CNWRA 97-010

AN ANALYSIS OF GALVANIC COUPLING EFFECTS ON THE PERFORMANCE OF HIGH-LEVEL NUCLEAR WASTE CONTAINER MATERIALS

Prepared for

Nuclear Regulatory Commission
Contract NRC-02-93-005

Prepared by

Center for Nuclear Waste Regulatory Analyses
San Antonio, Texas

August 1997

CNWRA 97-010

AN ANALYSIS OF GALVANIC COUPLING EFFECTS ON THE PERFORMANCE OF HIGH-LEVEL NUCLEAR WASTE CONTAINER MATERIALS

Prepared for

Nuclear Regulatory Commission
Contract NRC-02-93-005

Prepared by

Darrell S. Dunn
Gustavo A. Cragnolino

Center for Nuclear Waste Regulatory Analyses
San Antonio, Texas

August 1997

ABSTRACT

The current U.S. Department of Energy (DOE) Waste Containment and Isolation Strategy proposes the use of a double barrier waste package (WP) for the disposal of high-level nuclear waste (HLW). The WP is designed to have its lifetime extended by galvanic protection of the inner barrier, constructed of a corrosion resistant material, by an outer corrosion allowance barrier that corrodes sacrificially. Although the current DOE performance assessment approach is not based on a mechanistic modeling of galvanic corrosion, calculations have been reported that show the lifetime of the WP can be extended for many thousands of years if the inner and outer WP barriers are galvanically coupled.

The purpose of this study is to improve the mechanistic understanding of the effect of galvanic coupling on the WP performance and to develop a methodology to estimate a reasonable range of values for the galvanic coupling efficiency. Corrosion potentials of the inner and outer barrier materials were separately calculated based on the kinetics of the corrosion reactions and the reduction of both water and oxygen on the metal surface. The galvanic corrosion potentials of the materials were then calculated and compared to experimentally measured values previously reported. The calculations were extended to examine a wide range of near-field environmental parameters expected in a HLW repository. In addition, the effects of several electrochemical parameters, area ratio of the two materials, and efficiency of the galvanic couple on the galvanic corrosion potentials were evaluated. The occurrence of localized corrosion of the inner barrier was determined by comparing the galvanic corrosion potential with the repassivation potential. This potential is conservatively adopted as the critical potential for the initiation of localized corrosion in the form of pitting and crevice corrosion.

The results of this investigation confirm that after the outer barrier of the WP is penetrated, galvanic protection of the inner corrosion resistant barrier will occur as long as it is galvanically coupled to the failed carbon steel overpack. Variations in the near-field environmental conditions as well as uncertainties associated with the electrochemical parameters have little negative impact on the galvanic protection of the inner corrosion resistant barrier. The galvanic coupling efficiency was related to the resistance of the galvanic couple and estimated to be sufficiently high for the bimetallic couple consisting of a corrosion resistant inner barrier and a carbon steel outer barrier perforated by pits to assure protection of the inner container against localized corrosion.

CONTENTS

CONTENTS (cont'd)

FIGURES

FIGURES (cont'd)

FIGURES (cont'd)

LIST OF PRINCIPAL SYMBOLS

A_a	area of the anode
A_c	area of the cathode
A^{825}	surface area of Alloy 825
A^{steel}	surface area of A516 steel
α_{Fe}	charge transfer coefficient for the dissolution of iron.
β_{H_2O}	charge transfer coefficient for the reduction of water
β_{O_2}	charge transfer coefficient for the reduction of oxygen
C_{O_2}	concentration of dissolved oxygen
$C_{O_2}^{bulk}$	concentration of dissolved oxygen in the bulk solution
D_{O_2}	diffusion coefficient for oxygen
δ	thickness of the diffusion layer
E	potential
$E_{Fe/Fe^{2+}}$	equilibrium potential for the dissolution of iron
$E^0_{Fe/Fe^{2+}}$	standard equilibrium potential for the dissolution of iron
E_{H_2O}	equilibrium potential for the reduction of water
$E^0_{H_2O}$	standard equilibrium potential for the reduction of water
E_{O_2}	equilibrium potential for the reduction of oxygen

LIST OF PRINCIPAL SYMBOLS (cont'd)

$E_{O_2}^0$	standard equilibrium potential for the reduction of oxygen
$E_{O_2}^{op}$	overpotential of the oxygen reduction reaction
E_{couple}	potential of a perfect galvanic couple
E_{corr}	corrosion potential
E_{corr}^{steel}	corrosion potential of A516 steel
$E_{corr}^{steel,WP}$	corrosion potential of the A516 steel waste package
E_{corr}^{825}	corrosion potential of Alloy 825
$E_{corr}^{825,WP}$	corrosion potential of the Alloy 825 waste package
E_p	pit initiation potential
E_{rp}	repassivation potential for localized corrosion
$\Delta H_{a,O_2}$	activation enthalpy for the reduction of oxygen
$\Delta H_{a,H_2O}$	activation enthalpy for the reduction of water
F	Faraday's constant
h_p	height of active area of pit
I	current
I_a	anodic reaction current
I_c	cathodic reaction current
I_{galv}	galvanic corrosion current
I_{corr}	corrosion current
i	current density
i_c	cathodic reaction current density
i_a	anodic reaction current density
i_{corr}	corrosion current density
i_0	exchange current density
i_{pass}^{825}	passive current density of Alloy 825
$i_{H_2O}^{825}$	cathodic current density for water reduction on Alloy 825

LIST OF PRINCIPAL SYMBOLS (cont'd)

$i_{H_2O}^{825,WP}$	cathodic current density for water reduction on the Alloy 825 waste package
$i_{O_2}^{825}$	cathodic current density for oxygen reduction on Alloy 825
i_{0,O_2}^{825}	exchange current density for oxygen reduction on Alloy 825
$i_{0,O_2,(298)}^{825}$	exchange current density for oxygen reduction on Alloy 825 at 298 K
$i_{O_2}^{825,WP}$	cathodic current density for oxygen reduction on the Alloy 825 waste package
i_{active}^{steel}	anodic current density for the active dissolution of A516 steel
$i_{H_2O}^{steel}$	cathodic current density for the reduction of water on A516 steel
$i_{0,\ Fe/Fe^{2+}}$	exchange current density for the dissolution of iron
$i_{O_2}^{steel}$	cathodic current density for oxygen reduction on A516 steel
i_{0,O_2}^{steel}	exchange current density for oxygen reduction on A516 steel
$i_{0,O_2,(298)}^{steel}$	exchange current density for oxygen reduction on A516 steel at 298 K
i_{0,H_2O}	exchange current density for water reduction
$i_{0,H_2O,(298)}$	exchange current density for water reduction at 298 K
$i_{corr}^{steel,WP}$	corrosion current density of the A516 steel waste package
$i_{H_2O}^{steel,WP}$	cathodic current density for water reduction on the A516 steel waste package
$i_{O_2}^{steel,WP}$	cathodic current density for oxygen reduction on the A516 steel waste package
$I_{0,H^+/H_2}^{M}$	exchange current for hydrogen reduction on metal M
$I_{0,H^+/H_2}^{N}$	exchange current for hydrogen reduction on metal N
$I_{0,M/M^+}$	exchange current for the dissolution of metal M
$I_{0,N/N^+}$	exchange current for the dissolution of metal N
I_{corr}^{M}	corrosion current for metal M
I_{corr}^{N}	corrosion current for metal N
I_{corr}^{couple}	corrosion current for a galvanic couple
$I_{corr}^{M,galv}$	corrosion current of metal M when galvanically coupled

LIST OF PRINCIPAL SYMBOLS (cont'd)

K_H	Henry's constant
η	eta, galvanic coupling efficiency
p_{O_2}	partial pressure of oxygen
ρ_{soln}	solution resistivity
R	gas constant
R_{couple}	resistance of the Alloy 825/A516 steel galvanic couple
R_{soln}	resistance of solution
r_p	radius of pit
r_{CRM}	radius of exposed corrosion resistant material
$R_{CAM\ oxide}$	resistance of the corrosion allowance material oxide
$R_{CRM\ oxide}$	resistance of the corrosion resistance material oxide
$R_{corr\ product}$	resistance of the corrosion products between the waste package barriers
σ	solution conductivity
T	temperature in K
W_p	Wagner parameter
W_n	Wagner number
z_{Fe}	number of electrons involved in the dissolution of iron
z_{O_2}	number of electrons involved in the reduction of oxygen
z_{H_2O}	number of electrons involved in the reduction of water

ACRONYMS

AML	Areal Mass Loading
BEM	Boundary Element Method
BWR	boiling water reactor
CAM	corrosion allowance material
CRM	corrosion resistant material
CDF	Cumulative Distribution Function
CNWRA	Center for Nuclear Waste Regulatory Analyses
DOE	U.S. Department of Energy
EBSPAC	Engineered Barrier System Performance Assessment Code
FDM	Finite Difference Method
FEM	Finite Element Method
HLW	high-level nuclear waste
LEFM	Linear Elastic Fracture Mechanics
MPC	multi-purpose canister
NRC	Nuclear Regulatory Commission
PWR	pressurized water reactor
RH	relative humidity
SHE	standard hydrogen electrode
SF	spent fuel
SS	stainless steel
TPA	Total-system Performance Assessment
TSPA-95	Total System Performance Assessment–1995
WAPDEG	WAste Package DEGradation code
WP	waste package
YM	Yucca Mountain

ACKNOWLEDGMENTS

This report was prepared to document work performed by the Center for Nuclear Waste Regulatory Analyses (CNWRA) for the Nuclear Regulatory Commission (NRC) under Contract No. NRC-02-93-005. The activities reported here were performed on behalf of the NRC Office of Nuclear Material Safety and Safeguards, Division of Waste Management. The report is an independent product of the CNWRA and does not necessarily reflect the views or regulatory position of the NRC.

The authors gratefully acknowledge useful discussions with N. Sridhar, as well as his technical review, the programmatic review of B. Sagar, and the editorial review of B. Long. Appreciation is due to C. Garcia for assistance in preparation of this report.

ANALYSES AND CODES: *Mathematica* Version 2.2.3, a commercial scientific computer software, is used in analyses contained in this report.

QUALITY OF DATA: Sources of data are referenced in each chapter. CNWRA-generated laboratory data contained in this report meet quality assurance (QA) requirements described in the CNWRA QA Manual. Data from other sources, however, are freely used. The respective sources of non-CNWRA data should be consulted for determining levels of QA.

EXECUTIVE SUMMARY

The U.S. Department of Energy (DOE) updated strategy for radioactive waste containment and isolation for the proposed repository at the Yucca Mountain (YM), Nevada, site is focused on two objectives: (i) to ensure near-complete containment of radionuclides within the waste packages (WPs) for thousands of years and (ii) to limit the dose to any member of the public throughout the compliance period. To accomplish these objectives, the proposed repository will be located in an arid site with a low annual precipitation rate and a low flow of groundwater into the repository horizon. In addition, the DOE has redesigned the WPs applying a double metallic barrier concept in an attempt to prolong the time during which the radioactive waste can be contained. In the current design, a corrosion allowance material (a carbon steel is the primary candidate) intended to corrode uniformly at a slow and predictable rate, constitutes the outer barrier. In the event the outer barrier is breached by pits, galvanic coupling of the inner corrosion resistant barrier (a Ni-base alloy) to the outer barrier is assumed to prevent pitting corrosion of the inner barrier, extending the lifetime of the WP to many thousands of years.

In support of the Nuclear Regulatory Commission High-Level Nuclear Waste Program, the Center for Nuclear Waste Regulatory Analyses is developing a performance assessment capability for the purpose of evaluating the overall performance of the proposed repository at YM. As part of the activities conducted initially in the Container Life and Source Term and later in the Total-System Performance Assessment and Integration Key Technical Issues, the Engineered Barrier System Performance Assessment Code (EBSPAC) Version 1.1 was developed as a deterministic code to provide a means for evaluating the WP lifetime and radionuclide release rates.

In EBSPAC Version 1.1, a simple model is used to evaluate the beneficial effect of galvanic coupling on WP life. The model is based on a parametric equation in which the parameter representing the efficiency of galvanic coupling controls the corrosion potential of the galvanic couple formed by the two metallic barriers. The value of the efficiency parameter varies between 0.0 (no coupling) and 1.0 (perfect coupling). From the results of this simple model, galvanic coupling between the outer and inner metallic barriers was identified as a key factor in increasing the WP lifetime over a wide range of repository conditions.

The objectives of the study reported here are to improve the mechanistic understanding of the effect of galvanic coupling, develop a methodology to estimate a reasonable range of values for the galvanic coupling efficiency, and to define a criterion to estimate the time interval over which the effect can last, to evaluate the adequacy of the DOE prediction of a substantive beneficial effect and reduce the uncertainties involved in the EBSPAC calculations. To accomplish these objectives it is necessary to calculate the corrosion potentials of the WP materials separately and then couple them to determine the effect of galvanic coupling on the performance of the WPs.

In this study, the electrochemical kinetics of the anodic dissolution and cathodic reduction reactions are used to calculate both the corrosion potentials of the individual materials and the galvanic corrosion potentials of the materials when coupled. Corrosion potentials are calculated by summing all anodic and all cathodic reaction currents to zero because electrical charge cannot be accumulated in the metals. The anodic dissolution of A516 carbon steel was described by the active dissolution of iron whereas passive dissolution was assumed for Alloy 825 (one of the primary candidates for the corrosion resistant barrier). The reduction reactions were considered limited to the reductions of water and oxygen as the predominant reducible species. Evaluation of the effects of galvanic coupling is performed by considering the dissolution and reduction reactions occurring on both A516 carbon steel and Alloy 825. The geometry of

the galvanic couple is based on a through-wall pit penetrating the outer A516 carbon steel barrier that exposes the inner corrosion resistant Alloy 825 to an acidified local environment. The gradient in chemical composition, and hence the variation of solution conductivity in the pit, is ignored to simplify the calculation. The criterion adopted for the occurrence of localized corrosion of the inner overpack material is conservatively based on the repassivation potential. If the galvanic corrosion potential of Alloy 825 is lower than the repassivation potential, it is assumed that localized corrosion will not occur and the alloy will corrode slowly under passive dissolution conditions. Through these calculations, good agreement is found between the calculated and measured values of both the corrosion potentials and the galvanic corrosion potentials.

The main interest in performing these calculations is to determine the electrochemical conditions that may suppress localized corrosion of the Alloy 825 inner barrier by depressing its corrosion potential below the repassivation potential (E_{rp}) by galvanic coupling. Because the near-field environment is expected to be both space and time dependent, the effects of a range of environmental parameters on the corrosion and galvanic corrosion potentials are analyzed. The environmental parameters that are varied over wide ranges included temperature, pH, partial pressure of oxygen, and thickness of the diffusion layer. Calculations conducted in this investigation confirm conditions under which localized corrosion of Alloy 825 can occur are more easily attained at temperatures close to 100 °C. Within the ranges examined in this investigation, the effects of pH and the diffusion layer thickness on the corrosion potentials of the coupled metals are minimal. On the other hand, the partial pressure of oxygen is found to have a significant effect on WP performance. Decreasing the partial pressure of oxygen reduces the corrosion rate of the outer carbon steel barrier and, if the environment becomes sufficiently well deaerated, the possibility of localized corrosion of Alloy 825 is eliminated.

Electrochemical parameters investigated include the transfer coefficients for the dissolution of iron and the reduction of oxygen, the exchange current densities for the iron dissolution and the oxygen reduction, and the passive current density for Alloy 825. In addition, the effects of the area ratio between the container materials and the efficiency of the galvanic couple are evaluated. As with the environmental parameters, the effect of the electrochemical parameters within the range of values reported in the literature is found to be small. Variations in area ratio for the geometry used in this analysis also had little effect on performance. The efficiency of the galvanic couple is determined to be much more significant to WP performance than the environmental and electrochemical parameters or the area ratio of the WP materials.

As previously reported for EBSPAC calculations, the propensity to localized corrosion of the inner barrier is strongly dependent on the efficiency of the galvanic couple. A characterization of the galvanic couple in terms of the resistance between the WP materials is developed by correlating the resistance of the galvanic couple with its efficiency. The resistance of the galvanic couple as a function of galvanic coupling efficiency is determined for all the parameters investigated and related to the resistivity of the pit solution. From the analysis, it is concluded that to attain conditions where the localized corrosion of Alloy 825 could be suppressed, resistance of the galvanic couple has to be smaller than 500 ohms. This value is anticipated to be at least 30 times greater than that of the solution expected to come in contact with both container materials after the outer barrier is perforated. Estimations of galvanic coupling efficiency ranged from 0.97 to 0.99, assuming that resistance of the galvanic couple is determined by resistance of the solution present between the WP barriers if the outer barrier fails by localized corrosion. In addition, efficiency of the galvanic coupling required to avoid initiation of the localized corrosion of Alloy 825 seems to be assured because the electronic conductive and semiconductive natures of the oxides and corrosion products present between the WP barriers, as preliminarily evaluated from literature data, may provide a sufficiently high conductivity path. For a material with a higher E_{rp} such as Alloy 625,

localized corrosion can be avoided by galvanic coupling even if the couple has a greater resistance and is therefore less efficient.

Results of this investigation confirm that after the outer barrier of the WP is penetrated, galvanic protection of the inner corrosion resistant barrier will occur as long as it is galvanically coupled to the failed A516 carbon steel overpack. Variations in the environmental conditions expected in the repository, as well as uncertainties associated with the electrochemical parameters, appear to have little negative impact on the galvanic protection of the inner corrosion resistant barrier. The total time over which galvanic coupling protects the inner barrier is determined by the corrosion rate of the perforated outer A516 carbon steel container. Several factors can affect the corrosion rate of the outer barrier. These factors include the time the WP is continuously wetted, the surface area of the WP that is wetted, the chemistry of the water in contact with the WP, and the stability of protective oxide layers as well as the diffusion of soluble corrosion products away from the metal. Complete consumption of the anode (outer barrier) will end galvanic protection. Calculations presented in this report support previous results of EBSPAC calculations indicating that without adequate galvanic protection, localized corrosion of the inner corrosion resistant barrier is estimated to occur in a few thousand years.

1 INTRODUCTION

1.1 BACKGROUND

The U.S. Department of Energy (DOE) updated waste containment and isolation strategy (U.S. Department of Energy, 1996) for the proposed high-level nuclear waste (HLW) repository at the Yucca Mountain (YM), Nevada, site has the primary goals of near-complete containment of radionuclides within waste packages (WPs) for several thousand years and acceptably low annual doses to a member of the public living near the site throughout the compliance period. The WP consists of containers, fillers, basket materials, and waste forms [spent fuel (SF) or vitrified reprocessed waste]. The container lifetime is one of the important system attributes recognized in this strategy that needs to be assessed to determine overall repository performance.

Many factors, including WP design and interactions of the WP materials with the near-field repository environment, will have an effect on container lifetimes. Over the history of the YM repository program, several WP designs have been proposed by the DOE. Of these designs, the canistered fuel design is considered the most likely to be used for the disposal of SF (TRW Environmental Safety Systems, Inc., 1996). In the largest of this design, either 21 pressurized water reactor (PWR) or 40 boiling water reactor (BWR) SF assemblies will be contained in a type 316L stainless steel (SS) multi-purpose canister (MPC). The MPC (3.5 cm wall thickness) will be surrounded by an inner overpack made of a corrosion-resistant material (CRM) with a 2.0 cm wall thickness, that will in turn be contained in an outer overpack made of a corrosion-allowance material (CAM) with a 10 cm wall thickness. The total surface area of such a WP will be about 37 m^2 with a loaded weight of about 65,000 kg. Alternate designs include WP for uncanistered fuel (no MPC), small canistered fuel (12 PWR or 24 BWR SF assemblies), and vitrified waste. Nickel base alloys, such as Alloys 825, 625, and C-22 are presently being evaluated for the inner corrosion resistant overpack (Roy et el., 1996). A carbon steel, A516 grade 55, is proposed as the primary candidate material for the outer corrosion allowance overpack (TRW Environmental Safety Systems, Inc., 1996).

If the container should come in contact with humid air or an aqueous environment, it is anticipated in the Total System Performance Assessment–1995 (TSPA-95) that uniform corrosion of the carbon steel overpack will proceed at a slow and predictable rate, although the occurrence of pitting corrosion is considered by using a pitting factor (TRW Environmental Safety Systems, Inc., 1995). Evaporation of the groundwater as a result of the heat generated by radioactive decay and interactions of the percolating water with concrete in the repository, however, may result in an alkaline aqueous environment able to induce passivity of the carbon steel overpack. In the presence of chloride anions, passivity breakdown may occur leading to localized corrosion in the form of pitting (Marsh et al., 1986). Perforation of the carbon steel overpack will result in exposure of some areas of the CRM to an acidified aqueous environment enriched in chloride ions. Localized corrosion of the inner overpack can be mitigated by the use of both a highly corrosion resistant alloy and its galvanic coupling to the carbon steel overpack (TRW Environmental Safety Systems, Inc., 1995; Mohanty et al., 1997).

Protection of the inner CRM by the remaining CAM used for the outer overpack has been recognized as one of the most important design features of the WP. Cathodic protection has typically been used to protect steel structures such as gas pipelines, offshore oil platforms, and ship hulls as well as other types of components in many engineering applications (Morgan, 1993). Protection of the inner CRM by galvanic coupling with the perforated CAM, however, differs significantly from the conventional

application of cathodic protection systems. As in any other cathodic protection application, the goal is to achieve the highest efficiency attainable in the galvanic coupling. Because the WPs are expected to perform for a period well beyond that acceptable for other engineering applications, a mechanistic understanding in conjunction with experimental testing will be useful in developing reasonably valid predictions. There are three general considerations in any cathodic protection scheme: (i) potential distribution or indirectly, galvanic efficiency, (ii) anode life and efficiency, and (iii) overprotection leading to hydrogen embrittlement. All of these are germane to the present analysis.

1.2 THE U.S. DEPARTMENT OF ENERGY APPROACH TO GALVANIC COUPLING

The DOE has performed a probabilistic analysis of container life in the TSPA-95 (TRW Environmental Safety Systems, Inc., 1995) using the WAste Package DEGradation (WAPDEG) Version 1.0 code (Atkins and Lee, 1996). WAPDEG is designed to run stochastic simulations, in which sampled parameter values are used to determine the WP failure time.

Consistent with the DOE Waste Containment and Isolation Strategy for the Yucca Mountain Site (U.S. Department of Energy, 1996), the WP environment in WAPDEG simulations is assumed to be humid air at elevated temperatures for a period extended over thousands of years. In WAPDEG, the time-dependent temperature and relative humidity (RH) at the WP surface are the inputs that drive the various corrosion models. As explained in the following sections, the chemistry of the environment used in these simulations neither corresponds to that expected under repository conditions nor to the bounding environments described in the DOE test program (McCright, 1995). Humid air corrosion is considered to be corrosion that occurs under a thin water film forming on the container surface above a critical RH range uniformly distributed between 65 and 75 percent. Aqueous corrosion refers to corrosion of metal in contact with bulk water, assumed to occur at RHs greater than a threshold value uniformly distributed between 85 and 95 percent.

For the carbon steel outer overpack, active general corrosion is assumed to occur in humid air and is modeled using a parametric equation exhibiting a dependence of the corrosion rate on time, RH, and absolute temperature. The parameter values are obtained by linear regression to fit the equation by using atmospheric corrosion data from tropical, urban, rural, and industrial locations (excluding marine sites) and considering only the time fraction during which RH was greater than 70 percent (time of wetness). Aqueous corrosion of the outer overpack is evaluated through a similar approach but using literature data acquired in polluted river water and tropical lake water combined with data in distilled water to determine the temperature effect. In both types of environments, pitting corrosion of carbon steel is modeled by multiplying the uniform corrosion rate by a pitting factor assumed to be normally distributed with a mean of 4 and a standard deviation of 1.

For the inner overpack material, only pitting corrosion in the aqueous environment is considered, assuming that humid air corrosion and general corrosion are negligible. The pit growth rate is calculated through an empirical expression following an Arrhenius dependence on temperature. No pit initiation time is considered and it is assumed that pits nucleate with an uniform distribution on the overall WP surface. Failure of the WP is defined as penetration by a single pit.

Once the outer container is breached by pits, cathodic protection of the inner overpack is evaluated in TSPA-95 by assuming that pitting corrosion would be delayed until the overall thickness of

the outer metallic barrier is reduced by 75 percent. This criterion was adopted following an expert elicitation. For an areal mass loading (AML) of 83 MTU/acre, without backfill and with a low water infiltration rate (q_{inf} = 0.05 mm/yr), the cumulative distribution function (CDF) without galvanic protection of the CRM exhibits the first WP failure at 2,200 yr and a median failure time slightly over 3,000 yr with 92 percent of the WPs failing in 10,000 yr. If galvanic protection of the CRM by the outer container is considered, the first failure occurs after 8,000 yr, the median failure time is extended to 40,000 yr and only 60 percent of the WPs fail in 100,000 yr. As stated in TSPA-95, however, the criterion for "cathodic protection provided by the elicitation..., was not developed from experimental data or detailed analysis...." Nevertheless, the need for a substantive technical basis and improvement in the modeling of galvanic coupling are clearly recognized in TSPA-95. In addition, the importance of maintaining a good metallic contact between the CRM and the perforated CAM to insure good cathodic protection efficiency is noted. It is also recognized that corrosion of the outer overpack leading to a decreasing wall thickness sets a time limit to the protection afforded. Although it is not evaluated in TSPA-95, the risk of crevice corrosion of the inner overpack as a consequence of the lack of adequate cathodic protection by the outer overpack and its detrimental influence on the performance of the WP is identified, indicating that crevice corrosion will be addressed in future performance assessment analyses.

1.3 APPROACH TO GALVANIC COUPLING ADOPTED IN THE ENGINEERED BARRIER SYSTEM PERFORMANCE ASSESSMENT CODE

The effects of AML, chemical composition of the near-field environment, and galvanic coupling on WP lifetimes have been calculated using the Engineered Barrier System Performance Assessment Code (EBSPAC), Version 1.1 (Mohanty et al., 1997). EBSPAC is also incorporated into the Total-system Performance Assessment (TPA) code (Manteufel et al., 1997) as a source term module. It can be used to perform probabilistic calculations and conduct sensitivity analyses in a stand-alone mode by using appropriate drivers.

In this code, dry-air oxidation, aqueous corrosion, and mechanical failure due to thermal embrittlement are incorporated. Aqueous corrosion processes are modeled using an electrochemical approach assuming that aqueous corrosion occurs only above a critical value of RH. Below this critical value only dry-air oxidation takes place. The aqueous environments considered in EBSPAC are derived, by adopting several simplifications, from coupled thermal-hydrological-chemical calculations. The aqueous corrosion processes for both the outer and inner overpacks are governed by the corrosion potential (E_{corr}) and the critical potential required to initiate localized corrosion in the form of pitting or crevice corrosion. The E_{corr} of the CAM is explicitly calculated by considering the combined electrochemical kinetics of the steel dissolution reaction under passive conditions, which is potential-independent, and the reduction reactions of both water and oxygen on the outer overpack surface, which depend on potential and environmental variables such as temperature, oxygen partial pressure, and pH. The repassivation potential (E_{rp}) is conservatively adopted as the critical potential for the initiation of localized corrosion. Pitting or crevice corrosion of the CAM is assumed to begin without an induction time when the pH of water in contact with the steel container is greater than 8.0, the chloride concentration is higher than a threshold value of 3.0×10^{-4} mol/L, and the E_{corr} exceeds the E_{rp}. The latter parameter has been experimentally measured and expressed in an equation as a function of both chloride concentration and temperature. When the E_{corr} is lower than the E_{rp}, uniform corrosion under passive conditions takes place. If pitting starts, the pit propagation rate is assumed to follow a time dependent rate, as experimentally determined by Marsh and Taylor (1988).

Following penetration of the outer container, electrical contact of the inner and outer containers through the presence of an electrolyte path (such as that provided by groundwater) promotes galvanic coupling, assuming that metallic contact always exists between both containers. The galvanic coupling model evaluates whether penetration of the inner container by localized corrosion is possible; if not, uniform corrosion under passive conditions or mechanical fracture becomes the predominant failure mechanism, because the inner container is protected against localized corrosion.

The effect of galvanic coupling on the inner overpack is included in EBSPAC Version 1.1 (Mohanty et al., 1997) through an equation that computes the corrosion potential of the galvanic couple formed when the wall of the outer container is penetrated by a pit. The corrosion potential of Alloy 825 WP, E_{corr}^{WP}, is determined from the corrosion potential of the uncoupled inner overpack, E_{corr}, and the corrosion potential of the perfect galvanic couple, E_{couple}, through use of an efficiency coefficient, η.

$$E_{corr}^{WP} = (1 - \eta)E_{corr} + \eta E_{couple} \qquad (1\text{-}1)$$

The corrosion potential of the inner overpack upon penetration of the outer overpack but prior to any galvanic coupling, E_{corr}, is calculated based on the passive dissolution kinetics of the CRM and the cathodic reductions of both oxygen and water. If the corrosion potential of the inner overpack under galvanic coupling, E_{corr}^{WP} (assumed to be identical to the corrosion potential of the WP operating as a couple) is lower than the E_{rp} for localized corrosion of the CRM, only passive dissolution with a current density of about 2×10^{-7} A/cm^2 will occur. Otherwise, localized corrosion will be initiated without an induction time and pit propagation will occur at a constant rate of 2×10^{-5} A/cm^2. Failure of the WP is defined as penetration of both overpacks by a single pit or by uniform general dissolution. A simplified mechanical failure model based on linear elastic fracture mechanics (LEFM) concepts is included in EBSPAC Version 1.1 to consider the propensity to fracture of the outer steel overpack as a result of thermal embrittlement.

By selecting a critical RH of about 65 percent, calculations performed with EBSPAC Version 1.1 indicated that wetting of the outer container corresponding to the formation of a liquid film on its surface occurs at about 108 °C for an AML of 80 MTU/acre without either ventilation or backfilling (Mohanty et al., 1997). The time to wetting is dependent on the AML, and at 80 MTU/acre the WP remains dry for about 2,400 yr. Localized corrosion begins as soon as the WP becomes wet because the corrosion potential for the A516 steel overpack, E_{corr}^{steel}, is greater than E_{rp} for A516 steel under the prevailing environmental conditions (e.g., temperature, pH, chloride concentration, and partial pressure of oxygen) and penetration of the outer container by pitting corrosion can occur in a few hundreds of years. After penetration of the outer container, the E_{corr}^{WP} is dependent on the efficiency of the galvanic coupling. At a low AML (20 MTU/acre) the E_{corr}^{WP} never exceeds the E_{rp} even when the coupling is completely inefficient ($\eta = 0$). As a result, the lifetime of the WP can be greater than 10,000 yr. At higher AMLs (40 and 80 MTU/acre), however, the WP lifetimes are strongly dependent on the efficiency of the galvanic coupling. For an AML of 80 MTU/acre (without either ventilation or backfilling), the calculated WP failure time is equal to 2,736 yr if η is less than 0.2 but it is extended to over 10,000 yr for η greater than 0.2.

1.4 UNCERTAINTIES AND NEED FOR ADDITIONAL CALCULATIONS

Although completely different approaches are used in the DOE TSPA-95 WAPDEG Version 1.0 code (Atkins and Lee, 1996) and in EBSPAC Version 1.1 (Mohanty et al., 1997) to calculate the WP failure times, and in particular the influence of galvanic coupling, it is apparent from the calculations conducted with both codes that the beneficial effect of galvanic coupling between the CRM and the CAM can be significant. At present, however, clear understanding of the factors influencing galvanic coupling efficiency and hence WP lifetimes is lacking. The limitations of the empirical method used in TSPA-95 have recently been discussed (Dunn et al., 1997).

It appears that a more fundamental approach based on electrochemical kinetics theory can provide adequate justification for selection of an appropriate range of η values. The value of η should be based on the physicochemical and electronic nature of the galvanic contact, including the resistance of the electrolytic path to the flow of current, the presence of deposited corrosion products acting as high-impedance surface contacts between the metallic barriers, and the geometry and size of the pits penetrating the outer container. In addition, it is desirable to calculate the corrosion potential of the perfect galvanic couple established between Alloy 825 and A516 steel. It should be noted that the value used for E_{couple} in EBSPAC, Version 1.1, instead of being calculated on the basis of electrochemical reaction kinetics, corresponds to the potential measured by Scully and Hack (1984) for the galvanic couple formed by Alloy 625 and carbon steel exposed to seawater. Finally, it is important to evaluate whether or not the beneficial effect of galvanic coupling is limited to times significantly shorter than 10,000 yr as a result of the enhanced galvanic corrosion of the outer A516 steel overpack that may lead to its premature consumption.

1.5 OBJECTIVES AND SCOPE OF THIS ANALYSIS

In support of the Nuclear Regulatory Commission (NRC) HLW program, the Center for Nuclear Waste Regulatory Analyses (CNWRA) is developing a performance assessment capability for the purpose of evaluating the overall performance of the proposed repository at YM. As part of the activities conducted initially in the Container Life and Source Term (CLST) and later in the Total-System Performance Assessment and Integration (TSPA&I) Key Technical Issues (KTIs), the EBSPAC Version 1.1 (Mohanty et al., 1997) was developed as a deterministic code to provide a means for evaluating the WP lifetime and radionuclide release rates.

As noted in section 1.3, by performing EBSPAC calculations over a wide range of repository conditions (Sagar, 1997), galvanic coupling between the outer and inner metallic barriers was identified as a key factor in increasing the WP lifetime. To overcome the uncertainties described in section 1.4, a stronger technical basis for modeling galvanic coupling than that presented in EBSPAC Version 1.1 (Mohanty et al., 1997) was required within the TSPA&I KTI through an auxiliary analysis. The objective of this analysis was to improve the mechanistic understanding of the beneficial effect of galvanic coupling and to develop a methodology to estimate a reasonable range of values for the galvanic coupling efficiency. Another expected result was an evaluation of the critical remaining thickness of the outer overpack able to sustain galvanic coupling as conceived in TSPA-95.

This report presents the approach adopted in the modeling of galvanic corrosion and the associated results. Chapter 2 contains a discussion on the fundamental aspects of the electrochemical theory of galvanic coupling followed by a brief review of the literature regarding the analytical and numerical modeling of potential and current distributions. The chapter provides a detailed description of

the approach and the geometry adopted in the modeling of the galvanic corrosion potential of the bimetallic WP. The text includes the electrochemical kinetic expressions for anodic dissolution and cathodic reduction reactions used to calculate individual corrosion potentials of the container materials and the galvanic corrosion potential of the couple. Chapter 3 presents results of the calculations, including the galvanic corrosion potentials determined as a function of η. The effects of several near-field environmental parameters and the area ratio of the two materials on the galvanic corrosion potentials are described in this chapter. Chapter 4 offers a detailed discussion of the results, including an evaluation of the lifetime of the outer container that establishes a limit to the period of galvanic protection. Values of η are correlated with the resistance of the galvanic couple and the resistivity of the solution present between the two materials. The role of oxide films and corrosion products affecting the value of the resistance are discussed taking into consideration their conductive and semiconductive properties. Chapter 5 offers a summary of the study, followed by conclusions and recommendations. The appendix contains the results of an evaluation of the effect of uncertainties in the values of the electrochemical kinetics parameters on the galvanic corrosion potential calculations.

2 FUNDAMENTAL ASPECTS AND MODELING OF GALVANIC COUPLING

2.1 OVERVIEW OF ELECTROCHEMICAL THEORY OF GALVANIC COUPLING

Cathodic protection of metallic structures is based on the application of the fundamental concepts that explain galvanic or bimetallic corrosion. Therefore, a brief review of galvanic corrosion is useful to understand the nature of the electrochemical processes that occur as a result of the galvanic coupling of the two metallic barriers forming the WPs. When a metal is immersed in an electrolytic solution, an electrical potential difference is established at the metal/solution interface named E_{corr} and the value of this potential is defined with respect to a specific reference electrode scale [e.g., standard hydrogen electrode (SHE)]. The E_{corr} is not a thermodynamically defined potential such as the electrode potentials (Bard et al., 1985) but a mixed potential determined by rates of the anodic (oxidation) reactions corresponding to metal dissolution and the cathodic (reduction) reactions that occur simultaneously over the whole exposed metal surface (Vetter, 1967). This concept of coupled anodic and cathodic processes in freely corroding systems was originally proposed by Wagner and Traud (1938) and requires the total anodic current be equal to the total cathodic current since accumulation of charge within the metal cannot occur.

Figure 2-1 shows a schematic of the current versus potential curves for coupled anodic and cathodic reactions according to the Wagner and Traud hypothesis. The anodic currents (I_a) are conventionally represented as positive currents whereas the cathodic currents (I_c) are negative. The potential scale follows the convention used to represent electrode potentials with the negative sign corresponding to active redox couples (e.g., Fe/Fe^{2+}) and the positive sign to noble couples (e.g., O_2/H_2O) with respect to the SHE [$H^+(a=1)/H_2(f=1)$, where a is activity and f is fugacity]. The simplified case of a single metal oxidation reaction and the coupled H^+ ion reduction is shown in figure 2-1 to illustrate the equality of anodic and cathodic currents required to define E_{corr}, a mixed potential with an intermediate value between the thermodynamically defined equilibrium electrode potentials for both reactions, $E_{e,a}$ and $E_{e,c}$. According to the theory on the kinetics of charge transfer reactions at metal/electrolyte interfaces (Vetter, 1967) for the anodic reaction of metal oxidation

$$M \rightleftharpoons M^{z+} + ze^- \tag{2-1}$$

the current density, i_a, which is equal to the current I_a divided by the anodic surface area, A_a, is given as a function of potential under complete activation control by

$$i_a = i_{0,a} \exp\left(\frac{[E-E_{e,a}]}{b_a}\right) \tag{2-2}$$

and the current density for the reduction of H^+ ions, i_c, is given by

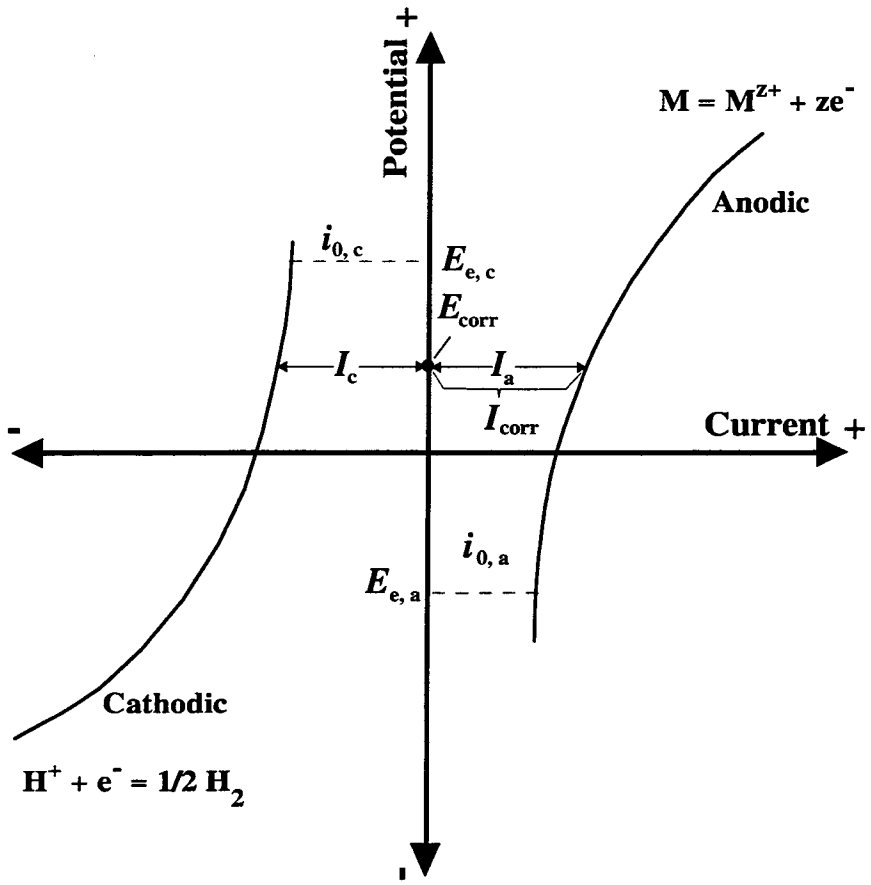

Figure 2-1. Schematic current versus potential curves for coupled anodic and cathodic partial reactions according to the Wagner and Traud hypothesis for metallic corrosion

$$i_c = i_{0,c} \exp\left(-\frac{[E-E_{e,c}]}{b_c}\right) \qquad (2\text{-}3)$$

where

i_0 — exchange current density
b — Tafel constant
E — potential
E_e — equilibrium potential

and the subscripts a and c designate anodic and cathodic processes. For simplicity the partial reduction reaction for M^{z+} and the partial oxidation reaction for H_2 are not included in Eqs. (2-2) and (2-3).

The anodic and cathodic Tafel constants (Vetter, 1967) can be expressed using more fundamental parameters as follows:

$$b_a = \frac{RT}{\alpha z F} \tag{2-4}$$

and

$$b_c = \frac{RT}{\beta z F} \tag{2-5}$$

where

α — anodic transfer coefficient
β — cathodic transfer coefficient
z — number of electrons transferred per mole
R — gas constant
T — absolute temperature
F — Faraday's constant

As illustrated in figure 2-1 when I_a is equal to I_c , $E=E_{corr}$. Under such conditions $i_a=i_c\ A_c/A_a$, that for the case of a single metal immersed in an aqueous solution becomes $i_a=i_c$ because all the area exposed is simultaneously available for the anodic and cathodic reaction ($A=A_a=A_c$), according to the Wagner and Traud theory. It is apparent from figure 2-1 that I_a is indeed the corrosion current, I_{corr}, from which the corrosion rate (e.g., in mm/yr) can be calculated by using Faraday's laws.

When two dissimilar metals are connected in a galvanic couple, the mixed potential theory is also applicable to determine I_{corr} of the couple and the E_{corr} of both metals. This is illustrated in figure 2-2, in which the logarithm of the absolute value of the currents are plotted against potentials in a single quadrant in the so-called Evans diagrams, a form of representation commonly used in the corrosion literature. The advantage of the Evans diagram arises from the fact that the logarithms of the absolute values of the anodic and cathodic currents can be used to obtain I_{corr} through the intersection of the potential versus current plots. Figure 2-2 shows the individual anodic currents as a function of potential for two actively corroding metals, M and N, in an acidic solution in which the reduction of H^+ ions is the cathodic reaction. When M is coupled to a more active metal such as N, the intersection of the total anodic current with the total cathodic current define the corrosion potential of the couple, E_{couple}. Although I_{corr} for the couple is greater than the corrosion currents corresponding to the uncoupled metals, the significant result is the decrease of the corrosion current of M from I_{corr}^{M} to $I_{corr}^{M,galv}$. Even more important for the purpose of this discussion is the observation that the current decrease is a result of the decrease in the potential of M from E_{corr}^{M} to $E_{corr}^{M,galv} = E_{couple}$ as a result of the galvanic coupling.

This analysis constitutes the electrochemical basis for the application of cathodic protection to industrial structures. Cathodic protection is accomplished by decreasing the potential of the metal M (e.g., Fe) to values lower than its equilibrium potential, shown in figure 2-2 as E_{M/M^+}, by using a sufficiently active metal (e.g., Zn, Mg) as a sacrificial anode. Thus, cathodic protection prevents the corrosion of the structure by displacing the E_{corr} of the steel into the region of thermodynamic immunity against corrosion (Pourbaix, 1974). The steel structure acts as a cathode where most of the reduction

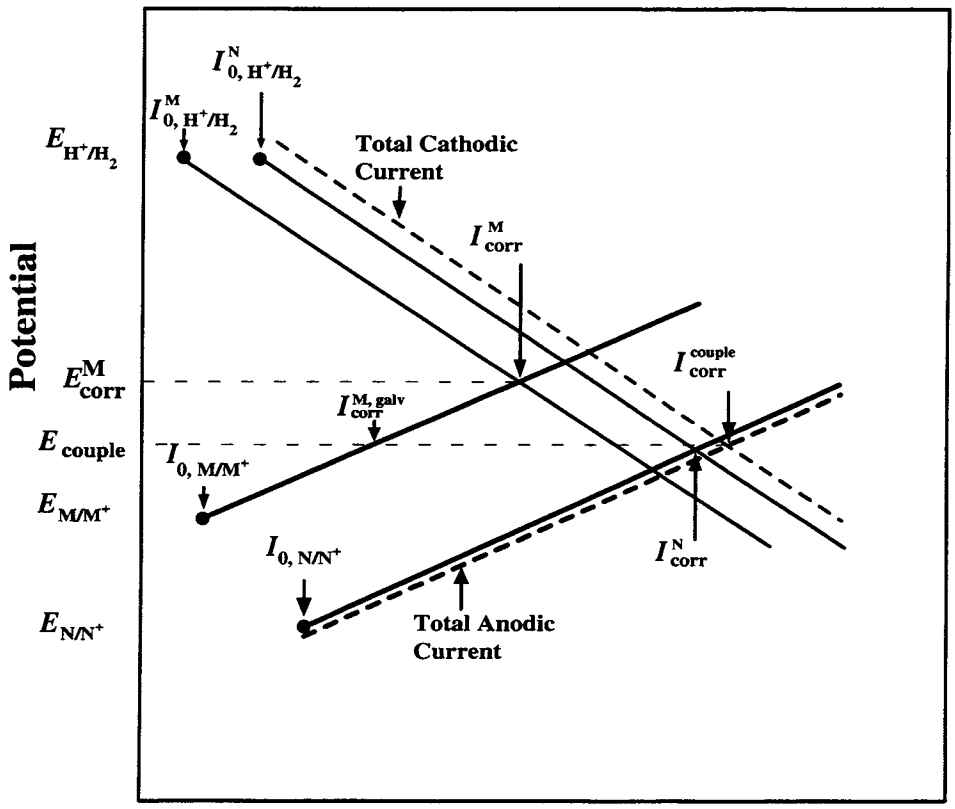

Figure 2-2. Evans diagram for the anodic and cathodic currents representing galvanic coupling between two active corroding metals

reactions of the available reducible species (e.g., H^+ ions, O_2) occur. As schematically shown in figure 2-2, the corrosion current of N, I^{N}_{corr}, is significantly higher than that of M, and as a consequence the life of the anode becomes the limiting factor for the existence of protection. If impressed current systems of cathodic protection are used, the structures are maintained as a cathode with either a constant current or a constant voltage source. Typically, the anodes used in impressed current systems are noble materials not consumed. Underprotection happens when the galvanic corrosion potential is above the potential needed for complete protection of the metal from corrosion. Overprotection takes place when the galvanic corrosion potential is significantly lower than the potential required for protection, in which case hydrogen generation may occur leading to hydrogen embrittlement.

Figure 2-3 illustrates the coupling of a CAM, an actively corroding metal, to a CRM exhibiting a wide potential range of passive behavior characterized by a low current density (typically 10^{-2} A/m^2), independent of potential, just above an active/passive transition. It is clearly seen that in this case galvanic coupling only decreases the E_{corr} of the passive metal without affecting its already low I_{corr}. In situations such as that represented in figure 2-3, the potential of the CRM is not usually maintained below the equilibrium potential for dissolution, E_{M/M^+}. The purpose is to provide anodic protection by galvanic coupling against the possible initiation of localized corrosion that can occur only above a certain critical

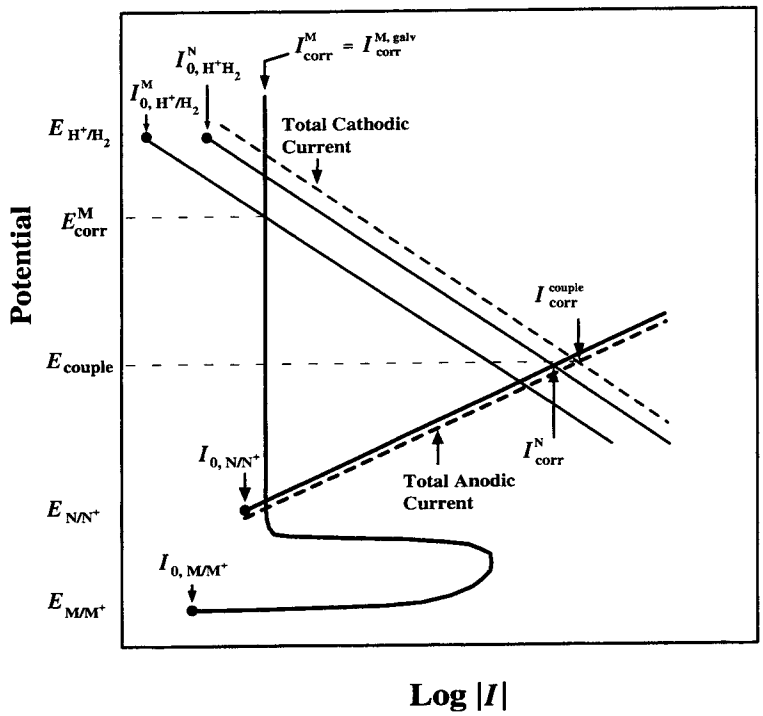

Figure 2-3. Evans diagram for the anodic and cathodic currents representing galvanic coupling between a passive corrosion resistant alloy and an active corroding metal

potential. Although the cathodic reaction takes place predominantly on the CRM surface, the protection differs from that in a typical cathodic protection system because the potential of the protected metal is maintained in the anodic range and not below its equilibrium potential, E_{M/M^+}, which could be even lower than that of the active metal, E_{N/N^+}, as noted in figure 2-3. Localized corrosion is avoided by maintaining its E_{corr} at values lower than the critical potential for the initiation of localized corrosion as a result of galvanic coupling. Under these conditions, localized corrosion does not occur and the CRM slowly corrodes at a rate determined by the passive current density under anodic protection conditions.

As previously noted, dissimilar metals exhibit different E_{corr} values when exposed separately to a given environment. If good metallic contact is established between the bimetallic couple, the corrosion potential of both metals is equal to E_{couple} as shown in figure 2-4 as the intersection between the total anodic and total cathodic currents from figure 2-2. The presence of a resistance, R_{couple}, between the metals creates a potential drop shown in figure 2-4 as I_{galv} R_{couple}. As the resistance increases, the potential drop becomes larger and the I_{galv} decreases.

2.2 CURRENT DISTRIBUTION AND WAGNER PARAMETER

Under galvanic coupling conditions there are three types of possible current distributions according to the geometry and the electrochemical characteristics of the bimetal/electrolyte system. The primary current distribution considers that only geometric and ohmic effects are involved, without influence of the polarization of the electrodes as a result of charge transfer kinetics across the metal/solution interfaces. The secondary current distribution considers the polarization of the electrodes

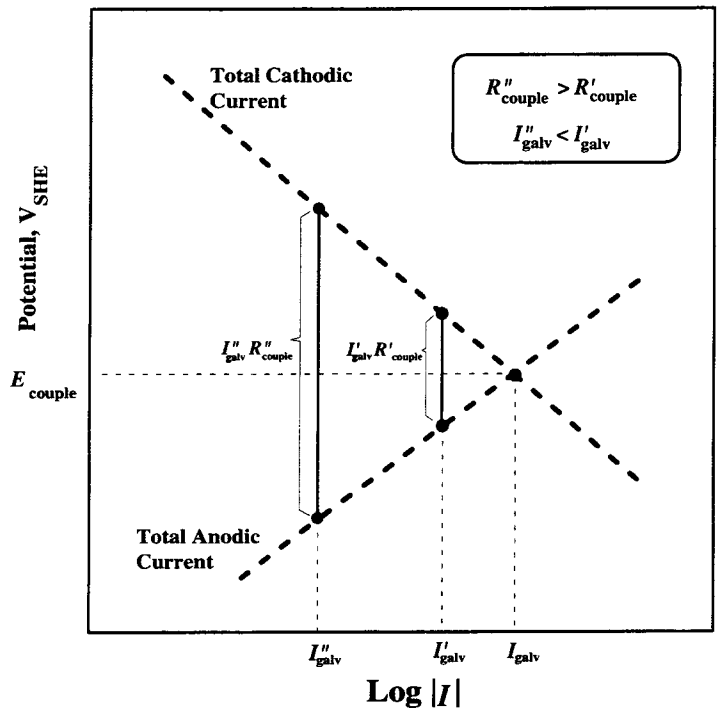

Figure 2-4. Evans diagram showing total anodic current and total cathodic current curves. The corrosion potential of a perfect galvanic couple is indicated by E_{couple}. Potential drops associated with two imperfect galvanic couples are indicated by $I'_{galv}\,R'_{couple}$ and $I''_{galv}\,R''_{couple}$.

due to charge transfer reactions in addition to ohmic effects in solution. Finally, the tertiary distribution considers mass transport effects on the kinetics of the charge transfer reactions in addition to the factors taken into account in the previous types of current distributions.

Wagner (1951) proposed a semiquantitative approach for current distribution using a polarization parameter of a given metal/electrolyte combination, defined as

$$W_p = \sigma\left(\frac{dE}{di}\right) \tag{2-6}$$

where σ is the conductivity of the solution in $ohm^{-1}\ m^{-1}$ and (dE/di) is the slope of the steady-state polarization curve where the current density, i, is expressed in A/m^2. As a consequence, the Wagner parameter, W_p, has dimensions of length in m. This parameter is important in galvanic corrosion studies because in the scale-up of a system, either for modeling or experimental simulations, the ratio of W_p to a characteristic length of the system, named the Wagner number, W_n, should be kept constant (Oldfield, 1988). As noted by Wagner (1951), the distribution of current will be nearly uniform if W_p is much greater than the characteristic length of the particular geometry (i.e., if W_n is a large number). For example, the flow of current along a condenser tube will be unidirectional if the tube radius (its characteristic length) is sufficiently smaller with respect to W_p. Astley (1988) noted that for copper base alloys in seawater service under stagnant conditions, W_p is about 5 m, whereas in a poorly conducting

electrolyte such as fresh water, W_p could be about 0.01 m. It can be concluded that the throwing power of the current arising from the dissolution of a sacrificial anode can be easily estimated by using W_p.

It is apparent from the previous discussion that in solutions of relatively high conductivity as those expected in localized geometries associated with pits or crevices, a uniform current distribution will exist regardless of the size of the pit or crevice. Associated with this current distribution, uniformly distributed equipotential surfaces will exist in the solution and distribution of the electrode potential on each metal will be uniform facilitating the analysis of galvanic coupling effects for a variety of simple geometries (Astley, 1988). In many cases, as noted by Astley (1983), analytical solutions are possible for the case of unidirectional current flow. It must be noted, however, that in pits and crevices, the solution conductivity may not be uniform due to concentration gradients.

2.3 NUMERICAL SIMULATION OF GALVANIC POTENTIAL AND CURRENT DISTRIBUTION

Modeling of cathodic protection systems has been performed to predict its life expectancy and to analyze the system for indications of both underprotection and overprotection. Numerical modeling techniques have also been used to characterize galvanic corrosion of systems with complex geometries. Applications for numerical modeling of cathodic protection and galvanic corrosion included offshore platforms (Adey et al., 1985; Strommen, 1992), underground pipelines (Orazem et al., 1997a, b; Esteban et al., 1995), and ocean going ships (Zamani, 1988). These models were constructed using three methods: the finite difference method (FDM), the finite element method (FEM), and the boundary element method (BEM).

Initially cathodic protection systems were analyzed using the FDM. A useful feature of FDM models is the ability to simulate nonhomogeneous electrolytes (Zamani et al., 1986). For many engineering applications, however, considerable difficulty was noted in defining the geometry and boundary conditions. The FEM can analyze more complex geometries than the FDM. The main limitation with the FEM method is that even though corrosion reactions only occur on the surface of the material, the analysis must consider the electrolyte. Much effort is required to construct a finite element mesh in the electrolyte from the anode to the cathode. In addition, the mesh must extend well beyond the area of interest to a realistic boundary (Adey et al., 1985). This results in a large number of computational nodes not located at places of interest and increases the complexity of the modeling task (Adey et al., 1985).

Several efforts focused on the BEM to model galvanic corrosion (Varela et al., 1997; Adey and Niku, 1992) and cathodic protection systems (Zamani, 1988; Yan et al., 1992; Zamani et al., 1986; Adey et al., 1985; De Giorgi et al., 1992). The principal advantage of the BEM is that all of the computational nodes are located on the surface of interest and not in the electrolyte. After computing the boundary values of current density and potential distributions at the surface, the potential and current density distributions in the medium can than be determined. Although nonhomogeneous electrolytes can be modeled by substructuring, this significantly increases the complexity of the modeling task.

Modeling either galvanic corrosion or cathodic protection systems requires equations for both the current flow through the medium and for reactions occurring on the metal surfaces. In BEM the partial differential equations are transformed to an integral equation on the boundary that is then discretizied (Zamani et al., 1986; Adey et al., 1985). The reactions occurring at the surface consist of dissolution of the metal and reduction of dissolved oxygen and hydrogen evolution. Equations relating the current density, i, at the electrode surface (either the anode or the cathode) may be expressed as

$$i = i_0 \, f(E - E_e) \tag{2-7}$$

where

i_0 — exchange current density for the reaction
f — function describing the relationship between current density and potential

This function f can be expressed as the Butler-Volmer equation

$$i = i_0 \left[\exp\left(\frac{\alpha F(E - E_e)}{RT} \right) - \exp\left(\frac{-(1-\alpha) F(E - E_e)}{RT} \right) \right] \tag{2-8}$$

where

α — transfer coefficient for the reaction

In the absence of the necessary electrochemical data it may not be possible to obtain an analytical expression for i as given by Eq. (2-8). In these cases, experimentally measured polarization curves can be used for the relationship between potential and current density.

For an electrolyte with uniform conductivity, the potential in solution must obey Laplace's equation.

$$\nabla^2 \phi = 0 \tag{2-9}$$

For most applications, the electrolyte is assumed to have a uniform concentration profile and a constant specific conductivity. The current density in the electrolyte is given by Ohm's law

$$i_n = \sigma \frac{\partial \phi}{\partial n} \tag{2-10}$$

where

i_n — current flowing in the n^{th} direction
σ — conductivity of the electrolyte

Laplace's equation can be discretized into a linear system of equations

$$GQ = H\Phi \tag{2-11}$$

where G and H are the matrices containing the influence coefficients of the system geometry. The terms Q and Φ are vectors of the potential gradient and potential on the boundaries of the system (Yan et al.,

1992). This system of equations relates the current flow in the system between the anode and the cathode and models the potential drop in the medium as a result of the resistance of the electrolyte. The main task in using the BEM to model corrosion systems is to solve this system of equations. This is accomplished using an iterative numerical procedure.

Modeling of cathodic protection systems for pipelines in seawater using sacrificial anodes with the BEM has been performed by Yan et al. (1992). Their calculations show that the potential of a 60 cm diameter cathodically protected pipeline is dependent on the number, dimensions, and placement of sacrificial anodes. Complete protection of the pipeline was only achieved using two anodes located at 0° and 180° with respect to the circular cross section of the pipe. Placement of the sacrificial anodes 1 cm from the pipe resulted in overprotection of the pipe surface in the area closest to the anode and incomplete protection at locations furthest from the anodes. Optimum placement of the anodes was determined to be 14 cm from the pipeline.

Orazem et al. (1997a, b) used the BEM to model the current and potential distributions at holidays of fusion bonded epoxy coated buried pipelines protected with sacrificial anodes. Conventional anode resistance formulas are available for bare pipes protected by remote anodes. Since for uncoated pipes the current density on the anode is much larger than the current density on the pipe, resistance formulas that ignore the potential and current distributions on the pipes can be used. The distributions, however, must be determined for a coated pipe with holidays or when anodes are placed in close proximity to the pipes. The BEM model was used to evaluate a variety of cathodic protection designs using both Zn and Mg anodes. In general it was found that the potential of the pipe at a holiday was $-0.65\ V_{Cu/CuSO_4}$ when Zn anodes were used in soils with resistivity greater than 5,000 ohm-cm. The current density lines converged on at the location of the holiday. At the holiday the current density was at least 6 or 7 orders of magnitude greater than that of the coated section of pipe. As the resistivity of the soil increased, the current density decreased. Adding Mg anodes to the system with the Zn anodes retained did not improve the performance of the system since the Mg anodes cathodically protected both the pipe and the Zn anodes. With Mg anodes alone, the potential of the pipe at the holiday was maintained below $-0.850\ V_{Cu/CuSO_4}$. An interesting outcome of the modeling work was that the potential measured at ground level above a coating holiday did not reflect that a significant shift in potential had occurred where the pipe coating was perforated unless the soil resistivity was at least 100,000 ohm-cm. As a result, determination of coating failures with surface potential measurements was shown to be limited to pipes buried in high resistivity soils.

The cathodic protection of seawater tanks on ships has been modeled both with the FEM and the FDM (Munn and Devereux, 1991a, b). The tanks were constructed of Monel and HY80 steel and protected using sacrificial Zn anodes. The calculated distribution of potentials using both methods was similar to the measured distribution of potentials. Based on results of the analyses, the number of cathodes was reduced to prevent overprotection of the tank that resulted in the formation of calcareous deposits. Similar efforts have been used to model the cathodic protection of ship hulls with sacrificial anodes (Zamani, 1988) using the BEM. Measurements on a docked ship revealed that the potentials on the ship hull were in the range of -0.80 to -0.86 $V_{Ag/AgCl}$. The maximum error in the predicted potentials of ten locations along the length of the hull was 15 percent.

The galvanic corrosion of carbon steel welded to stainless steel (SS) in different electrolytes was investigated by Bardal et al. (1984). Using the BEM, the current density for both the corrosion of carbon steel and the reduction of oxygen on the SS surface was calculated as a function of distance from the weld

region. Experimental measurements were also performed using specimens composed of multiple sections of carbon and SS electrically insulated from each other. Each corresponding section of carbon steel and SS was connected to each other through a zero resistance ammeter. The geometry of this specimen allowed measurement of both potential and current density distributions. Again modeling calculations agreed well with the experimentally measured values. For the dissolution of carbon steel, the corrosion current density varied between 0.8 A/m^2 (0.94 mm/yr) near the weld to 0.1 A/m^2 (0.11 mm/yr), a distance of 20 cm from the weld with a 360 ohm cm electrolyte. Under flowing conditions current densities as high as 1.5 A/m^2 were observed. With static conditions and a more conductive electrolyte (resistivity = 22.5 ohm cm), the current density distribution was 0.7 to 0.3 A/m^2 over the same distance. The much more uniform current density across the carbon steel surface in the more conductive electrolyte is expected with a high electrolyte conductivity (Pryor and Astley, 1994). Because of the low solution resistance, R_{soln}, the potential drop through the electrolyte, IR_{soln}, is small. As a result, the area ratio of the anodic material to the cathodic material is equivalent to the geometrical surface area. As the conductivity of the electrolyte decreases, however, the ohmic drop through the electrolyte causes the effective area ratio to be substantially different than the geometric area. As a result, only the anodic and cathodic areas near the point of the galvanic contact are significant and the local current densities under these conditions can be quite high. Schematic illustrations of the current density distributions for a galvanic contact in low and high conductivity electrolytes are shown in figure 2-5.

Varela et al. (1997) conducted both experimental measurements and modeling calculations of the corrosion potential and corrosion current density of Type 304 SS and carbon steel galvanic couples in 3.5 percent NaCl with dissolved CO_2 at temperatures from 50 to 150 °C. Experimental measurements were conducted with sectioned specimens similar to those of Bardal et al. (1984).The calculated values of the corrosion potentials of the galvanic couple were found to agree well with the predicted values based on polarization curves. Modeling calculations showed the corrosion rates increased with temperature up to 100 °C. The maximum corrosion current density for carbon steel, obtained at 100 °C close to the contact with type 304 SS, was 6 A/m^2 compared to 1 A/m^2 at 50 °C. Above 100 °C, the corrosion rates decreased substantially. The authors concluded that the rate-determining step for the galvanic process is the cathodic reaction rate below 100 °C and the dissolution rate for iron above 100 °C.

In this report, galvanic corrosion potential calculations are not performed using the modeling methods discussed here. Instead, a simplified calculation method is used to determine the effects of galvanic coupling of the WP materials based on a bimetallic couple geometry created assuming failure of the outer CAM barrier by localized corrosion.

2.4 GALVANIC CORROSION POTENTIAL CALCULATIONS FOR HIGH-LEVEL WASTE CONTAINERS

Several key differences exist between the behavior of the WPs in a repository environment and the engineering applications where numerical modeling techniques have been successfully exercised to either evaluate cathodic protection systems using sacrificial anodes or model galvanic corrosion of metals in well characterized environments. For offshore engineering applications, such as ships, pipelines, and platforms, the environmental conditions are relatively constant. The successful use of cathodic protection schemes in these applications is the result of system designs specifically tailored to the characteristics of the environment as well as to monitoring and routine maintenance. Cathodic protection systems for underground pipelines are also tailored to the specific application. The anode material, size, placement, resistivity of the soil, and composition of the groundwater are all factors considered to optimize system performance.

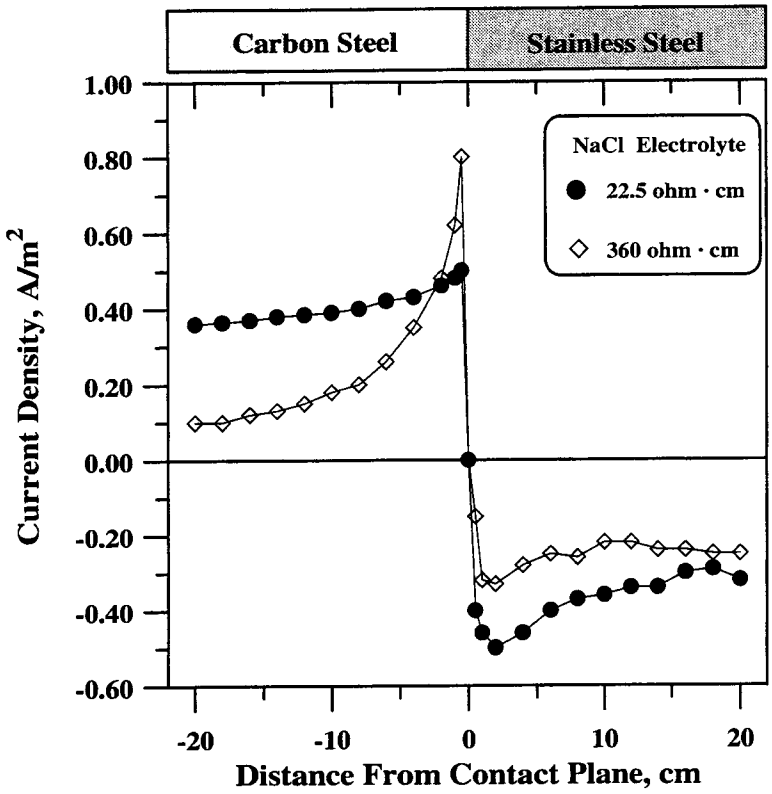

Figure 2-5. Galvanic current density distribution as a function of the distance from the contact plane for the galvanic coupling of carbon steel welded to stainless steel in NaCl solutions of different resistivities. Note the positive sign of the galvanic current associated with dissolution of carbon steel (Bardal et al., 1984)

In contrast, the outer barrier of the WP is not designed solely for the purpose of cathodic protection. As with all cathodic protection systems that use sacrificial anodes, the two container barriers should be in both electrolytic and electronic contact. That is, the electrolyte (groundwater) must be in contact with both the inner and outer barriers to provide an ionic path to the galvanic current. In addition, the inner and outer barriers must be electrically connected to each other through a low impedance contact which allows the flow of galvanic current by electronic conduction. A specific condition for the current WP design is the potential of the galvanic couple be maintained below the repassivation potential of the inner barrier material in the enclosed environment formed as a result of the penetration of the outer barrier.

There are several conceivable difficulties to any approach used to model the galvanic coupling behavior of the double barrier WP:

- In addition to the materials, the detailed design and methods of construction used for the WP will have a strong influence on the galvanic behavior.

- The chemistry of the electrolytic environment that will be present between the inner and outer barriers may undergo significant variations in time.

- If the outer barrier is perforated by localized corrosion such as pitting or crevice corrosion, then the environment present between the two materials is likely to be an acidic, concentrated chloride solution (Lou et al., 1992; Sugimoto and Asano, 1987; Suzuki et al., 1973; Alavi and Cottis, 1987). Additionally there will be a significant gradient in solution chemistry and conductivity.

- If the outer barrier fails by mechanical fracture, the environment contacting the container barriers can be expected to be groundwater modified by evaporation and refluxing effects.

- If good electronic contact is not assured through appropriate fabrication methods, the metallic contact between both metal barriers may be significantly degraded by exposure to the local environment after penetration of the outer barrier.

- Films of oxides or deposits of corrosion products on both metal barriers can introduce important kinetic and resistive effects that may have a major influence on the galvanic current flow (Pryor and Astley, 1994).

The last bullet item is important because it is known that metals covered with unreduceable oxides or corrosion products are far less efficient as cathodes when compared to noble metals. The oxygen reduction reaction on an oxide coated cathode is much more polarized than on a bare metal which in turn limits the flow of galvanic current. It may be possible that passivation of the A516 steel outer barrier will also limit the galvanic protection afforded to the inner corrosion resistant barrier by increasing the electronic contact resistance between the barriers and will significantly alter the anodic polarization behavior of the A516 steel. Electrical impedance of the corrosion products between the two barriers will depend on the electronic and physical properties of the products formed. For example, a dry, nonporous, high resistivity oxide layer will impede the flow of galvanic current much more than a solution saturated, porous, semiconductive corrosion product.

A final aspect to emphasize is that the uncertainties surrounding the chemical composition of the near-field environment are significant and also time dependent. As a result, the use of experimental studies to corroborate model calculations is necessary to overcome the difficulties noted previously in evaluating the degree of effective galvanic coupling between the container barriers through modeling and numerical calculations.

2.5 CALCULATION OF GALVANIC CORROSION POTENTIAL

Calculation of the galvanic corrosion potential was performed using *Mathematica* Version 2.2.3. Several simplifying assumptions were made as follows:

- The galvanic couple is a one-dimensional model of two parallel plates consisting of Alloy 825 and A516 steel.

- The current flow in the galvanic couple is perpendicular to the plates and hence the equipotential surfaces are parallel to the plates.

- The conductivity of the electrolyte was constant and does not contain any spacial variability related to concentration gradients.

- Corrosion potentials of the individual materials are calculated by summing the currents of all anodic and cathodic reactions to zero.

- The corrosion of A516 steel is described by the active dissolution of iron.

- The dissolution of Alloy 825 occurs at a rate determined by the passive current density.

- Oxygen and water reduction are the only cathodic reactions. Oxygen reduction is controlled by a combination of surface activation and transport controlled reactions whereas water reduction is controlled only by surface activation.

The groundwater contacting the containers may vary in pH as a result of many processes occurring in the repository near field. The interactions of the groundwater with concrete used in drift walls and inverts, as well as evaporative and refluxing effects associated with radioactive decay heat and rock fracture flow, may result in significant increases in pH (Mohanty et al., 1997). As discussed elsewhere (Sridhar et al., 1994; Mohanty et al., 1997) alkaline aqueous solutions (pH $\geq$ 9) confer passivity to carbon steels but the presence of chloride ions will result in localized corrosion of the A516 steel outer container barrier above a critical potential dependent on temperature and chloride concentration.

Previous investigations indicated that the alkaline, chloride-containing water expected to contact the WPs will induce failure of the A516 steel corrosion allowance material by localized corrosion. A schematic illustration of this scenario is shown in figure 2-6. The magnified schematic view of this through-wall pit in penetrating the outer barrier is shown in figure 2-7. While the pit is active, dissolution of iron, shown as Eq. (2-12), occurs at the bottom of the pit.

$$Fe \rightarrow Fe^{2+} + 2e^{-} \tag{2-12}$$

Hydrolysis of the Fe^{2+} species inside the pits occurs by the reaction shown in Eq. (2-13).

$$Fe^{2+} + H_2O \rightarrow FeOH^{+} + H^{+} \tag{2-13}$$

At the mouth of the pit, a membrane of Fe_3O_4 and FeOOH is formed that separates the bulk environment from the environment formed within the pit. The presence of dissolved oxygen at the pit mouth promotes the oxidation of $FeOH^{+}$ and Fe^{+} according to Eqs. (2-14) and (2-15).

$$2FeOH^{+} + \tfrac{1}{2}O_2 + 2H^{+} \Rightarrow 2FeOH^{2+} + H_2O \tag{2-14}$$

$$2Fe^{2+} + \tfrac{1}{2}O_2 + 2H^{+} \Rightarrow 2Fe^{3+} + H_2O \tag{2-15}$$

Both $FeOH^{2+}$ and Fe^{3+} are hydrolyzed according to Eqs. (2-16) and (2-17).

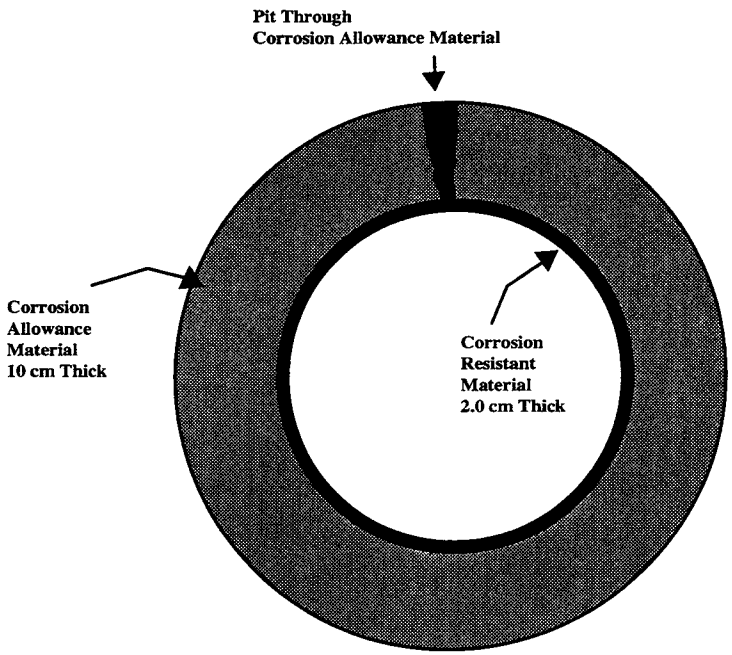

Figure 2-6. Schematic view of a through-wall pit penetrating the outer A516 steel overpack exposing the corrosion resistant inner overpack

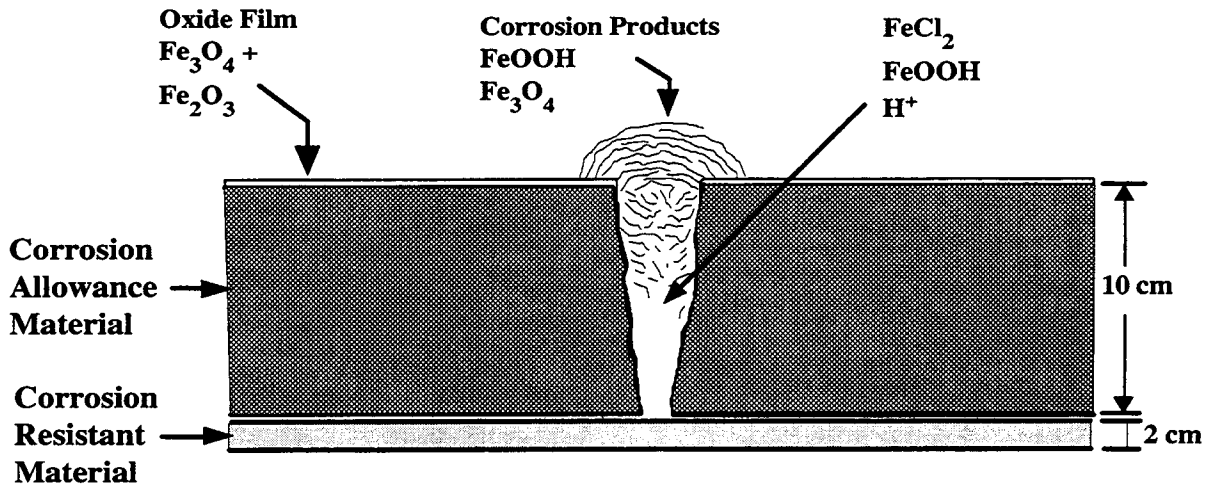

Figure 2-7. Schematic view of the pit penetrating the outer A516 steel overpack with the mouth covered by corrosion products and the passive oxide film over the surface of the outer overpack

$$FeOH^{2+} + H_2O \Rightarrow Fe(OH)_2^+ + H^+ \quad (2\text{-}16)$$

$$Fe^{3+} + H_2O + FeOH^{2+} + H^+ \quad (2\text{-}17)$$

Corrosion products of magnetite, Fe_3O_4, and red rust, FeOOH, precipitate at the mouth of the pit according to Eqs. (2-18) and (2-19).

$$2FeOH^{2+} + Fe^{2+} + 2H_2O \Rightarrow Fe_3O_4 + 6H^+ \quad (2\text{-}18)$$

$$Fe(OH)_2^+ + OH^- \Rightarrow FeOOH + H_2O \quad (2\text{-}19)$$

These corrosion products are porous and allow the transport of corrosion products out of the pit or the migration of Cl^- ions into the pit. Outside the pit, the surface is passivated and covered with an oxide containing Fe_3O_4 and Fe_2O_3. The reduction of oxygen occurs on the outside surface near the mouth of the pit. This reaction is shown as Eq. (2-20).

$$O_2 + 2H_2O + 4e^- \Rightarrow 4OH^- \quad (2\text{-}20)$$

Under acidic conditions, the reduction of hydrogen can occur as follows:

$$2H^+ + 2e^- \Rightarrow H_2 \quad (2\text{-}21)$$

The geometry of the galvanic couple between the inner Alloy 825 barrier and the outer A516 steel corrosion allowance material is modeled considering that the galvanic contact will occur at the base of a pit that propagates through the A516 steel barrier. A schematic illustration of the geometry is shown in figure 2-8 as a cut-away view of the perforated A516 steel barrier in contact with the Alloy 825 inner barrier. After the pit penetrates the A516 steel, the area ratios of Alloy 825 and A516 steel will depend on the relative areas of each material exposed to the electrolyte. For Alloy 825, this area is defined by the radius of the electrolyte puddle on the CRM surface, r_{CRM}. The anodic area of A516 steel is determined by both the radius of the pit, r_p, and the height of the pit above the Alloy 825 surface that is active, h_p. In these calculations, the r_p was assumed to be between 1 and 5 mm. The r_{CRM} varied between 5 and 50 mm. The h_p was assumed to be between 20 and 100 mm. With these limits, the area ratio of Alloy 825 to A516 steel will vary between 8:1 and 1:40.

The kinetics of both the metal dissolution along with the oxygen and water reduction reactions are used as the basis for calculating the galvanic corrosion potential of the multibarrier WP. Charge balance is maintained by summing all anodic and cathodic currents to zero. The general equation is

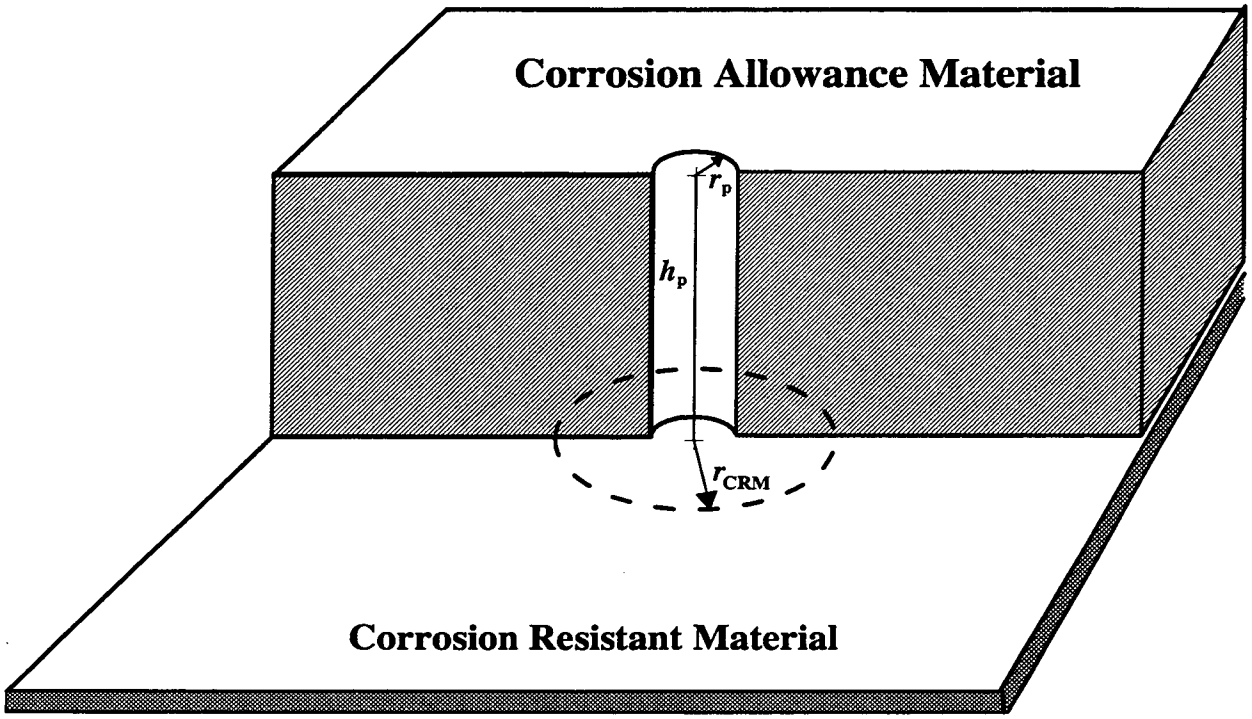

Figure 2-8. Schematic view of the pit geometry used for galvanic coupling modeling showing the surface areas of the steel overpack and the corrosion resistant material exposed to the pit electrolyte, assuming the existence of a narrow gap between both containers

$$\sum_{j=1}^{n} I_{a,j} - \sum_{j=1}^{n} I_{c,j} = \sum_{j=1}^{n} i_{a,j}^{a} A_{a,j} + \sum_{j=1}^{n} i_{a,j}^{c} A_{a,j} - \sum_{j=1}^{n} i_{c,j}^{a} A_{a,j} - \sum_{j=1}^{n} i_{c,j}^{a} A_{a,j} = 0 \quad (2\text{-}22)$$

where

$I_{a,j}$ — current from the j^{th} anodic reaction

$I_{c,j}$ — current from the j^{th} cathodic reaction

$i_{a,j}^{a}$ — current density of the j^{th} anodic reaction at the anode

$i_{a,j}^{c}$ — current density of the j^{th} anodic reaction at the cathode

$A_{a,j}$ — area of the anode for the j^{th} reaction

$i_{c,j}^{a}$ — current density of the j^{th} cathodic reaction at the anode

$i_{c,j}^{c}$ — current density of the j^{th} cathodic reaction at the cathode

$A_{c,j}$ — area of the cathode for the j^{th} reaction

In the present calculation, only the active area of the A516 steel is considered and the surface of Alloy 825 is passive. The areas of the anode and cathode are considered to be independent of the reaction. The reduction of water and oxygen are assumed to occur on both the Alloy 825 and the A516 steel surfaces. Under these assumptions, the expression in Eq. (2-22) reduces to

$$A^{\text{steel}}\, i_{\text{active}}^{\text{steel}} + A^{825}\, i_{\text{pass}}^{825} = \tag{2-23}$$

$$(A^{825}\, i_{H_2O}^{825} + A^{825}\, i_{O_2}^{825} + A^{\text{steel}}\, i_{H_2O}^{\text{steel}} + A^{\text{steel}}\, i_{O_2}^{\text{steel}})$$

where

A^{steel} — surface area of the A516 steel

A^{825} — surface area of Alloy 825

i_{pass}^{825} — anodic current density for the passive dissolution of Alloy 825

$i_{\text{active}}^{\text{steel}}$ — anodic current density for the active dissolution of A516 steel

$i_{H_2O}^{\text{steel}}$ — cathodic current density for the reduction of water on A516 steel

$i_{H_2O}^{825}$ — cathodic current density for the reduction of water on Alloy 825

$i_{O_2}^{\text{steel}}$ — cathodic current density for the reduction of oxygen on A516 steel

$i_{O_2}^{825}$ — cathodic current density for the reduction of oxygen on Alloy 825

2.5.1 A516 Carbon Steel

The current density for the active dissolution of A516 steel, $i_{\text{active}}^{\text{steel}}$, is described by the Tafel equation

$$i_{\text{active}}^{\text{steel}} = i_{0,Fe/Fe^{2+}}\left[\exp\left(\frac{\alpha_{Fe} z_{Fe} F\left(E - E_{Fe/Fe^{2+}}\right)}{RT}\right)\right] \tag{2-24}$$

where

$i_{0,Fe/Fe^{2+}}$ — exchange current density for the dissolution of iron

α_{Fe} — charge transfer coefficient for the dissolution of iron

z_{Fe} — number of electrons involved in the dissolution of iron

F — Faraday's constant

E — potential

$E_{Fe/Fe^{2+}}$ — equilibrium potential for the dissolution of iron

R — gas constant

T — temperature in K

The value of $i_{0,Fe/Fe^{2+}}$ has been reported by Heusler (1976) to be 10^{-10} A/m^2. Bockris et al. (1961) presented values in the range of 10^{-1} to 10^{-6} A/m^2 depending on the concentration of Fe^{2+}, pH, and the anionic species in solution. Conway (1952) noted values of 10^{-2} A/m^2 as being typical for the exchange current densities for the dissolution of iron and nickel. The z_{Fe} is assumed to be 2. The $E_{Fe/Fe^{2+}}$ is given by the Nernst equation

$$E_{Fe/Fe^{2+}}\ (V_{SHE}) = E^0_{Fe/Fe^{2+}} + 2.303\frac{RT}{zF}Log[Fe^{2+}] \qquad (2\text{-}25)$$

The cathodic current density for the reduction of oxygen on the surface of A516 steel, $i_{O_2}^{steel}$, is given by

$$i_{O_2}^{steel} = i_{0,O_2}^{steel}\frac{\exp\left(\frac{-\beta_{O_2} z_{O_2} F\left(E-E_{O_2}\right)}{RT}\right)}{\left[1+\left[\frac{i_{0,O_2}^{steel}\ \delta\ \exp\left(\frac{-\beta_{O_2} z_{O_2} F\left(E-E_{O_2}\right)}{RT}\right)}{4FD_{O_2}C_{O_2}^{bulk}}\right]\right]} \qquad (2\text{-}26)$$

where

i_{0,O_2}^{steel} — exchange current density for the reduction of oxygen on steel

β_{O_2} — charge transfer coefficient for the reduction of oxygen

z_{O_2} — number of electrons involved in the reduction of oxygen

E_{O_2} — equilibrium potential for the reduction of oxygen

δ — thickness of the diffusion layer

D_{O_2} — diffusion coefficient for oxygen

$C_{O_2}^{bulk}$ — concentration of dissolved oxygen in the bulk solution

It is important to note that δ is not the water film thickness but rather thickness of the diffusion layer over which a concentration gradient of oxygen exists. The value of δ for a stationary system is on the order of 5×10^{-4} m. This decreases with convection, and for a well agitated system δ can be as low as 5×10^{-5} m (Bockris and Reddy, 1977). E_{O_2} is calculated according to the Nernst equation as follows:

$$E_{O_2} = E^0_{O_2} - \frac{2.303\ R\ T\ pH}{F} + \frac{0.576\ R\ T\ Log[p_{O_2}]}{F} \quad (2\text{-}27)$$

where

$E^0_{O_2}$ — standard potential for the reduction of oxygen

p_{O_2} — partial pressure of oxygen

The temperature dependence for $E^0_{O_2}$ is based on data published by Macdonald et al. (1972).

$$E^0_{O_2} = (1.47172 - E^{op}_{O_2}) - 0.000815(T) \quad (2\text{-}28)$$

where

$E^{op}_{O_2}$ — overpotential of the oxygen reduction reaction on the metal surface

The D_{O_2} is calculated as a function of temperature according to

$$D_{O_2} = \frac{0.063 \exp\left(\frac{14.612}{0.001R}\left(\frac{1}{298.15} - \frac{1}{T}\right)\right)}{31536000} \quad (2\text{-}29)$$

and the $C^{bulk}_{O_2}$ is calculated using Eq. (2-30).

$$C^{bulk}_{O_2} = K_H\ p_{O_2} \quad (2\text{-}30)$$

where

K_H — Henry's law constant

The dependence of K_H on temperature is calculated according to Eq. (2-31).

$$K_H = 1000 \exp\left(0.2984 - \frac{5596.17}{T} + \frac{1049670}{T^2}\right) \quad (2\text{-}31)$$

The effect of salt concentration on oxygen solubility is ignored for these calculations. The exchange current density for the reduction of oxygen on A516 steel, i_{0,O_2}^{steel}, is calculated as follows:

$$i_{0,O_2}^{steel} = i_{0,O_2(298)}^{steel} \exp\left[\frac{\Delta H_{a,O_2}}{0.001R}\left(\frac{1}{298} - \frac{1}{T}\right)\right] \quad (2\text{-}32)$$

where

$i_{0,O_2,(298)}^{steel}$ — exchange current density for the reduction of oxygen on steel at 298 K

$\Delta H_{a,O_2}$ — activation enthalpy for the reduction of oxygen

From the work of Calvo and Schiffrin (1988) $i_{0,O_2,(298)}^{steel}$ measured on passivated iron is in the range of 1×10^{-6} A/m^2. Calvo (1979) reported the $\Delta H_{a,O_2}$ to be 40 kJ/mol.

The cathodic current density for the reduction of water on A516 steel is given by

$$i_{H_2O}^{steel} = i_{0,H_2O} \exp\left(\frac{-\beta_{H_2O} z_{H_2O} F \left(E - E_{H_2O}\right)}{RT}\right) \quad (2\text{-}33)$$

where

i_{0,H_2O} — exchange current density for the reduction of water

β_{H_2O} — charge transfer coefficient for the reduction of water

z_{H_2O} — number of electrons involved in the reduction of water

E_{H_2O} — equilibrium potential for the reduction of water

E_{H_2O} is calculated according to Eq. (2-34).

$$E_{H_2O} = E^0_{H_2O} - \left(\frac{2.303\ R\ T}{F}\ pH\right) \tag{2-34}$$

where

$E^0_{H_2O}$ — standard potential for the reduction of water

The exchange current density for water reduction at 298 K, $i_{0,H_2O,(298)}$, is calculated as a function of pH according to Eq. (2-35).

$$i_{0,H_2O,(298)} = 2\ F\ k_1\ [H^+]^{\beta_{H_2O}} \tag{2-35}$$

Where k_1 has been determined by Bockris and Reddy (1977) to be 5.18×10^{-8} mol m^{-2} s^{-1} and $i_{0,H_2O,(298)}$ is 10^{-2} A/m^2 at pH 0. The exchange current density at any temperature can than be calculated according to Eq. (2-36).

$$i_{0,H_2O} = i_{0,H_2O(298)}\ \exp\left[\frac{\Delta H_{a,H_2O}}{0.001R}\left(\frac{1}{298} - \frac{1}{T}\right)\right] \tag{2-36}$$

where

$\Delta H_{a,H_2O}$ — activation enthalpy for the reduction of water

By combining Eqs. (2-24), (2-26), and (2-33), the E^{steel}_{corr}, which is the potential, E, at which the sum of all the anodic and cathodic currents is equal to zero, can be obtained from Eq. (2-37).

$$i_{0,Fe/Fe^{2+}}\left[\exp\left(\frac{\alpha_{Fe} z_{Fe} F\left(E_{corr}^{steel}-E_{Fe/Fe^{2+}}\right)}{RT}\right)\right] =$$

$$i_{0,H_2O}\left[\exp\left(\frac{-\beta_{H_2O}\, z_{H_2O}\, F\left(E_{corr}^{steel}-E_{H_2O}\right)}{RT}\right)\right] +$$

$$i_{0,O_2}^{steel}\frac{\exp\left(\frac{-\beta_{O_2}\, z_{O_2} F\left(E_{corr}^{steel}-E_{O_2}\right)}{RT}\right)}{\left[1+\left[\frac{i_{0,O_2}^{steel}\,\delta\,\exp\left(\frac{-\beta_{O_2} z_{O_2} F\left(E_{corr}^{steel}-E_{O_2}\right)}{RT}\right)}{4FD_{O_2}C_{O_2}^{bulk}}\right]\right]} \qquad (2\text{-}37)$$

2.5.2 Alloy 825

For Alloy 825, the dissolution rate is assumed to be controlled by the passive current density, i_{pass}^{825}, which has been measured to be 10^{-3} A/m^2 (Dunn et al., 1995).

The cathodic current density for the reduction of oxygen, $i_{O_2}^{825}$, is given by

$$i_{O_2}^{825} = i_{0,O_2}^{825}\frac{\exp\left(\frac{-\beta_{O_2}\, z_{O_2} F\left(E-E_{O_2}\right)}{RT}\right)}{\left[1+\left[\frac{i_{0,O_2}^{825}\,\delta\,\exp\left(\frac{-\beta_{O_2} z_{O_2} F\left(E-E_{O_2}\right)}{RT}\right)}{4FD_{O_2}C_{O_2}^{bulk}}\right]\right]} \qquad (2\text{-}38)$$

where

i_{0,O_2}^{825} — exchange current density for the reduction of oxygen on Alloy 825

i_{0,O_2}^{825} is calculated according to

$$i_{0,O_2}^{825} = i_{0,O_2(298)}^{825} \exp\left[\frac{\Delta H_{a,O_2}}{0.001R}\left(\frac{1}{298} - \frac{1}{T}\right)\right] \tag{2-39}$$

The exchange current density for the reduction of oxygen on Alloy 825 at 298 K, $i_{0,O_2,(298)}^{825}$, is assumed to be similar to that for passivated iron at 298 K (Calvo, 1979) and is varied over the range of 10^{-8} to 10^{-6} A/m^2.

The cathodic current density for the reduction of water on Alloy 825, $i_{H_2O}^{825}$, is given by

$$i_{H_2O}^{825} = i_{0,H_2O} \exp\left(\frac{-\beta_{H_2O}\, z_{H_2O}\, F\left(E - E_{H_2O}\right)}{RT}\right) \tag{2-40}$$

Combining the Eqs. (2-38) and (2-40) and setting i_{pass}^{825} equal to the cathodic current density, the E_{corr}^{825} is the potential where the sum of all the anodic currents and all cathodic currents is equal to zero.

$$i_{pass}^{825} = i_{0,H_2O}^{825}\left[\exp\left(\frac{-\beta_{H_2O}\, z_{H_2O}\, F\left(E_{corr}^{825} - E_{H_2O}\right)}{RT}\right)\right] +$$

$$i_{0,O_2}^{825} \frac{\exp\left(\dfrac{-\beta_{O_2}\, z_{O_2} F\left(E_{corr}^{825} - E_{O_2}\right)}{RT}\right)}{\left[1 + \left[\dfrac{i_{0,O_2}^{825}\, \delta \exp\left(\dfrac{-\beta_{O_2} z_{O_2} F\left(E_{corr}^{825} - E_{O_2}\right)}{RT}\right)}{4FD_{O_2}C_{O_2}^{bulk}}\right]\right]} \tag{2-41}$$

2.5.3 Galvanic Coupling of Alloy 825 and A516 Steel

The corrosion potential of the galvanic couple between A516 steel and Alloy 825 can be calculated by summing the anodic dissolution reactions for A516 steel and Alloy 825 with the oxygen and water reduction reactions. The surface areas of the A516 steel and Alloy 825 must also be included. For

the case where Alloy 825 and A516 steel are in good metallic contact, E_{corr}^{825} is equal to E_{corr}^{steel}. Therefore, the potential of the perfect galvanic couple, E_{couple}, can be obtained from

$$A^{steel} \times i_{0,Fe/Fe^{2+}} \left[\exp\left(\frac{\alpha_{Fe} z_{Fe} F\left(E_{couple} - E_{Fe/Fe^{2+}}\right)}{RT} \right) \right] + A^{825} \times i_{pass}^{825} =$$

$$A^{steel} \times i_{0,H_2O} \left[\exp\left(\frac{-\beta_{H_2O} z_{H_2O} F\left(E_{couple} - E_{H_2O}\right)}{RT} \right) \right] +$$

$$A^{steel} \times i_{0,O_2}^{steel} \frac{\exp\left(\frac{-\beta_{O_2} z_{O_2} F\left(E_{couple} - E_{O_2}\right)}{RT} \right)}{\left[1 + \left[\frac{i_{0,O_2}^{steel} \delta \exp\left(\frac{-\beta_{O_2} z_{O_2} F\left(E_{couple} - E_{O_2}\right)}{RT} \right)}{4FD_{O_2} C_{O_2}^{bulk}} \right] \right]} +$$

$$A^{825} \times i_{0,H_2O} \left[\exp\left(\frac{-\beta_{H_2O} z_{H_2O} F\left(E_{couple} - E_{H_2O}\right)}{RT} \right) \right] + \qquad (2\text{-}42)$$

$$A^{825} \times i_{0,O_2}^{825} \frac{\exp\left(\frac{-\beta_{O_2} z_{O_2} F\left(E_{couple} - E_{O_2}\right)}{RT} \right)}{\left[1 + \left[\frac{i_{0,O_2}^{825} \delta \exp\left(\frac{-\beta_{O_2} z_{O_2} F\left(E_{couple} - E_{O_2}\right)}{RT} \right)}{4FD_{O_2} C_{O_2}^{bulk}} \right] \right]}$$

It is important to note that Eq. (2-42) is only valid when the electronic and the electrolytic contact are ideal. As a result of the resistance of the electrolyte, an IR_{soln} drop will be present between the two materials. The magnitude of the IR_{soln} drop is dependent on the conductivity of the corrosive electrolyte in the distance between the galvanic couple. In addition, the resistance of the electronic contact between the materials must also be considered. Low resistance contacts are required for cathodic protection systems using sacrificial anodes. If the resistance is high, then the galvanic coupling efficiency, η, is reduced and cathodic protection may not be obtained. For the WP, η will be determined by the resistance of both the oxide scales and corrosion products as well as the conductivity of the electrolyte between the A516 steel and Alloy 825 barriers. The relationship between the corrosion potential of the imperfectly coupled Alloy 825 WP, $E_{corr}^{825,WP}$, and η has been assumed (Mohanty et al., 1997) to be

$$E_{corr}^{825,WP} = (1 - \eta)\, E_{corr}^{825} + (\eta\, E_{couple}) \tag{2-43}$$

The value of η may vary from 0 to 1 corresponding to no galvanic coupling and perfect galvanic coupling.

The corrosion potential of the A516 steel WP in contact with the Alloy 825 inner container material will also depend on η. The corrosion current density, $i_{corr}^{steel,WP}$, of the A516 steel WP is calculated based on the corrosion potential of the A516 steel WP, $E_{corr}^{steel,WP}$, according to Eq. (2-44).

$$i_{corr}^{steel,WP} = i_{0,Fe/Fe^{2+}} \exp\left[\frac{\alpha_{Fe}\, z_{Fe}\, F\, (E_{corr}^{steel,WP} - E_{Fe/Fe^{2+}})}{RT}\right] \tag{2-44}$$

Similarly, the cathodic current for the reduction of oxygen at the A516 steel WP surface is given by

$$i_{O_2}^{steel,WP} = i_{0,O_2}^{steel} \frac{\exp\left[\dfrac{-\beta_{O_2}\, z_{O_2} F \left(E_{corr}^{steel,WP} - E_{O_2}\right)}{RT}\right]}{\left[1 + \left[\dfrac{i_{0,O_2}^{steel}\, \delta\, \exp\left(\dfrac{-\beta_{O_2} z_{O_2} F \left(E_{corr}^{steel,WP} - E_{O_2}\right)}{RT}\right)}{4FD_{O_2} C_{O_2}^{bulk}}\right]\right]} \tag{2-45}$$

The cathodic current density for the reduction of water on the A516 steel WP surface, $i_{H_2O}^{steel,WP}$, is given by Eq.(2-46).

$$i_{H_2O}^{steel,WP} = i_{0,H_2O} \exp\left(\frac{-\beta_{H_2O}\, z_{H_2O}\, F\left(E_{corr}^{steel,WP} - E_{H_2O}\right)}{RT}\right) \tag{2-46}$$

The value of $E_{corr}^{steel,WP}$ is determined by solving Eq. (2-47).

$$\begin{aligned}
&A^{steel} \times i_{0,Fe/Fe^{2+}}\left[\exp\left(\frac{\alpha_{Fe} z_{Fe} F\left(E_{corr}^{steel,WP} - E_{Fe/Fe^{2+}}\right)}{RT}\right)\right] + A^{825} \times i_{pass}^{825} = \\
&A^{steel} \times i_{0,H_2O}\left[\exp\left(\frac{-\beta_{H_2O}\, z_{H_2O}\, F\left(E_{corr}^{steel,WP} - E_{H_2O}\right)}{RT}\right)\right] + \\
&A^{steel} \times i_{0,O_2}^{steel} \frac{\exp\left(\frac{-\beta_{O_2}\, z_{O_2} F\left(E_{corr}^{steel,WP} - E_{O_2}\right)}{RT}\right)}{\left[1 + \left[\frac{i_{0,O_2}^{steel}\, \delta\, \exp\left(\frac{-\beta_{O_2} z_{O_2} F\left(E_{corr}^{steel,WP} - E_{O_2}\right)}{RT}\right)}{4FD_{O_2} C_{O_2}^{bulk}}\right]\right]} + \\
&A^{825} \times i_{0,H_2O}\left[\exp\left(\frac{-\beta_{H_2O}\, z_{H_2O}\, F\left(E_{corr}^{825,WP} - E_{H_2O}\right)}{RT}\right)\right] + \\
&A^{825} \times i_{0,O_2}^{825} \frac{\exp\left(\frac{-\beta_{O_2}\, z_{O_2} F\left(E_{corr}^{825,WP} - E_{O_2}\right)}{RT}\right)}{\left[1 + \left[\frac{i_{0,O_2}^{825}\, \delta\, \exp\left(\frac{-\beta_{O_2} z_{O_2} F\left(E_{corr}^{825,WP} - E_{O_2}\right)}{RT}\right)}{4FD_{O_2} C_{O_2}^{bulk}}\right]\right]}
\end{aligned} \tag{2-47}$$

The resistance of the galvanic couple between the Alloy 825 surface and the A516 steel material, R_{couple}, is calculated by dividing the potential difference between the materials by the absolute value of the cathodic current as follows:

$$R_{couple} = \left| \frac{E_{corr}^{825,WP} - E_{corr}^{steel,WP}}{\sum_{j=1}^{n} i_{c,j} A_{c,j}} \right| \quad (2\text{-}48)$$

Hence, if R_{couple} is known either from measurement or independent calculation, simultaneously solving Eqs. (2-47) and (2-48) would yield values of $E_{corr}^{825,WP}$ and $E_{corr}^{steel,WP}$. Additionally, the potential of the perfect galvanic couple can be obtained from Eq. (2-42). Finally, these values can then be used to calculate η from Eq. (2-43). Since the values of R_{couple} are not well known at present, however, the relationship between η and various parameters, including R_{couple}, is explored in subsequent chapters.

In summary, the galvanic corrosion potentials of the WP materials are calculated using a combination of equations that describes the electrochemical kinetics of the anodic oxidation and cathodic reduction reactions. The geometry of the galvanic couple is defined by a pit penetrating through the outer A516 steel container and exposing the inner Alloy 825 barrier to the aqueous environment. Corrosion of the barrier metals is considered as the single anodic oxidation reaction, whereas cathodic reduction reactions are limited to the reduction of O_2 and H_2O. Corrosion of A516 steel is described by active dissolution in an acidified solution, taking into consideration the conditions existing in a pit once the outer container is breached. Passive dissolution is postulated to describe the behavior of Alloy 825 prior to the occurrence of localized corrosion.

In the first step of the calculations, the diffusion coefficient of O_2 and the bulk concentration of O_2 are determined using Eqs. (2-29) and (2-30). The equilibrium potential for the reduction of O_2 is then determined using Eqs. (2-27) and (2-28), whereas the equilibrium potential for the reduction of H_2O is computed using Eq. (2-34). Then, the equilibrium potential for the anodic oxidation of iron is determined from Eq. (2-25). After the equilibrium potentials are defined for a given set of environmental and electrochemical parameters, the corrosion potentials for A516 steel and Alloy 825 are computed independently of each other by solving for the potential at which the anodic current from the metal dissolution reactions is equal in magnitude to the total current from the cathodic reduction reactions. The corrosion potential of A516 steel is obtained by solving Eq. (2-37) for E_{corr}^{steel}. Similarly, the corrosion potential of Alloy 825, E_{corr}^{825}, is computed using Eq. (2-41). The corrosion potentials of the metals and

the equations describing the electrochemical kinetics of the anodic dissolution and cathodic reduction reactions are then used to calculate the galvanic corrosion potentials of the container materials. The galvanic corrosion potential of a perfect galvanic couple between Alloy 825 and A516 steel, E_{couple}, is calculated using Eq. (2-42). The galvanic corrosion potential of the Alloy 825 WP, $E_{corr}^{825,WP}$, is obtained based on the assumed relationship (Mohanty et al., 1997) in which E_{corr}^{825} and E_{couple} are combined through the use of the galvanic coupling efficiency, η, according to Eq. (2-43). The efficiency of the galvanic couple is varied from 0.0, corresponding to the total absence of galvanic interactions between the materials, to 1.0 corresponding to perfect galvanic coupling. The value of $E_{corr}^{825,WP}$ from Eq. (2-43) is then used as an input into Eq. (2-47) to compute the galvanic corrosion potential of the A516 steel WP, $E_{corr}^{steel,WP}$. Finally, the resistance of the galvanic couple, R_{couple}, is calculated by dividing the difference between the galvanic corrosion potentials of the WP barriers by the galvanic corrosion current according to Eq. (2-48).

3 RESULTS

3.1 CORROSION POTENTIALS OF THE UNCOUPLED WASTE PACKAGE MATERIALS

Both E_{corr}^{steel} and E_{corr}^{825} are determined from the potential dependent kinetics of the metal dissolution and the reduction reactions for O_2 and H_2O. As discussed in section 2.5, E_{corr} corresponds to the potential at which the sum of the anodic current balances the total cathodic current. Figure 3-1 shows the calculated kinetics of the O_2 and H_2O reactions superimposed on the Fe dissolution reaction at a temperature of 368 K (95 °C) in a potential versus logarithm of current plot. The curve for the reduction of O_2, calculated using Eq. (2-26), has both an activation controlled region, where the potential is linearly dependent on the logarithm of the reduction reaction current, and a diffusion limited current region, where the current is independent of potential. In the diffusion limiting region, the kinetics of the reaction are controlled by the diffusion of oxygen to the metal surface. The current for the reduction of H_2O, calculated with Eq. (2-33), only exhibits the activation controlled region. The sum of the current for the two cathodic reactions is also shown in figure 3-1. Since A516 steel is predominantly Fe, the dissolution kinetics of this metal are used to describe the anodic behavior of the steel. In addition, dissolution of the steel at the bottom of a propagating pit can be considered as active dissolution in an acidified solution (Galvele, 1978). In a detailed review, Turnbull (1983) reported that the minimum pH value in a localized corrosion cavity for Fe, in the absence of Fe^{3+} ions, varies from 3.8 at potentials ≈ -0.33 V_{SHE} to 6.6 at potentials ≈ -0.46 V_{SHE}. Therefore, a pH of 5.0 was selected for the baseline calculations. Under such conditions, the active dissolution of the A516 steel is under activation control and is calculated using Eq. (2-24) with a Tafel slope of 40 mV/decade (De Waard and Milliams, 1975; Ogundele and White, 1986).

In fully deaerated solutions the E_{corr}^{steel} is determined by the intersection of the A516 steel anodic dissolution and the H_2O cathodic reduction curves, shown as $E_{corr(1)}$ (−0.510 V_{SHE}) in figure 3-1. For air saturated solutions the E_{corr}^{steel} is determined by the intersection of the A516 steel dissolution curve with the total cathodic current (O_2 + H_2O) reduction curve. When a dilute solution is in equilibrium with air (p_{O_2} = 0.21 atm), the total dissolved oxygen concentration at 368 K (95 °C) is approximately 5.2 mg/L (5.2 ppm) and the E_{corr}^{steel} is -0.450 V_{SHE} as indicated in figure 3-1 by $E_{corr(2)}$. Since the dissolution rate of the A516 steel is potential dependent, the I_{corr} in a deaerated solution is approximately 3.0×10^{-2} A for a surface area of 1 m^2 and is shown in figure 3-1 as $I_{corr(1)}$. The I_{corr} increases more than ten times to 0.77 A when the solution is air saturated, as indicated by $I_{corr(2)}$.

For Alloy 825 the dissolution kinetics are governed by the passive current density independent of potential. The E_{corr}^{825} in a completely deaerated solution is defined by the intersection of the anodic passive dissolution and the H_2O reduction curves. This point, labeled $E_{corr,(1)}$ on figure 3-2, is equal to −0.310 V_{SHE}. When the solution is in equilibrium with air (p_{O_2} = 0.21 atm) the E_{corr}^{825}, as indicated by $E_{corr(2)}$, increases to 0.66 V_{SHE}. At intermediate levels of deaeration, the E_{corr}^{825} lies between the air saturated and deaerated values shown in figure 3-2. Since Alloy 825 is passive, the dissolution rate, shown

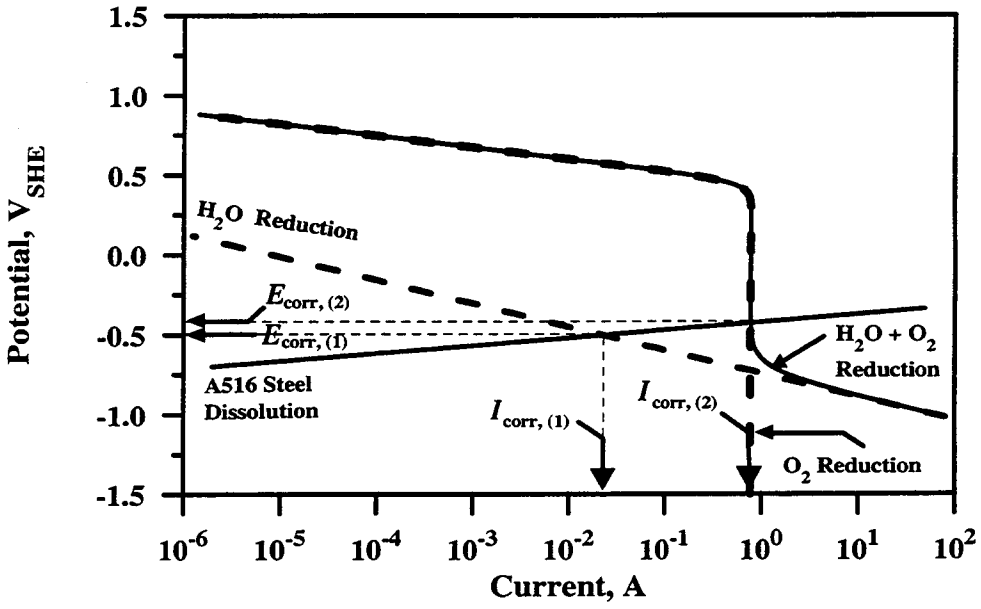

Figure 3-1. Evans diagram showing the calculated cathodic currents for the reduction of O_2 and H_2O, total cathodic current, and anodic current for the active dissolution of A516 steel as a function of potential in a solution of pH 5 at 368 K. Corrosion potentials and corrosion currents are indicated for two conditions: 1 deaerated solution; and 2 air saturated solution.

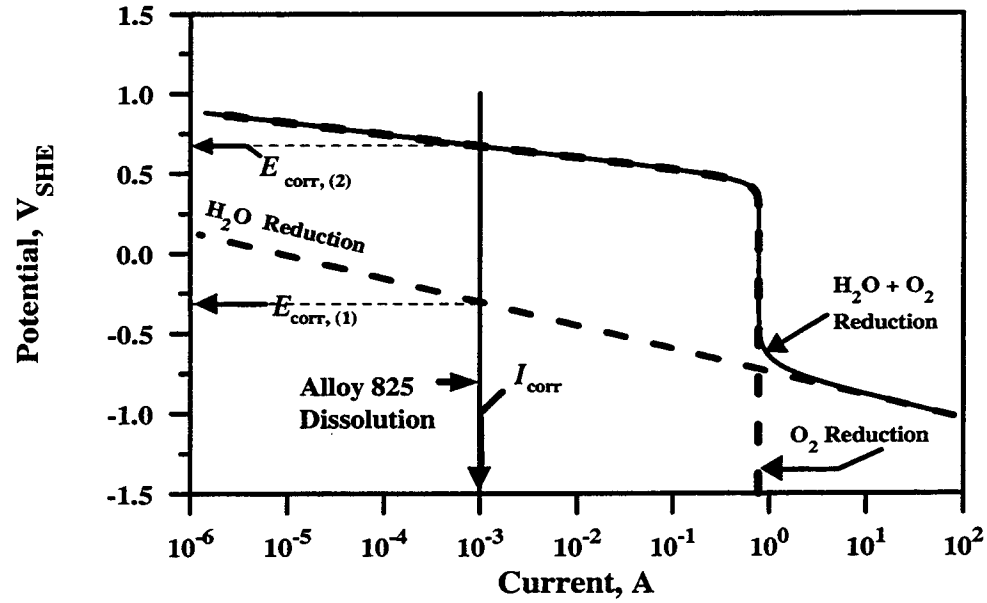

Figure 3-2. Evans diagram showing the calculated cathodic currents for the reduction of O_2 and H_2O, total cathodic current, and anodic current for the passive dissolution of Alloy 825 as a function of potential in a solution of pH 5 at 368 K. Corrosion potentials are indicated for two conditions: 1 deaerated solution; and 2 air saturated solution.

as I_{corr}, is equal to the passive current density remaining at 1.0×10^{-3} A for a surface area of 1 m^2 for both air saturated and deaerated solutions. If the environment contains deleterious species such as chlorides, Alloy 825 will not exhibit passive current density at all potentials, but will initiate localized active dissolution (localized corrosion) above a critical potential associated with the breakdown of passivity.

3.2 CALCULATION OF GALVANIC CORROSION POTENTIALS

A number of environmental and electrochemical parameters are used to calculate the galvanic corrosion potential of an A516 steel/Alloy 825 couple. The relevant environmental parameters considered in this analysis are temperature, pH, and p_{O_2}. In addition, thickness of the diffusion layer, δ, is also an environment-related parameter because it depends on the hydrodynamics of the metal/solution system. The influence of the values assigned to some of the relevant electrochemical kinetics parameters included in Eqs. (2-24), (2-26), and (2-38), such as $i_{0,Fe/Fe^{2+}}$, i_{pass}^{825}, i_{0,O_2}, α_{Fe}, and β_{O_2}, are discussed in some detail in the appendix. In addition to the environmental and electrochemical related parameters, the effects of the area ratio between Alloy 825 and A516 steel and the characteristics of the galvanic coupling on the galvanic corrosion potentials deserve a separate evaluation. As discussed in chapter 2, if both metals are perfectly coupled ($\eta = 1$), such that there is no resistive voltage drop between the WP materials, then $E_{corr}^{825,WP}$ and $E_{corr}^{steel,WP}$ are equivalent and equal to the galvanic corrosion potential, E_{couple}. If the galvanic couple is not perfect ($0 \leq \eta \leq 1$), however, a voltage drop resulting from several electrical impedances in series is present between the metal barriers and, as a result, $E_{corr}^{steel,WP}$ will not equal to $E_{corr}^{825,WP}$. These resistances may be caused by surface oxides, formed or deposited on the metal surfaces affecting the transfer of electrons required by the cathodic reduction reactions. In addition, the resistance of the solution associated with ion migration, can affect ionic conduction.

In this study, it was of interest to compare the effect of these parameters on both the E_{corr} of the WP materials without galvanic coupling, as well as on the E_{couple} of the bimetallic couple. The kinetics of the anodic dissolution and cathodic reduction reactions for Alloy 825 and A516 steel were calculated using a range of values for each parameter. In addition, the effects of these parameters on both the $E_{corr}^{825,WP}$ and the $E_{corr}^{steel,WP}$ were calculated as a function of η.

Evans diagrams, similar to those presented in figures 3-1 and 3-2, are used in this report to show the effect of the environmental parameters on the corrosion potentials of the container materials. In these diagrams, the anodic dissolution and the cathodic reduction kinetics for both A516 steel and Alloy 825 are shown on the same graph. Although the effects of the environmental parameters are shown on the same figure, the anodic dissolution kinetics for each material are determined separately without galvanic interaction. The reduction kinetics of both O_2 and H_2O are assumed to have the same electrochemical parameters on both the A516 steel and Alloy 825. Therefore, the kinetics of the reduction reactions plotted in these figures are valid for either Alloy 825 or A516 steel. The E_{corr} of both alloys is determined as described previously for figures 3-1 and 3-2.

A second type of plot is used to present the results of the E_{couple} computations. In these representations, the $E_{corr}^{825,WP}$ is calculated as a function of η using Eq. (2-43) after calculating E_{corr}^{825} from

Eq. (2-41) and E_{couple} from Eq. (2-42). The value of $E_{corr}^{steel,WP}$ is then calculated using Eq. (2-47). As previously indicated, when $\eta = 0$, $E_{corr}^{825,WP} = E_{corr}^{825}$ and $E_{corr}^{steel,WP} = E_{corr}^{steel}$. Likewise, when $\eta = 1$, $E_{corr}^{825,WP} = E_{corr}^{steel,WP}$. The E_{rp} for Alloy 825 measured in a 1,000 ppm Cl^- solution at 95 °C (Sridhar et al., 1995; Dunn et al., 1997) is also included in the plots to indicate at what values of η localized corrosion can be initiated. As discussed previously (Mohanty et al., 1997), Alloy 825 is susceptible to localized corrosion when $E_{corr}^{825,WP} > E_{rp}$ and the lifetime of the container is determined by the localized corrosion propagation rate. On the contrary, Alloy 825 is considered to be immune to localized attack when $E_{corr}^{825,WP} < E_{rp}$ and the lifetime of the container is determined by the passive current density of the material. In addition to the galvanic corrosion potentials, the resistance of the galvanic couple, R_{couple}, calculated using Eq. (2-48), is also shown in complementary plots as a function of η.

3.3 ENVIRONMENTAL PARAMETERS

3.3.1 Temperature

Raising the temperature from 273 to 368 K (0 to 95 °C) increases the kinetics of both the iron dissolution and the O_2 and H_2O reduction reactions. The dissolved oxygen concentration is reduced and hence, the electrode potential for the reduction of oxygen decreases. As shown in figure 3-3, a slight increase in the E_{corr}^{steel} is observed as the temperature rises due to both the change in the dissolution kinetics of iron and an escalation in the diffusion limited current for oxygen reduction. In contrast, the E_{corr}^{825} is inversely dependent on temperature as a result of the reduction in the dissolved oxygen concentration. These two opposite effects produce an increase of $E_{corr}^{steel,WP} = E_{corr}^{825,WP}$ of less than 100 mV when $\eta = 1$ (figure 3-4a). In figure 3-4a, $E_{corr}^{825,WP}$ and $E_{corr}^{steel,WP}$ are plotted as a function of η. As shown in this plot, the $E_{corr}^{825,WP}$ is a linear function of η. The linear dependence of $E_{corr}^{825,WP}$ on η is a result of the relationship assumed in Eq. (2-43). Also plotted in figure 3-4a is the E_{rp} of Alloy 825 obtained in a 1,000 ppm chloride solution at 368 K. Under these conditions the E_{rp} is in the range of 0.24 to 0.34 V_{SHE}. Values of E_{rp} are shown covering about 100 mV to indicate the dispersion found experimentally in the measurement of this parameter (Dunn et al., 1997). The active behavior of A516 steel is observed to dramatically reduce $E_{corr}^{825,WP}$ below E_{rp} for all values of η >0.3. The most significant result occurring in the temperature range of interest, as illustrated in figure 3-4a, arises from the decrease in the E_{rp}, from 0.50 ± 0.05 V_{SHE} to 0.29 ± 0.05 V_{SHE}, as the temperature increases from 273 to 368 K (Sridhar et al., 1995; Dunn et al., 1997). By comparing the plots of $E_{corr}^{825,WP}$ and the E_{rp} shown in figure 3-4a, it is evident that the propensity for localized corrosion of the Alloy 825 waste container decreases by lowering the temperature, therefore requiring a far less efficient galvanic coupling to avoid the occurrence of localized corrosion.

In figure 3-4b, the value of η is plotted as a function of R_{couple}. It may be observed from this figure that for low values of R_{couple}, η is close to 1.0 indicating a highly efficient galvanic couple.

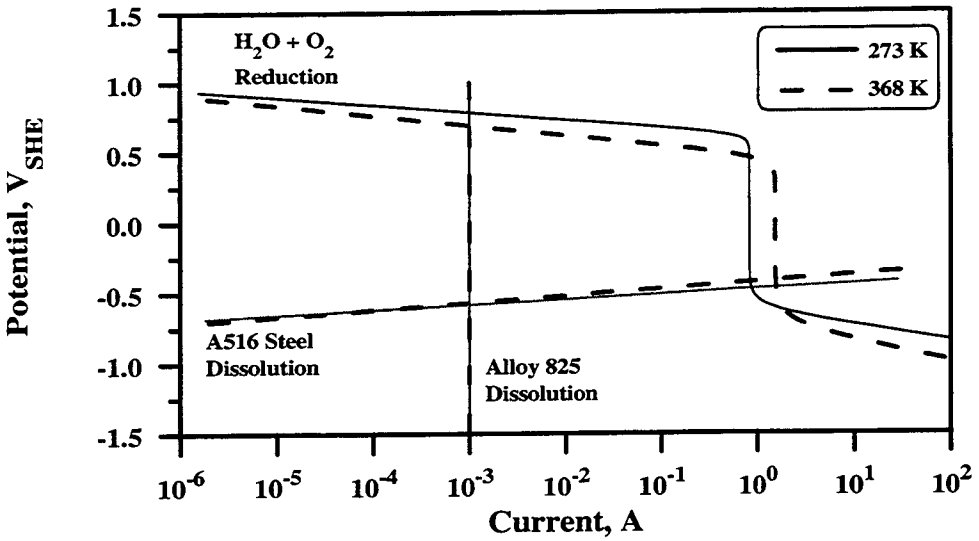

Figure 3-3. Evans diagram showing the effect of temperature (273 and 368 K) on the calculated total cathodic current for the reduction of O_2 and H_2O, and anodic currents for the passive dissolution of Alloy 825 and the active dissolution of A516 steel as a function of potential in an air saturated solution of pH 5

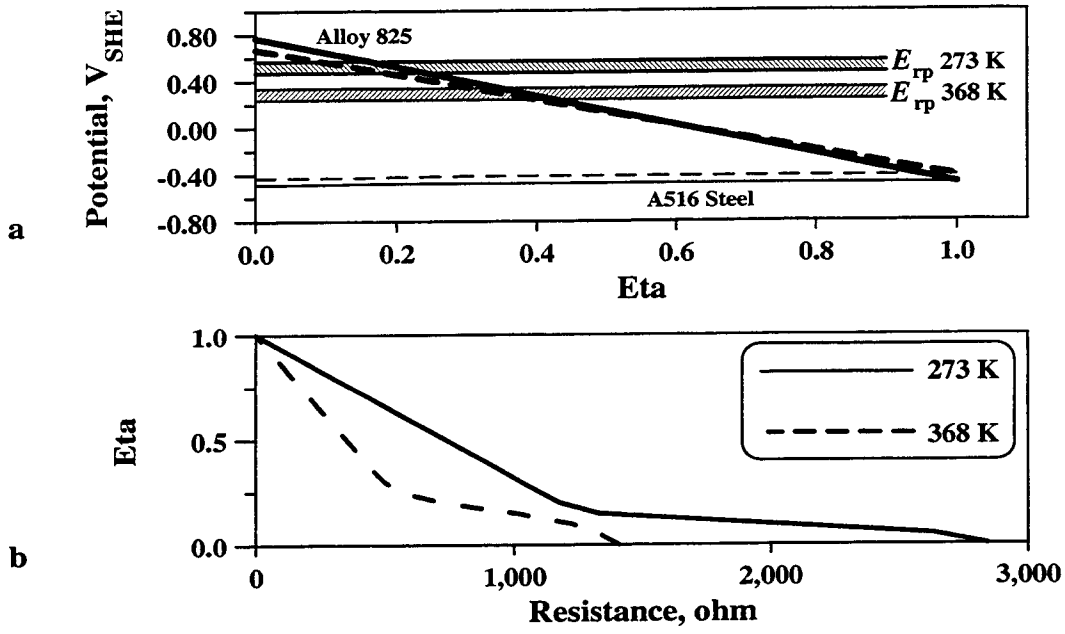

Figure 3-4. (a) Plot of the calculated galvanic corrosion potentials of Alloy 825 and A516 steel as a function of the efficiency, η, of the galvanic coupling at two temperatures (273 and 368 K). Values of the repassivation potential of Alloy 825 in solutions containing 1,000 ppm chloride at 273 and 368 K are included. (b) Value of η as a function of the resistance of the galvanic couple showing the effect of temperature (273 and 368 K).

Figure 3-4b, as well as similar figures presented in later sections of this chapter, can be used to estimate the value of η provided that R_{couple} is known. For the two cases plotted in this figure, it is apparent that at higher temperatures a much lower R_{couple} is needed to produce an efficient galvanic couple that may avoid the initiation of localized corrosion. This is primarily the result of the increased kinetics of both the O_2 and H_2O reduction reactions as the temperature is elevated. Using both figures 3-4a and 3-4b, it can be concluded that R_{couple} of 400 ohms is needed to reduce η below 0.4 at a temperature of 368 K, and thus initiate localized corrosion of Alloy 825.

3.3.2 pH

After localized corrosion in the form of pitting has penetrated through the outer barrier, the pH of the solution contacting both the Alloy 825 and the A516 barriers is expected to be about 5 or lower due to the hydrolysis of Fe^{2+} cations, as discussed previously. In figure 3-5, the effect of pH on the E_{corr}^{825} and the E_{corr}^{steel} is shown at pH values of 3 and 7. No significant change in the E_{corr}^{steel} is observed. For simplicity, in the calculations provided in figure 3-5, it is assumed the dissolution of A516 steel is independent of pH within the 3 to 7 pH range. Figure 3-5, indicates the main effect of decreasing the pH from 7 to 3 is an increase in the E_{corr}^{825}. The effect of pH on the variation of $E_{corr}^{825,WP}$ and $E_{corr}^{steel,WP}$ with η is given in figure 3-6a. At low pH values, the E_{corr} of the WP materials is controlled by the reduction of H^+ ions. At near neutral pH, the reduction of O_2 is the most significant cathodic reduction reaction for both materials. By comparing $E_{corr}^{825,WP}$ to the E_{rp}, it is apparent in figure 3-6a that a decrease of the pH from 7 to 3 does not alter significantly the value of η required to avoid the occurrence of localized attack of Alloy 825. From figure 3-6b, it is apparent that the pH of the bulk solution over the range of 3 to 7 has little influence on the magnitude of R_{couple} necessary to obtain a given value of η. It should be noted however, that at pH 3, localized corrosion of Alloy 825 is possible for $\eta<0.5$, which in turn corresponds to a R_{couple} of 300 ohms. Localized corrosion of Alloy 825 may only occur if $\eta<0.3$ at pH 7, which is the case of R_{couple} approximately equal to 450 ohms.

3.3.3 Partial Pressure of Oxygen

The effect of p_{O_2} on the E_{corr} of both materials is shown in figure 3-7. The E_{corr}^{825} is much higher than E_{corr}^{steel} when the solution is in equilibrium with air (p_{O_2} = 0.21 atm). When the p_{O_2} is reduced to 2.1×10^{-5} atm, which represents a well deaerated condition, the primary reduction reaction is switched from the reduction of O_2 to the reduction of H_2O. This deaeration reduces the E_{corr}^{825} by almost 1.0 V and also reduces both the E_{corr}^{steel} and the I_{corr}^{steel}. In the case of a completely deaerated environment ($p_{O_2} \rightarrow 0$ atm), the E_{corr} of both WP materials is only determined by the kinetics of the metal dissolution and H_2O reduction reaction. Figure 3-8a presents the effect of the p_{O_2} on the galvanic corrosion potentials of the WP materials. Decreasing the p_{O_2} reduces the diffusion limited current for the reduction of O_2 resulting in a lowering of the galvanic corrosion potentials. As indicated in this figure, when the p_{O_2} is

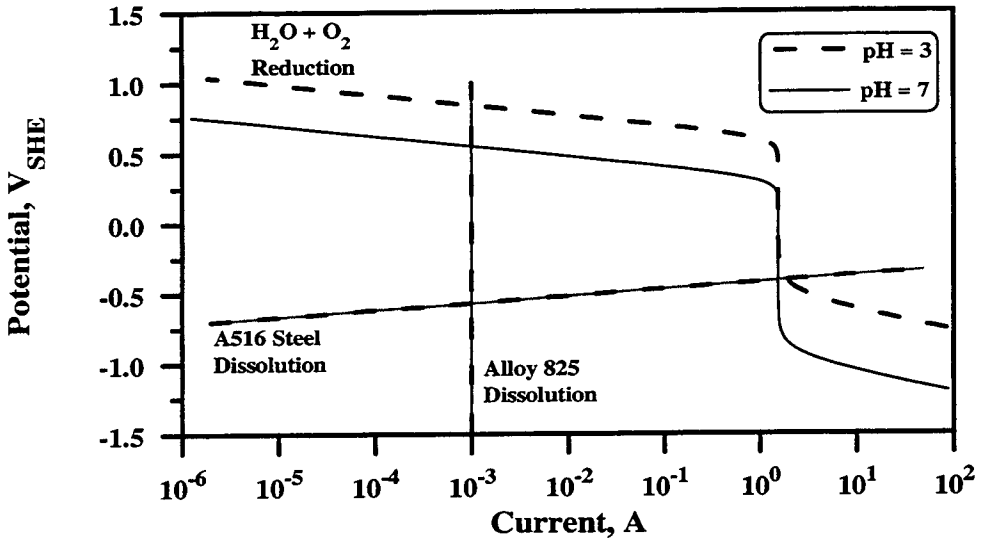

Figure 3-5. Evans diagram showing the effect of pH (3 and 7) on the calculated total cathodic current for the reduction of O_2 and H_2O, and anodic currents for the passive dissolution of Alloy 825 and the active dissolution of A516 steel as a function of potential in an air saturated solution at 368 K

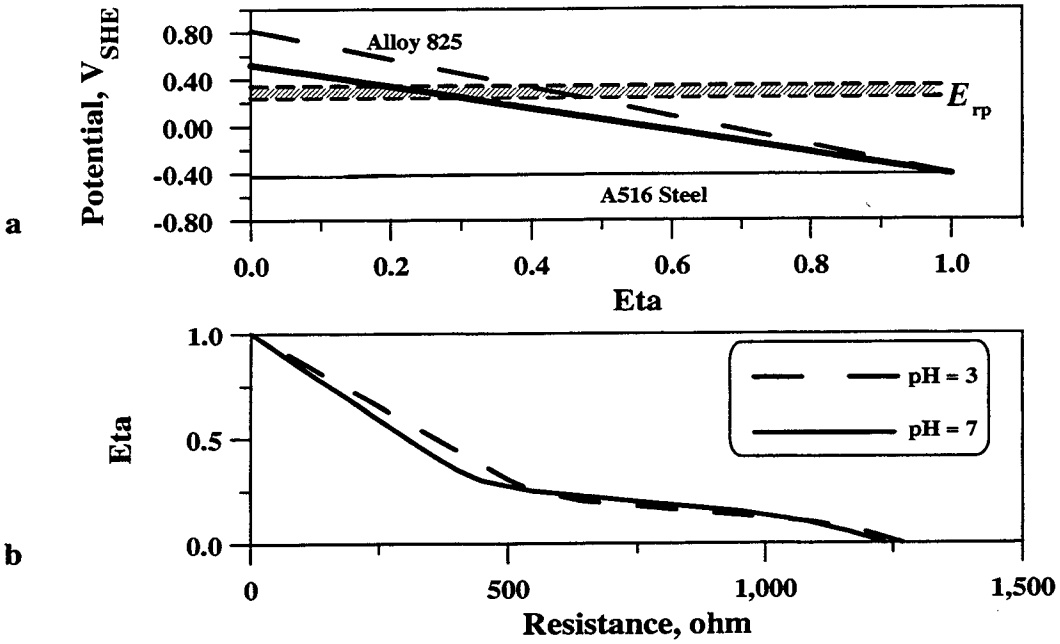

Figure 3-6. (a) Plot of the calculated galvanic corrosion potentials of Alloy 825 and A516 steel as a function of the efficiency, η, of the galvanic coupling at two pH values (3 and 7). The value of the repassivation potential of Alloy 825 in a solution containing 1,000 ppm chloride at 368 K is included. (b) Value of η as a function of the resistance of the galvanic couple for two pH values (3 and 7).

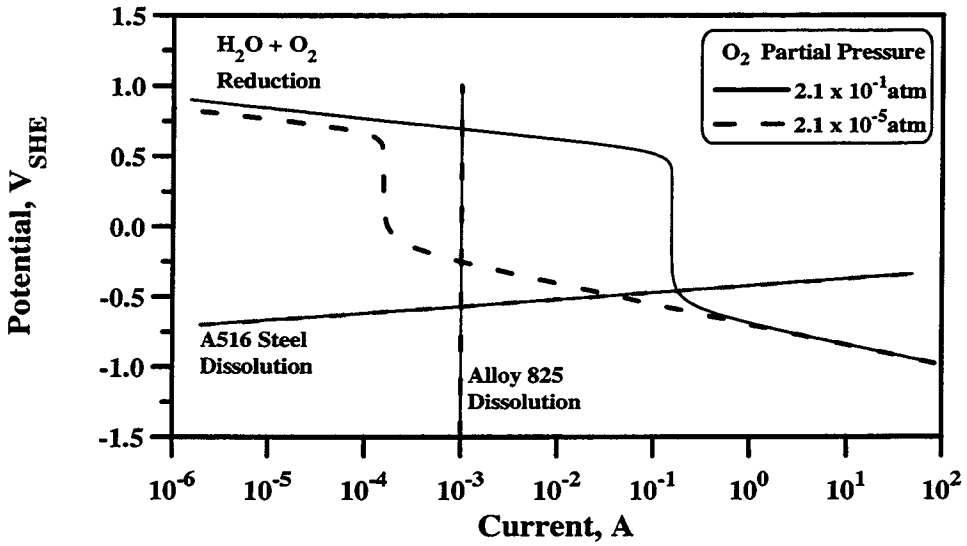

Figure 3-7. Evans diagram showing the effect of the partial pressure of oxygen (2.1×10^{-1} and 2.1×10^{-5} atm) on the calculated total cathodic current for the reduction of O_2 and H_2O, and anodic currents for the passive dissolution of Alloy 825 and the active dissolution of A516 steel as a function of potential in a solution of pH 5 at 368 K

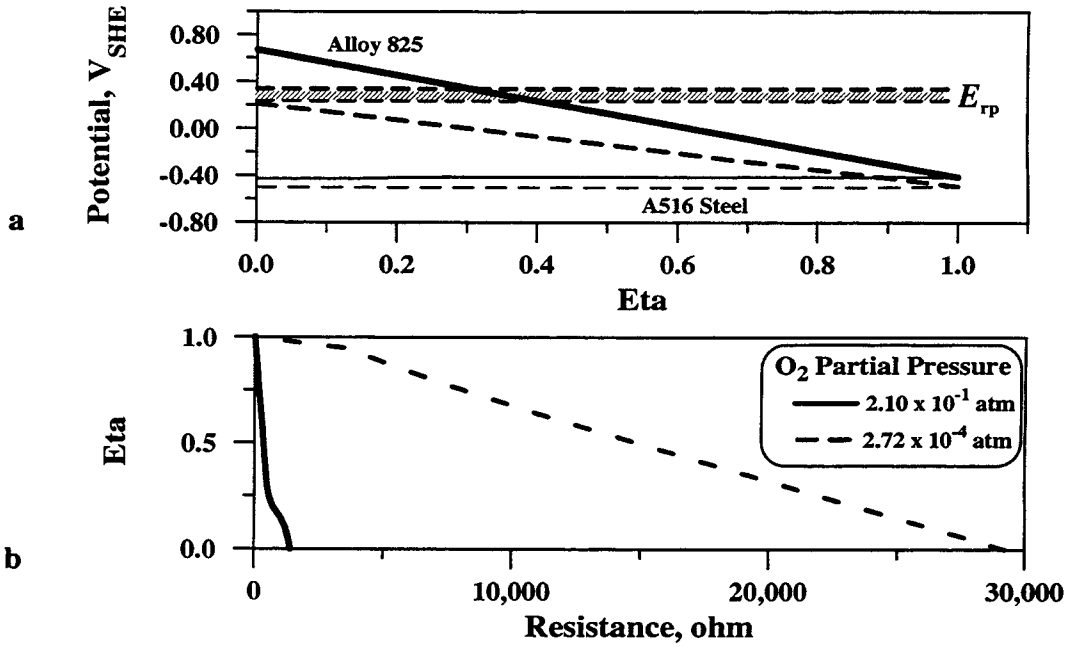

Figure 3-8. (a) Plot of the calculated galvanic corrosion potentials of Alloy 825 and A516 steel as a function of the efficiency, η, of the galvanic coupling at two partial pressures of oxygen (2.1×10^{-1} and 2.72×10^{-4} atm). The value of the repassivation potential of Alloy 825 in a solution containing 1,000 ppm chloride at 368 K is included. (b) Value of η as a function of the resistance of the galvanic couple for two oxygen partial pressures.

less than 2.72×10^{-4} atm, the $E_{corr}^{steel,WP}$ is always lower the E_{rp}. Lower values of p_{O_2} result in further reductions in the $E_{corr}^{825,WP}$ and $E_{corr}^{steel,WP}$. In figure 3-8b, η is plotted as a function of R_{couple} for the air saturated and partially deaerated cases provided in figure 3-8a. It should be noted that for the air saturated case, the curve for η versus R_{couple} is exactly the same as the 368 K curve shown in figure 3-4a. For the deaerated case in figure 3-8b, it is seen that the value of η remains close to 1 unless the R_{couple} is greater than 5,000 ohms. This result indicates that the value of η under deaerated conditions is consistently high and galvanic protection of the inner overpack can be assured.

3.3.4 Diffusion Layer Thickness

The effect of δ on E_{corr}^{825} and E_{corr}^{steel} is presented in figure 3-9. From Eqs. (2-26) and (2-38) it is apparent the rate of O_2 reduction on the metal surfaces increases as δ is reduced. This is reflected in figure 3-9 where the limiting current for the reduction of O_2 is inversely proportional to δ. Decreasing δ results in an increase of both the E_{corr}^{steel} and the I_{corr}^{steel} since the intersection of the anodic dissolution curve for A516 steel occurs in the diffusion controlled region for O_2 reduction. Since δ has no effect on the O_2 reduction kinetics in the activation controlled region, no significant change in E_{corr}^{825} is observed. Figure 3-10a shows that $E_{corr}^{825,WP}$ and $E_{corr}^{steel,WP}$ are not too sensitive to the value of δ. Although an increase in $E_{corr}^{825,WP}$ is observed as δ is reduced, the effect is small but more pronounced for $\eta \rightarrow 1$. A decrease in δ has a more noticeable effect on $E_{corr}^{steel,WP}$. The strong dependence of $E_{corr}^{steel,WP}$ on δ is a result of the intersection of the anodic dissolution curve for A516 steel and the reduction of O_2 occurring in the diffusion limited region for O_2 reduction. It is apparent from figure 3-9, that the kinetics of O_2 reduction in the diffusion limited region increase significantly when δ is reduced. For the range of δ values given in figure 3-10a the localized corrosion of Alloy 825 is possible only for η <0.3. In figure 3-10b, the value of η is indicated as a function of R_{couple}. The kinetics of the O_2 and H_2O reduction reactions are accelerated when δ is small. This increases the corrosion rate of the A516 steel and reduces its durability as a sacrificial anode. A δ value of 10^{-4} m can only be expected under flowing conditions, whereas for stagnant conditions the value of δ is expected to be on the order of 5×10^{-4} m.

3.4 AREA RATIO

Figure 3-11a provides results of galvanic corrosion calculations for two surface area ratios of Alloy 825 and A516 steel corresponding to the extremes expected for the geometry depicted in figure 2-8. The linear dependence of $E_{corr}^{825,WP}$ on η is clearly shown in figure 3-11a. The active behavior of the A516 steel reduces $E_{corr}^{825,WP}$ below E_{rp} for all values of η >0.35. The effect of the area ratio is minimal, however, resulting at the most in a 100 mV increase in both $E_{corr}^{825,WP}$ and $E_{corr}^{steel,WP}$ with a 500 times decrease in the area ratio when $\eta \rightarrow 1$, but no change for $\eta \rightarrow 0$. It is apparent from this figure that the value of η above which localized corrosion is avoided ($\eta \approx 0.35$) is not affected by the change in the area ratio.

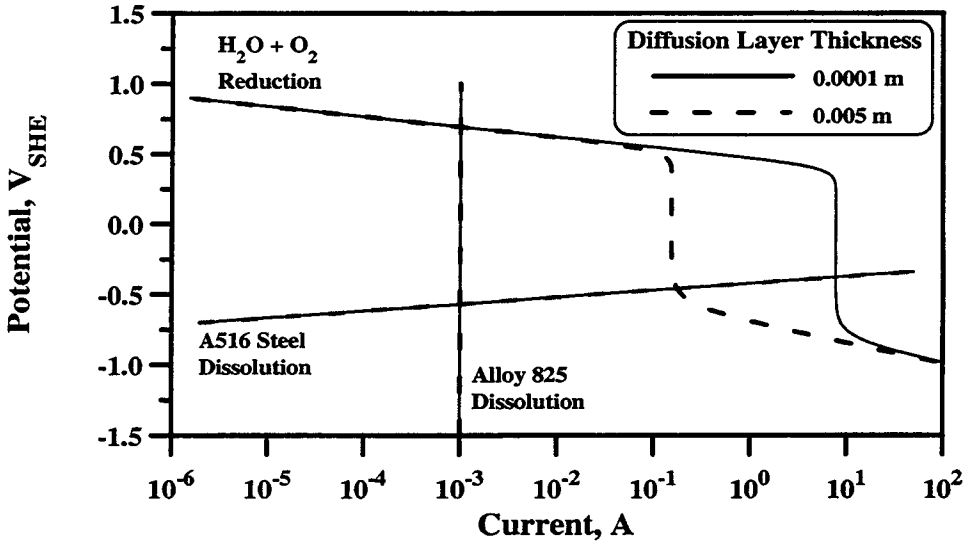

Figure 3-9. Evans diagram showing the effect of the diffusion layer thickness (0.0001 and 0.005 m) on the calculated total cathodic current for the reduction of O_2 and H_2O, and anodic currents for the passive dissolution of Alloy 825 and the active dissolution of A516 steel as a function of potential in an air saturated solution of pH 5 at 368 K

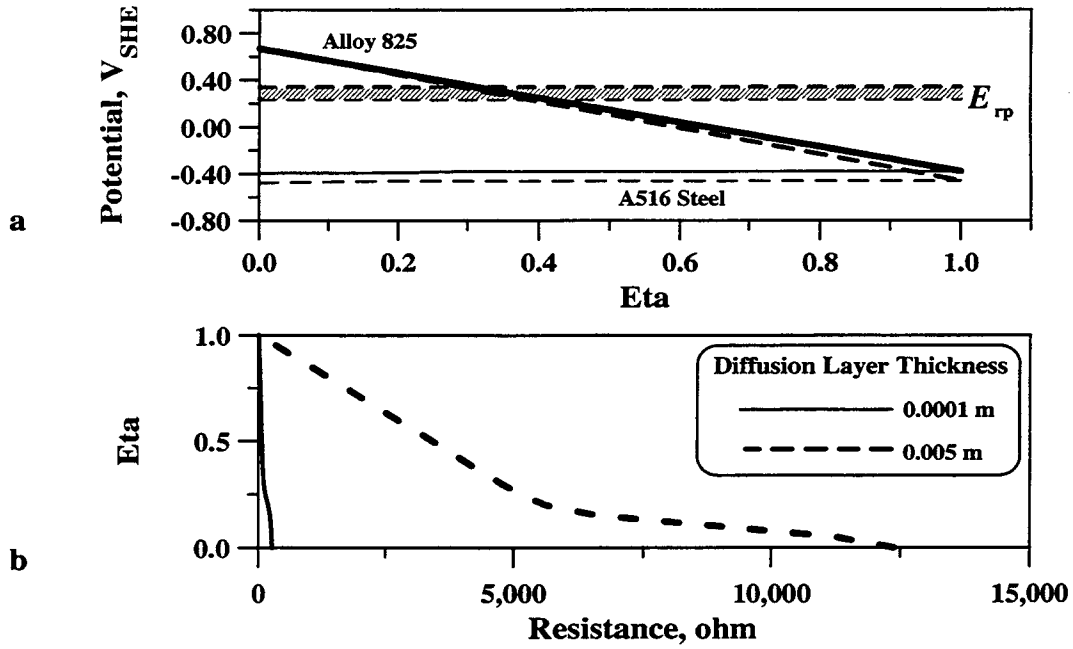

Figure 3-10. (a) Plot of the calculated galvanic corrosion potentials of Alloy 825 and A516 steel as a function of the efficiency, η, of the galvanic coupling for two values of the diffusion layer thickness (0.0001 and 0.005 m). The value of the repassivation potential of Alloy 825 in a solution containing 1,000 ppm chloride at 368 K is included. (b) Variation of η as a function of the resistance of the galvanic couple showing the effect of diffusion layer thickness.

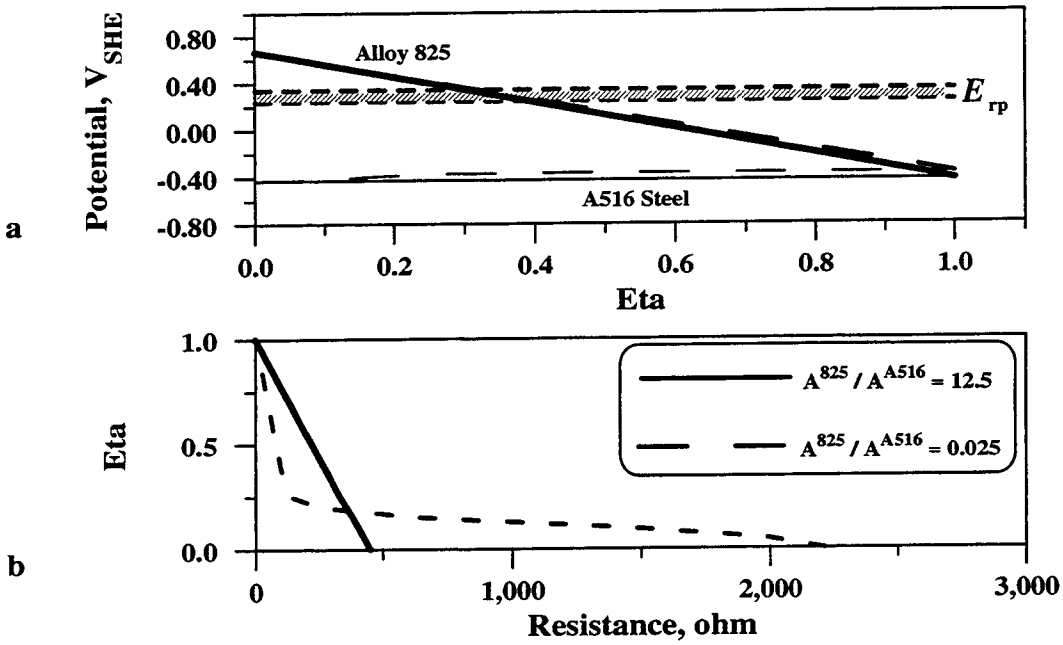

Figure 3-11. (a) Plot of the calculated galvanic corrosion potentials of Alloy 825 and A516 steel as a function of the efficiency, η, of the galvanic coupling for two values of the surface area ratio between Alloy 825 and A516 steel (12.5 and 0.025). The value of the repassivation potential of Alloy 825 in a solution containing 1,000 ppm chloride at 368 K is included. (b) Value of η as a function of the resistance of the galvanic couple for the upper and lower limits of Alloy 825: A516 steel area ratio.

The values of η determined from R_{couple} for the extremes of the area ratios considered in this study are graphically depicted in figure 3-11b. For an Alloy 825: A516 steel area ratio of 12.5:1, a linear relationship between η and R_{couple} is observed. In this case, the value of R_{couple} necessary to initiate localized corrosion of Alloy 825 is approximately 300 ohms. When the area of A516 steel is many times greater than that of Alloy 825 however, localized corrosion can be initiated with a lower value of R_{couple} on the order of 150 ohms.

4 DISCUSSION

4.1 COMPARISON OF CALCULATED AND MEASURED POTENTIALS

A comparison of calculated and measured E_{corr} is necessary to confirm the validity of the calculations performed in this study. For Alloy 825, the E_{corr} in both air saturated and deaerated environments has previously been reported (Sridhar et al., 1995; Dunn et al., 1997). In deaerated solutions of pH 9 at 368 K (95 °C), the measured E_{corr}^{825} varies between –0.50 and –0.25 V_{SHE}. As shown in figure 4-1, the calculated value of E_{corr}^{825} in a completely deaerated environment is –0.74 V_{SHE}. This relatively large (about 365±125 mV) difference between the measured and calculated values is a strong indication that the experimental data were obtained in environments not completely deaerated. Work by Gilroy and Mayne (1962) has shown that the dissolved O_2 concentration in solutions deaerated by bubbling an inert gas, such as prepurified nitrogen or argon, can vary from 0.5 to 140 µg/L at room temperature depending on choice of the deaeration method. With a p_{O_2} of 0.00027 atm (dissolved O_2 concentration of 7 µg/L), the limiting current density for the reduction of O_2 on Alloy 825 is approximately equal to the passive current density for Alloy 825 (10^{-3} A/m^2). Slight variations in the p_{O_2} (0.00027 ± 0.00005 atm) may result in variations in the E_{corr} in the range of –0.60 to –0.20 V_{SHE}, which is comparable to the range of the measured values as noted previously. In addition, to reach a better agreement between measured and calculated values, the experimental data should be obtained using a deaerating gas containing a mixture of hydrogen (i.e., 90 percent N_2 + 10 percent H_2) to attain conditions closer to the equilibrium value for the H_2O reduction reaction due to a partial pressure of H_2 of 0.1 atm in equilibrium with the solution.

In air saturated solutions the calculated values of E_{corr}^{825} were found to agree reasonably well with the experimental measurements. An E_{corr}^{825} of 0.38 V_{SHE} was calculated for an air saturated solution of pH 9 at 368 K (figure 4-1). Measured values of the E_{corr}^{825} have been as high as 0.41 V_{SHE} in an air saturated 1,000 ppm chloride solution at 368 K (Dunn, et al., 1997). It must be emphasized that the E_{corr}^{825} in an air saturated solution is expected to be time dependent because decreases in the passive current density result in changes in the E_{corr}^{825}. As the passive film on a corrosion resistant material ages without the initiation of localized corrosion, the resistive properties of the film improve. As a result, the passive current density will tend to decrease causing an increase in the E_{corr} over time. Conversely, the continuous nucleation and repassivation of metastable pits on an oxide covered surface may tend to increase the average anodic current density that in turn decreases the E_{corr}.

Although good agreement was found between the calculated and measured values of E_{corr}, several factors that can significantly alter the E_{corr} should be discussed. The reduction of O_2 on the metal surface is a complex electrochemical reaction with many intermediate steps (Vetter, 1967; Damjanovic, 1969). The measured potential of the O_2 electrode is never as high as indicated from theoretical calculations of the electrode potential. Even for almost inert electrodes such as platinum or carbon, the

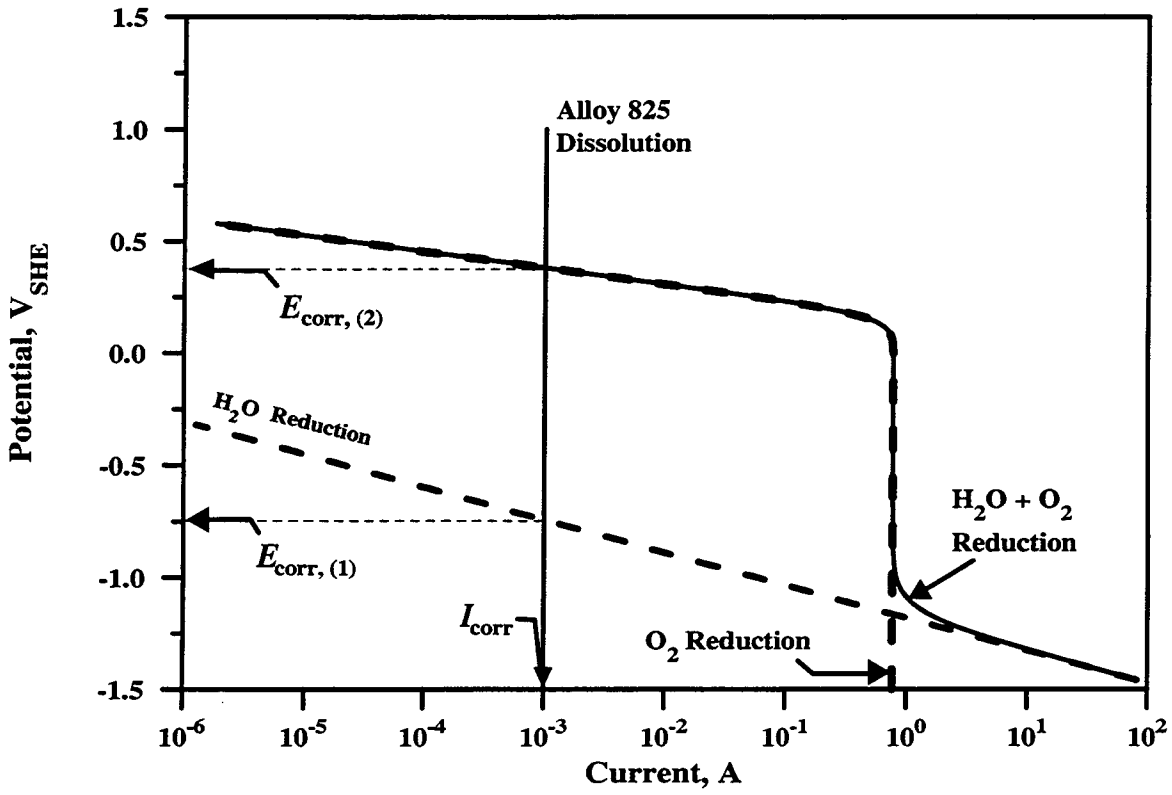

Figure 4-1. Evans diagram showing the calculated cathodic currents for the reduction of O_2 and H_2O, total cathodic current, and anodic current for the passive dissolution of Alloy 825 as a function of potential in a solution of pH 9 at 368 K. Corrosion potentials are indicated for two conditions: (1) deaerated solution and (2) air saturated solution.

O_2 reduction potential has been reported in the range of 0.8 to 1.1 V_{SHE}, well below the theoretical calculated value of 1.2 V_{SHE} (Oldfield, 1988). The 0.1 to 0.4 V overpotential is due to the surface condition of the electrode and the lack of a substantive catalytic activity. The adsorption of ions such as Cl^- or the formation of an oxide film covering the metal surface can also increase the overpotential for the reduction of O_2. The surface of the platinum electrodes is not truly inert but is actually covered with an oxide film. As a result, the potential measured on platinum electrodes is the mixed potential of the oxide/oxygen system and not the metal/oxygen system (Hoare, 1967). The effect of a 0.2 V overpotential is shown in figure 4-2. The limiting current density is not affected by the O_2 reduction overpotential because it is only dependent on mass transport limitations and, consequently E_{corr}^{steel} does not change. Since the overpotential alters the kinetics in the activation controlled region for the O_2 reduction reaction, a 0.2 V overpotential reduces E_{corr}^{825} by approximately the same value.

The presence of high concentrations of dissolved salts tends to decrease the concentration of dissolved O_2 in the bulk solution which is accompanied by a corresponding decrease in the E_{corr}. Cramer

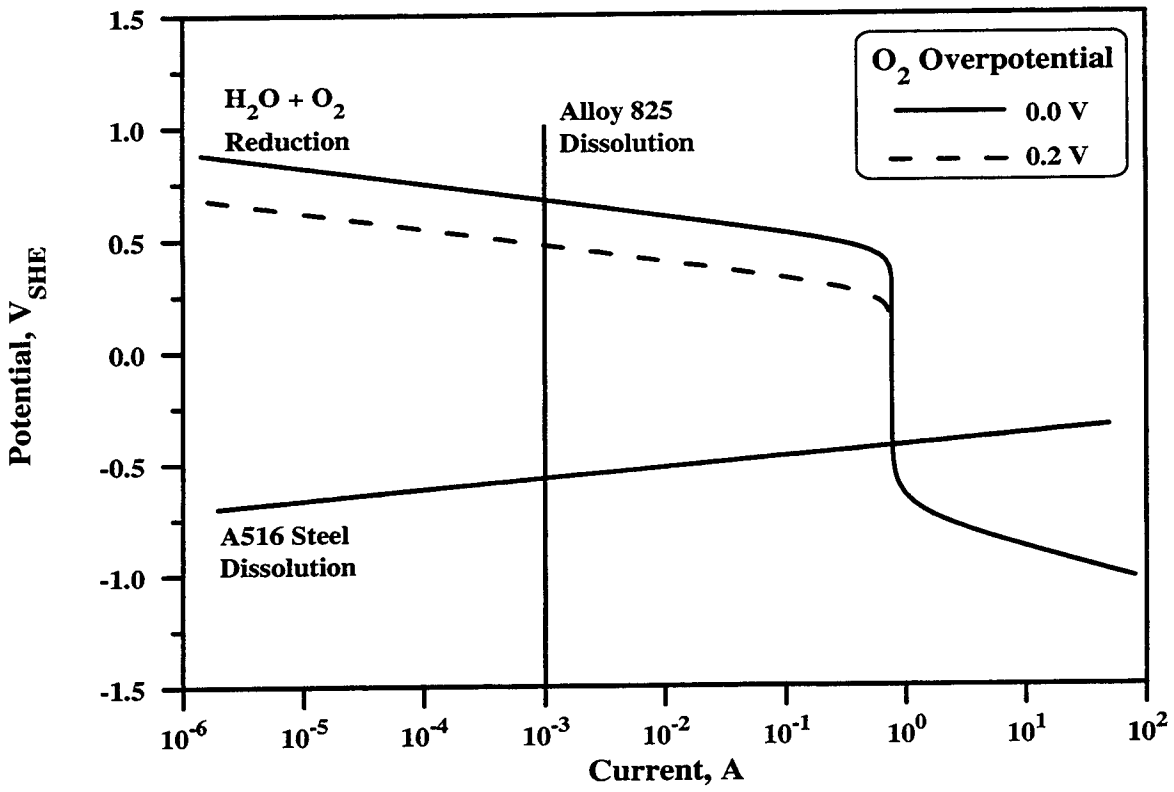

Figure 4-2. Evans diagram showing the effect of a 0.2 V overpotential for the oxygen reduction reaction on the calculated corrosion potential of Alloy 825 in an air saturated solution of pH 5 at 368 K, considering the calculated total cathodic current for the reduction of O_2 and H_2O, and anodic currents for the passive dissolution of Alloy 825 and the active dissolution of A516 steel as a function of potential

(1982) examined the salting out effect and measured the equilibrium concentration of dissolved O_2 in pure water and in NaCl solutions ranging in concentration from 0.87 to 5.69 molal over the temperature range of 0 to 120 °C (273 to 393 K). The concentration of dissolved O_2 in these solutions is given in figure 4-3. For all solutions, the concentration of dissolved O_2 is highest at low temperatures and decreases monotonically with increasing temperature, as well as with escalating salt concentration. As a result, the E_{corr} of both materials should decrease according to the reduction in the O_2 solubility, particularly in solutions with relatively high chloride concentrations.

The most significant effect of augmenting the chloride concentration however, is related to the aggressive effect of this anion on the susceptibility to localized corrosion of CRM. Both the pitting nucleation potential, E_p, and the E_{rp} for CRM such as stainless steels and Ni-base Fe-Cr-Ni-Mo alloys have been shown to decrease linearly with the logarithm of the chloride concentration (Szklarska-Smialowska, 1986; Sridhar et al., 1993). For Alloy 825 in a 1,000 ppm (0.028 mol/L) Cl^- solution at 368 K (95 °C), the E_{rp} is in the range of 0.24 to 0.34 V_{SHE} and is reduced to 0.07 V_{SHE} in a 5.8 mol/L

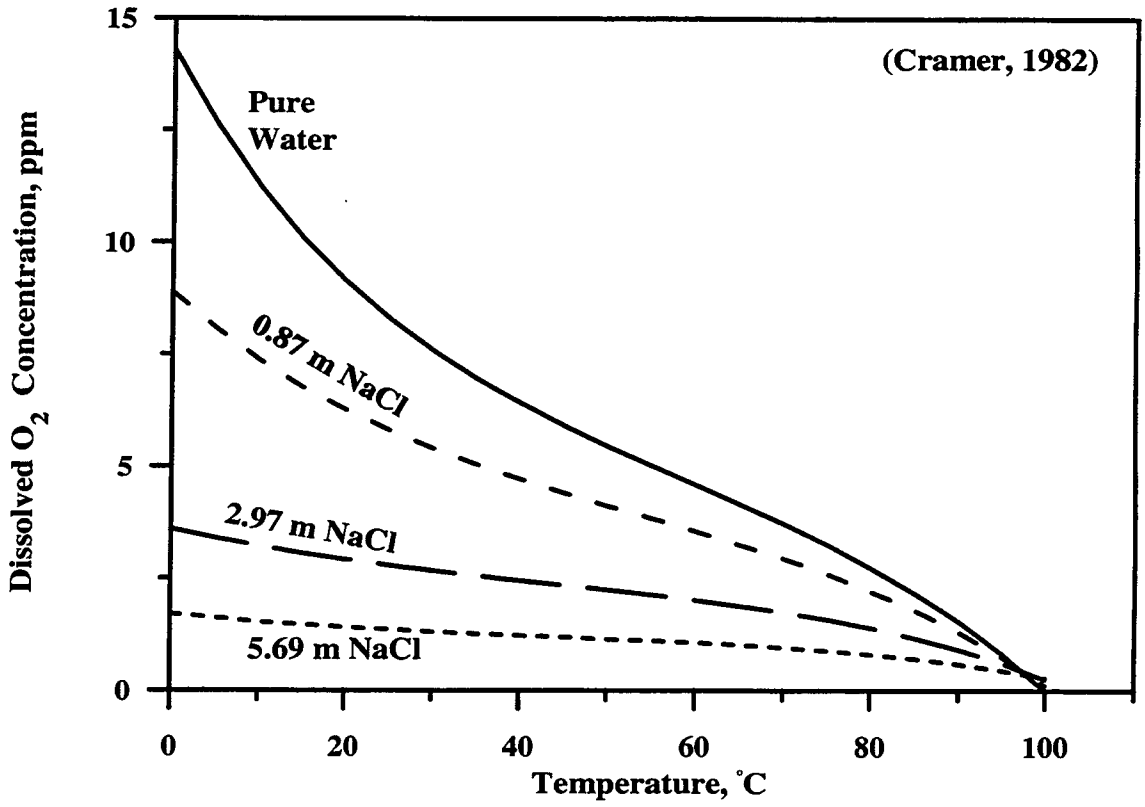

Figure 4-3. Effect of NaCl concentration on the solubility of oxygen in water as a function of temperature (Cramer, 1982).

Cl^- solution (Sridhar et al., 1995). Thus, while an increase in the dissolved NaCl concentration tends to reduce E_{corr}, large reductions in the E_{rp} values result in an increase of the susceptibility to localized corrosion in solutions with high Cl^- concentrations.

The E_{couple} calculated in this study are compared to previously obtained values to verify the accuracy of the parameters used in the calculations. Scully and Hack (1984) measured the galvanic corrosion potential of an Alloy 625/carbon steel couple with an area ratio of 1:1 in seawater at ambient temperature. They reported a value of $-0.466\ V_{SHE}$. For comparison, a calculation was performed using a temperature of 298 K in a solution of pH 7. Assuming perfect galvanic coupling (η=1), the E_{couple} was calculated to be $-0.462\ V_{SHE}$. The excellent agreement between the calculated and measured values lends support to both the methods used in these calculations and to the values selected for the electrochemical parameters. Further experimental investigation is in progress at the CNWRA as a part of the Evolution of the Near-Field Environment (ENFE) KTI.

4.2 EFFECT ON ENVIRONMENTAL PARAMETERS

4.2.1 Temperature

Although increases in temperature decrease E_{corr}^{825}, the E_{couple} of the Alloy 825/A516 steel couple is raised slightly. This is the result of an elevation in E_{corr}^{steel} due to increases in both the limiting current density for O_2 reduction and the dissolution kinetics of the steel. The most important effect of elevation the temperature, as shown in figure 3-4a, is the substantial decline E_{rp}. In addition, significant changes in the chemical composition of the solution contacting the WP surface can be expected at high temperatures as a result of water evaporation. In the emplacement drift, water is first presumed to contact the WPs when temperature is close to the boiling point and the RH at the WP surface exceeds the critical RH necessary to stabilize a water film of sufficient thickness on the metal surface able to sustain electrochemical reactions. The time necessary to penetrate the outer CAM must be considered to determine the temperature of the WP when galvanic corrosion begins. The temperature ranges given in figure 3-4a represent the bounding values of the WP temperatures that can be expected at the time galvanic corrosion is initiated. Fast penetration of the outer containment barrier will result in galvanic corrosion starting at temperatures close to 368 K. If penetration of the outer barrier takes many thousands of years, then the WP temperatures will have substantially decreased and the likelihood of localized corrosion of the inner barrier will be reduced. The main effect of temperature is the required increase in η from approximately 0.2 to 0.4 to avoid localized corrosion of Alloy 825 when the temperature at which galvanic coupling occurs is raised from 273 to 368 K.

4.2.2 pH

The effect of pH is provided in figures 3-5 and 3-6. As already noted, groundwater contacting the containers is expected to be alkaline (pH $\geq$ 9). The effect of temperature on the HCO_3^-/CO_3^{2-} concentration ratio, as a consequence of the removal of CO_2 from the solution, will cause the pH to increase. In addition, interactions with the concrete used to construct the underground facilities will increase the pH of the groundwater. The most important effect of the elevated pH is the passivation of the A516 steel overpack (Uhlig and Revie, 1985). The purpose of the outer overpack is to provide a corrosion allowance barrier that will corrode in a uniform and predictable manner. As long as the outer overpack is intact, the thickness of this barrier will act as a gamma radiation shield preventing radiolysis of the groundwater and subsequent formation of highly oxidizing species such as H_2O_2. Failure of the WP by uniform corrosion will take many hundreds of years. The extended time for the failure of the outer barrier is a design feature of the WP and will allow a significant period for the decay of the radioactive waste. When the inner barrier is exposed after the failure of the outer barrier by uniform corrosion, radiolysis of the groundwater will no longer occur and the temperature of the WP will be substantially reduced.

As previously noted, passivation of the A516 steel overpack occurs if the pH is above 9 leading to a decrease in the uniform corrosion rate of the overpack. When passivated, however, carbon steels become susceptible to localized corrosion. Marsh et al., (1986) reported pitting of steel in simulated groundwater of pH 9.2 containing 0.001 M HCO_3^-/CO_3^{2-} in the presence of 10 ppm Cl^- at 50 °C (323 K). A similar or even more aggressive environment in terms of Cl^- concentration and temperature can be expected to contact the WP emplaced in a repository located in the unsaturated zone. If initiated, penetration of the A516 steel overpack by localized corrosion will occur much faster than failure by

uniform corrosion. Figure 3-6 shows the calculated $E_{corr}^{825,WP}$ and the E_{rp} of Alloy 825 measured in a 1,000 ppm Cl^- solution. A substantially different environment exists inside localized corrosion enclaves independent of the bulk environment. The environment inside pits is known to be enriched in H^+ ions as a result of the hydrolysis of Fe^{2+} cations and contains a high concentration of Cl^- ions to maintain electroneutrality. After pits penetrate through the outer barrier, the inner barrier will then be exposed to the aggressive pit electrolyte. As previously indicated, the E_{rp} of the corrosion resistant barrier is strongly dependent on Cl^- concentration. The end result of the high pH in the near-field environment is a reduction in the uniform corrosion rate of the A516 steel barrier due to passivity accompanied by the initiation and growth of pits that generate a localized environment in which Alloy 825 is prone to localized corrosion. The main effect of the lower pH in the pit environment is the need of a more efficient galvanic couple to avoid localized corrosion of Alloy 825 because the threshold value for η increases from 0.3 to 0.45 with a pH decrease from 7 to 5, as noted in figure 3-6a.

4.2.3 Partial Pressure of Oxygen

In figure 3-7, the main effect of decreasing the p_{O_2} is the reduction in $E_{corr}^{825,WP}$. For A516 steel in an alkaline environment in which passive conditions prevail, a substantial decrease in the E_{corr}^{steel} is also expected. Pitting corrosion however, may occur even in deaerated environments due to the very low values of E_p and E_{rp} for A516 steel in Cl^- solutions (Sagar, 1997). Nevertheless, passivity of A516 steel may not be sustained in a fully deaerated environment and hence, the high aspect ratio characteristic of a pit cannot be maintained. The pits will tend to spread laterally and coalesce together, leading to less-localized, nonuniform corrosion. This form of corrosion can also occur if the pH of the near-field environment is lower than 9. This morphology of the attack, although not defined in relation to the pH, is assumed in the aqueous corrosion model for carbon steel adopted in TSPA-95 (TRW Environmental Systems Inc., 1995).

For the pit geometry depicted in figure 2-8, since the passive dissolution rate for Alloy 825 is independent of the concentration of oxygen, C_{O_2}, reducing the $E_{corr}^{825,WP}$ below the E_{rp} for all values of η requires that the diffusion limiting current for the reduction of oxygen be less than the passive current density of Alloy 825. This condition is fulfilled when the p_{O_2} is 2.7×10^{-4} atm for a i_{pass}^{825} of 10^{-3} A/m^2. As presented in figure 3-8a, no localized corrosion of Alloy 825 can occur under these conditions since the $E_{corr}^{825,WP}$ is always less than E_{rp}.

The effect of C_{O_2} on the E_{corr}^{steel} can be understood considering the diffusional flux

$$j_{O_2,\delta} = -D_{O_2}\left(\frac{dC_{O_2}}{dx}\right)_{(x = \delta)} \qquad (4\text{-}1)$$

where

$j_{O_2,\delta}$ — Mass flux of oxygen across the diffusion layer thickness

D_{O_2} — Diffusion coefficient of oxygen

C_{O_2} — Concentration of oxygen

The $j_{O_2,\delta}$ increases with increasing C_{O_2}, which in turn results in a faster rate of O_2 reduction. In the case of steel (see figure 3-7), the rising cathodic current is balanced by an increase in the I_{corr}^{steel} resulting in a reduced lifetime for the outer overpack.

Figure 3-8a, shows localized corrosion of Alloy 825 in air-saturated solutions is avoided when $\eta > 0.4$, whereas E_{rp} is not reached in deaerated solutions even in the absence of galvanic coupling ($\eta = 0$). Under deaerated conditions, the lifetime of both the A516 steel overpack and the CRM inner barrier will be significantly extended. The lifetimes of Ti based alloys as well as Cu alloys, considered as possible container materials for the disposal of SF in Canada, have also been reported to be strongly influenced by the amount of available O_2 in the repository (King and Kolar, 1996; Shoesmith et al., 1996). In the Canadian program, complete consumption of the available O_2 is expected to occur in a few hundred years as a result of partial oxidation of the containers when emplaced in a sealed repository located in deep, water-saturated geologic formations. Afterwards, the corrosion rate of the containers is expected to be so low that containment of the waste will be assured for many thousands of years. Significant reductions in the O_2 concentrations in the proposed YM repository however, have not been reported. As a consequence, corrosion rates of the materials in an air saturated environment must be considered.

4.2.4 Diffusion Layer Thickness

From the plot in figure 3-9 it is apparent that variations in δ do not change the kinetics of O_2 reduction in the activation controlled region and, therefore, the E_{corr}^{825} is not affected by changes in δ. Slight changes in δ however, have a pronounced effect on the kinetics of O_2 reduction in the mass transfer controlled region, and both the E_{corr}^{steel} and the I_{corr}^{steel} become strongly dependent on δ. In the mass transfer controlled region under stagnant conditions, the rate limiting step for O_2 reduction is its diffusion to the metal surface. Fick's law is also used to describe the changes in the O_2 reduction kinetics as δ varies. Since the value of D_{O_2} is only dependent on temperature, for a constant value C_{O_2} under isothermal conditions, $j_{O_2,\delta}$ increases with decreasing δ. The escalated rate of the O_2 reduction reaction must be balanced by an increase in the I_{corr}^{steel}. As noted in figure 3-10a, the rise in the kinetics of the iron dissolution reaction results in a slight increase in both the $E_{corr}^{825,WP}$ and the $E_{corr}^{steel,WP}$. Since $E_{corr}^{825,WP}$ is slightly affected by δ, the minimum value of η required to maintain $E_{corr}^{825,WP}$ below E_{rp} does not change with δ.

Since neither flowing conditions nor short term cyclic variations in the RH are expected in the proposed YM repository, variations in δ can only occur from changes in the water film thickness on the

WP surface. Such deviations may occur as a result of condensed water dripping of on the container surfaces followed by evaporation of the water film. The corrosion rate of iron base materials under cyclic wet and dry conditions has been shown by Tsuru et al. (1995) to be accelerated by a factor of at least 4 compared to a continuously immersed exposure. At present, determination of the corrosion rate of the WP as a result of water dripping on the container is not addressed in either EBSPAC or WAPDEG. This exclusion is primarily because of uncertainties regarding the fracture flow through the rock.

4.3 AREA RATIO

In this investigation, the effect of area ratio on the $E_{corr}^{825,WP}$ and the $E_{corr}^{steel,WP}$ was found to be minimal as presented in figure 3-11. Even with an 12.5:1 area ratio of Alloy 825 to A516 steel, the dissolution of the steel decreases the $E_{corr}^{825,WP}$ below the E_{rp} for $\eta > 0.3$. The area ratio however, has a pronounced effect on the dissolution rate of carbon steel. Figure 4-4 shows the i_{steel} for a 1 m^2 area of steel with three values for the area ratio. An increase in i_{steel} from 0.8 to 10 A/m^2 is predicted as a result of the elevation in Alloy 825 to A516 steel area ratio from 0.025:1 to 12.5:1. For an area ratio equal to 1, the current density is 1.3 A/m^2. It should be noted for comparison that Zamani et al. (1986) measured the corrosion current density in seawater to be in the range of 0.3 to 0.7 A/m^2 for a carbon steel/SS couple with a 1:1 area ratio. The results indicate that as long as a small amount of A516 steel is coupled to the Alloy 825 inner overpack, galvanic protection of the Alloy 825 barrier should occur. These calculations do not consider the effect of potential and current density distributions. When the geometry of the galvanic couple is similar to that in figure 2-8, then the effect of potential and current density distributions are negligible. Significant variations of the potential and current density distributions may be present after much of the A516 steel overpack has corroded away. The DOE model of WP performance considers that galvanic protection of the inner barrier will occur until 75 percent of the outer barrier has corroded. Although no justification is provided for the 75 percent criteria, results of previous modeling efforts of galvanic corrosion and cathodic protection systems where the potential and current density distributions were calculated, suggest there should be a minimum amount of A516 steel necessary to galvanically protect the inner corrosion resistant barrier.

4.4 ELECTROCHEMICAL PARAMETERS

Several electrochemical parameters were varied within the range of values reported in the literature. The variation of these parameters was performed to determine the effect on the potential of the galvanic couple. Results of these calculations are shown in detail in the appendix. Although the i_{pass}^{825} had the largest effect on $E_{corr}^{825,WP}$, it is important to note that this parameter was varied over four orders of magnitude. In addition, a i_{pass}^{825} of 10^{-5} A/m^2 is approximately one order of magnitude lower than what has been experimentally measured, even with thermally oxidized specimens (Dunn et al., 1995) in which a protective passive film is formed. The effect of the i_{0,O_2} was also examined and as expected, a higher i_{0,O_2} escalates the rate of O_2 reduction in the activation controlled region resulting in a higher $E_{corr}^{825,WP}$. Changing the value of β_{O_2} also alters the kinetics of the O_2 reduction in the activation controlled region. As the Tafel slope decreases with an increase in β_{O_2}, as indicated by Eq. (2-5), the intersection of the

anodic passive dissolution curve for Alloy 825 with the curve for the cathodic reduction of O_2 is displaced toward higher potentials. Although this change in β_{O_2} has a negligible effect on $E_{corr}^{steel,WP}$, the $E_{corr}^{825,WP}$ is raised in about 200 mV. Decreasing the $i_{0,Fe/Fe^{2+}}$ results in a rise in both $E_{corr}^{steel,WP}$ and $E_{corr}^{825,WP}$. Similarly, reducing the α_{Fe} equivalent to an increase in the anodic Tafel slope for iron dissolution according to Eq. (2-4) also elevates the galvanic corrosion potentials.

In general, the effect of the electrochemical parameters on both $E_{corr}^{steel,WP}$ and $E_{corr}^{825,WP}$ was minor. Because of the assumed relationship, however, the $E_{corr}^{825,WP}$ is strongly dependent on the value of η. The galvanic corrosion potentials do not vary significantly by changing the values selected for the electrochemical parameters, although they were diversified over a wide range to assess the propagation of uncertainties in certain values reported in the literature. This fact suggests that future modeling efforts on the efficiency of galvanic coupling, in addition to evaluation of environmental effects, should be focused on the effect of WP geometry, including consideration of potential and current density distributions for the more complex case of an outer barrier having a large number of pits of different sizes.

4.5 GALVANIC COUPLING EFFICIENCY

By far, the dominant factor in determining $E_{corr}^{825,WP}$ is the value of η as a result of the assumed relationship between parameters discussed in previous subsections. Because of the active behavior of steel, the value of η is not so significant in determining $E_{corr}^{steel,WP}$. As indicated in the calculations presented in chapter 3, the highest resistance that would yield the minimum value of η required to avoid the occurrence of localized corrosion for Alloy 825 is typically smaller than 500 ohms.

To illustrate this assertion better, a plot of $E_{corr}^{825,WP}$ and $E_{corr}^{steel,WP}$ as a function of the resistance of the galvanic couple, R_{couple}, is shown in figure 4-5a. It is seen that the $E_{corr}^{825,WP}$ increases linearly with the resistance up to values equal to approximately 500 ohms. This is indeed the range of efficient galvanic coupling (η>0.5), as noted in figure 4-5b. For this range of η the $E_{corr}^{825,WP}$ is lower than E_{rp} for localized corrosion as shown in figure 4-5a. If any potential difference within this range is divided by the corresponding resistance, a current density of about 1.5 A/m^2 is obtained representing that provided by the anodic dissolution of A516 steel required to galvanically protect Alloy 825 against the occurrence of localized corrosion. The recently measured E_{rp} for Alloy 625 (Gruss et al., 1997) is also plotted in figure 4-5a. The electrochemical parameters for Alloys 825 and 625 are similar and therefore the $E_{corr}^{825,WP}$ plot can be considered valid for both alloys. It is seen that galvanic protection of an alloy with a higher E_{rp} than that of Alloy 825 can be assured even with a high resistance of the couple and therefore a smaller value of η.

As it can be inferred from the linear relationship exhibited at low values of R_{couple} in figure 4-5a, it is possible to conclude in that range the potential difference between the anode and the cathode is only associated with ohmic drop in the solution because of the electrolyte resistivity. This is the regime of high conductivity in which W_p exhibits high values. An uniform current and potential distribution can be

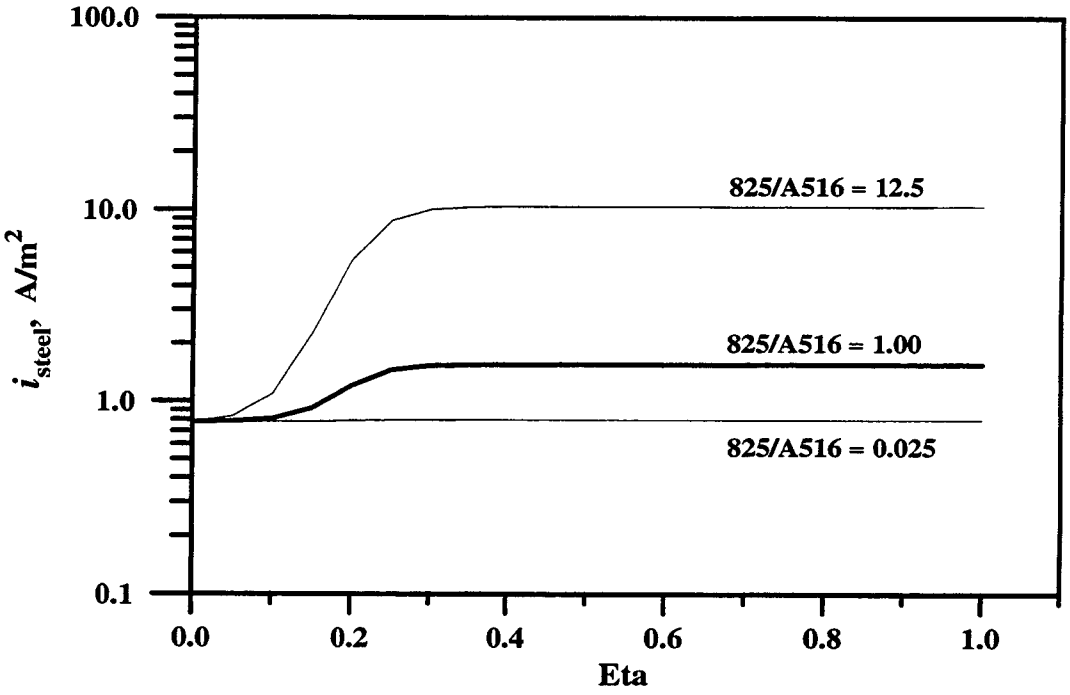

Figure 4-4. Effect of the area ratio between Alloy 825 and A516 steel (12.5, 1, and 0.025) on the dissolution current density of A516 steel coupled to Alloy 825 in an air saturated solution of pH 5 at 368 K as a function of η.

expected within the geometry depicted in figure 2-8. The estimated value of W_p can be calculated from Eq. (2-6) and is about 3.4 m, which takes into account a Tafel constant for the anodic dissolution of iron, b_a, equal to 0.040 V/decade, a corrosion current of about 0.7 A, a surface area of A516 steel of about 3×10^{-3} m, and a resistivity of the electrolyte of 5×10^{-5} ohm m. In contrast, the characteristic dimension which may be either r_p (5 mm) or h_p (100 mm) is quite small.

At high resistance values, corresponding to low galvanic coupling efficiency ($\eta < 0.25$), no linear relationship between the potential difference and the resistance exists, suggesting that additional resistances in series significantly affect the flow of current from the anode to the cathode. The R_{couple} is the sum of all the resistances between the WP barriers, as given by Eq. (4-2)

$$R_{couple} = R_{soln} + R_{CAM\ oxide} + R_{CRM\ oxide} + R_{corr\ product} \qquad (4\text{-}2)$$

where

R_{soln} — resistance of the solution
$R_{CAM\ oxide}$ — resistance of the oxide on the CAM barrier
$R_{CRM\ oxide}$ — resistance of the oxide on the CRM barrier

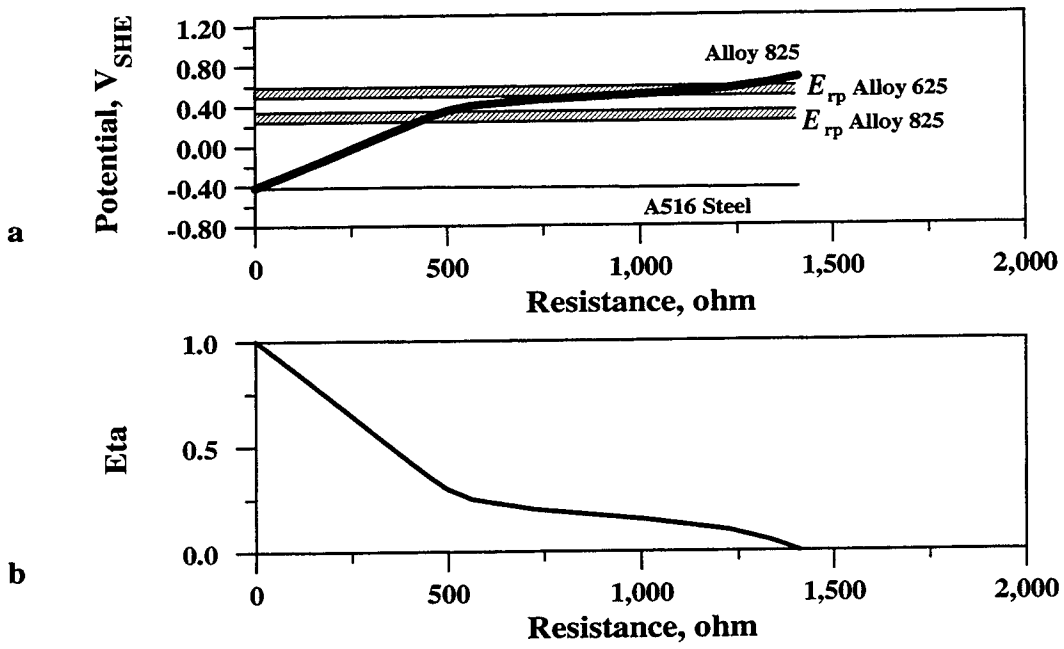

Figure 4-5. (a) Plot of the calculated galvanic corrosion potentials of Alloy 825 and A516 steel as a function of the resistance of the galvanic couple in an air saturated solution of pH 5 at 368 K. The values of the repassivation potential of Alloys 825 and 625 in a solution containing 1,000 ppm chloride at 368 K is included. (b) Value of η as a function of the resistance of the galvanic couple.

$R_{corr\ product}$ — resistance of the corrosion products between the WP barriers

The resistance of the oxides and corrosion products may have a capacitive component instead of being purely resistive as in the case of the electrolyte. The solution resistance can be determined from the resistivity of the electrolyte (the inverse of the ionic conductivity) and the geometry of the galvanic couple depicted in figure 2-8, according to the following equation

$$R_{soln} = \rho_{soln} \frac{l}{A} \qquad (4\text{-}3)$$

where

ρ_{soln} — resistivity of the solution in ohm m
l — length between the anode materials constituting the galvanic couple
A — area

If only the electrolyte resistivity is considered in Eq. (4-2), $R_{couple} = R_{soln}$. According to the geometrical dimensions in figure 2-8, l can vary from a low value to 0.1 m. The value of A corresponds

to the area of Alloy 825 exposed to the pit environment. A value of 7.8×10^{-5} m^2 obtained when r_{CRM} = 5mm was used in this calculation. The value of ρ_{soln} may range from 5×10^{-5} to 1×10^{-2} ohm m, taking into consideration the resistivity of a 5 mol/L $FeCl_2$ solution (the solution composition within a pit in steel) is 5×10^{-5} ohm m. For this specific geometry, the value of R_{soln} ranges from a low value to 13 ohms, which in turn corresponds to η values ranging from 1 to 0.97, based on figure 4-5.

It is unlikely the resistivity of a solution in contact with the A516 steel/Alloy 825 couple will be lower than that given previously. In addition to the electrolyte, however, oxide films and corrosion products could be present between the inner and outer container barriers. Therefore, the contribution of resistances in Eq. (4-2) should be discussed. Wilhelm (1988) investigated the electronic properties of different oxides and their effect on galvanic corrosion. In Wilhelm's study, oxides were classified as insulators, conductors, n-type semiconductors, and p-type semiconductors based on the band gap between the conduction and valance bands. The p-type oxides include NiO. These oxides can support the reduction of O_2 and H^+ ions but may also be reduced. Iron oxides such as Fe_2O_3 are n-type semiconductors (the oxide is deficient in oxygen) and can readily support the reduction of O_2 or H^+ ions. As a result, materials coated with n-type oxides are at risk for localized attack. Materials coated with insulator oxides such as Al_2O_3 or ZrO_2 can be subject to localized attack but only if electron conduction by tunneling occurs through a thin oxide layer.

The interface between the A516 steel overpack and the Alloy 825 inner barrier may consist of Fe_2O_3, Fe_3O_4, corrosion products containing Fe^{2+} and Fe^{3+}, Cr_2O_3, and a solution between the materials. The resistance of the interface is determined by the resistances of these layers. The Cr_2O_3, which is expected to form on the Alloy 825 surface, is an electronic conductive oxide that facilitates electron transfer for the cathodic reduction of O_2 and H_2O. Wilhelm (1988) did not investigate corrosion products such as FeOOH. The porosity of other corrosion products is expected to be high and conduction dominated by the electrolyte present in the pores. The low resistivity of the phases present at the interface suggests the value of η can be expected to be close to 1.0. Under these conditions, the galvanic corrosion potentials of the container materials will be reduced to low values because of the dominating effect of the iron dissolution kinetics. Localized corrosion of Alloy 825 will be prevented until significant loss of the steel corrosion allowance barrier has occurred and large potential and current density distributions are present. More sophisticated techniques such as the boundary element method will be required to model such potential and current density distributions.

4.6 LIFETIME OF THE OUTER OVERPACK

Calculation of the outer barrier lifetime is significant to the container performance regardless of whether or not the outer overpack fails by either uniform or localized corrosion. The calculations presented in this report indicate that the breached outer overpack can galvanically protect the inner corrosion resistant barrier from localized corrosion. Thus, an important factor in the lifetime of the WP is the period of galvanic protection. Several factors determine the length of time over which galvanic protection of the inner overpack by the breached outer overpack can occur. Failure of the outer overpack by uniform corrosion will result in a significant portion of the outer barrier being completely corroded leaving only a small fraction of the A516 steel to provide galvanic protection of the inner CRM barrier. In contrast, perforation of the outer barrier by localized corrosion may occur more rapidly than uniform corrosion, however, the majority of the A516 steel which may then act as a sacrificial anode will remain coupled to the CRM barrier. In either case the minimum amount of A516 steel necessary to protect the inner overpack will be determined by the potential and current density distributions of the galvanic couple.

The time necessary to exhaust the galvanic protection of the inner overpack will be controlled by the time dependent corrosion rate of the A516 steel outer overpack. Calculating the galvanic protection time requires knowledge of both the fraction of the WP surface that is wet, which can vary with time as well as the chemistry of the water, which will determine the corrosion mechanism for the steel. If it is assumed that the entire surface of the A516 steel overpack is wet and the chemistry of the water is such that the A516 steel surface is completely passivated, then the lifetime of the A516 steel is only determined by the passive current density. For a passive current density ranging from 10^{-2} to 10^{-3} A/m^2, the lifetime of the A516 steel overpack will vary from approximately 9,000 to 90,000 yr. Onset of pitting of the A516 steel overpack may significantly increase the corrosion rate which will in turn result in a decreased outer container lifetime. In a deaerated environment, the corrosion rate of A516 steel will be low and pitting of the outer overpack may be prevented. If the outer barrier fails in a deaerated environment, the calculations presented here indicate that localized corrosion of the inner barrier will not occur.

Other factors also need to be considered. As previously indicated, one of the main purposes of modeling cathodic protection systems is to prevent overprotection of the engineered structure that can eventually result in hydrogen embrittlement. A preliminary assessment of the hydrogen absorption and embrittlement of several candidate container materials has been performed by Sridhar et al. (1991). This assessment, based on short term tests and literature data, indicates the alloys containing higher amounts of Fe are less susceptible to embrittlement than low-Fe, Ni-base alloys such as Alloy C-22. In addition, it was determined that raising the temperature decreased the susceptibility to embrittlement. Based on the short term hydrogen embrittlement data and the expected corrosion potential of the galvanic couple determined in this report, the susceptibility of the inner CRM barrier to hydrogen embrittlement appears to be low.

5 SUMMARY, CONCLUSIONS, AND RECOMMENDATIONS

The corrosion potentials of the proposed HLW container materials are calculated using the electrochemical kinetics of the anodic dissolution and cathodic reduction reactions. In this simplified calculation, corrosion of the barrier metals is considered as the single anodic oxidation reaction. Corrosion of A516 steel is assumed to be described by the active dissolution of the metal in an acidified solution taking into consideration the conditions existing in a pit once the outer container is breached. Passive dissolution is postulated to describe the behavior of Alloy 825 prior to the occurrence of localized corrosion. The reduction reactions considered are limited to the cathodic reductions of O_2 and H_2O. Corrosion potentials of the metals are then determined by the potential at which the anodic current from the metal dissolution reactions is equal in magnitude to the total current from the cathodic reduction reactions.

The corrosion potentials of the metals and the electrochemical kinetics of the anodic dissolution and cathodic reduction reactions are then used to calculate the galvanic corrosion potentials of the container materials. A pit penetrating through the outer A516 steel container and exposing the inner Alloy 825 barrier to an acidified environment is used as the geometry of the galvanic couple. Based on this geometry, area ratios of Alloy 825 to A516 steel ranging from 12.5:1 to 1:40 are analyzed. Environmental parameters are varied in a manner consistent with that expected in the near field of a HLW repository located in the unsaturated zone to determine the effect of environmental variations on the galvanic corrosion potentials of the container materials. Electrochemical parameters are also varied over the range of the values reported in the literature, making allowance for uncertainties in the experimental data. The efficiency of the galvanic couple is varied from 0.0, corresponding to the total absence of galvanic interactions between the materials, to 1.0 (perfect galvanic coupling). The galvanic coupling efficiency is determined as a function of the resistance of the galvanic couple.

Temperature and the partial pressure of oxygen are found to be the most significant environmental parameters in determining the lifetime of the WP. Changes in temperature do not have a significant effect on the galvanic corrosion potentials of the container materials. The repassivation potential, which is conservatively chosen as the critical potential for the initiation of localized corrosion on Alloy 825, decreases significantly with increasing temperature. As a result, Alloy 825 becomes less susceptible to localized corrosion at lower temperatures. On the other hand, significant changes in the galvanic corrosion potentials are calculated as the partial pressure of oxygen abates. The corrosion rate of A516 steel is reduced by over an order of magnitude when the environment was fully deaerated. A significant decline in the galvanic corrosion potential of Alloy 825 is also estimated. As a consequence, for partial pressures of oxygen less than 2.7×10^{-4} atm, Alloy 825 can be protected against localized corrosion even in the absence of galvanic coupling to A516 steel. Variations in the electrochemical parameters and the area ratio of Alloy 825 to A516 steel have only a minimal influence on the galvanic corrosion potentials and do not modify the value of the galvanic coupling efficiency required to avoid the occurrence of localized corrosion of Alloy 825. Nevertheless, the study of other geometries, covering a wide distribution of pit sizes and locations needs to be performed using other methods to attain a more complete understanding of the influence of the effective area ratio between both container materials.

An analysis of the resistance of the galvanic couple between Alloy 825 and A516 steel is also performed for the pit geometry considered in this study. The analysis suggests that galvanic protection of the inner barrier by the perforated A516 steel overpack can be accomplished if a good metallic contact exists between both barriers. Therefore, localized corrosion of the Alloy 825 inner container can be avoided by galvanic coupling to the outer container if the resistance of the couple is lower than 500 ohms. On the

basis of literature information and simple calculations, it appears the oxide films on the materials and the solution in contact with the barrier layers have a relatively low resistance, suggesting a conductive path for the flow of galvanic current exists. Galvanic protection of the inner Alloy 825 barrier can be achieved unless electronic conduction is affected by the lack of metallic contact between the barriers.

A methodology for estimating the galvanic coupling efficiency from the resistance of the galvanic couple is developed. Considering only the resistance of the electrolyte solution, the value of the galvanic coupling efficiency is estimated to range from 0.97 with a low conductivity solution to more than 0.99 with a high conductivity solution. Oxides formed on Cr-containing corrosion resistant alloys are good conductors. As a result, the presence of a Cr oxide on an inner barrier constructed of an alloy such as Alloys 825, 625, or C-22 will not significantly reduce the galvanic coupling efficiency. The semiconductive nature of the oxides formed on A516 steel should also provide a conductive path that will not significantly impede the flow of galvanic current.

From this investigation it may be concluded that failure of the outer A516 steel corrosion allowance barrier by localized corrosion will result in galvanic protection of the inner corrosion resistant barrier. Since the efficiency of the galvanic couple is not strongly dependent on either the environmental variations, electrochemical parameters, or area ratio of the galvanic contact, complete protection of the inner corrosion resistant barrier from localized corrosion can be expected. The environmental conditions in the repository near field will have a significant impact on the time that galvanic protection of the inner barrier will be maintained.

Results of this investigation may provide a means of improving calculation of the corrosion and galvanic corrosion potentials in the EBSPAC. These results also provide a methodology for estimating the galvanic coupling efficiency critical to performance of the WP in the near-field repository environment. Although a simple functional relationship cannot be established that relates η to environmental parameters, electrical conductivity of the environment, and the electrochemical behavior of the outer and inner overpacks, it is confirmed that these parameters are implicitly considered in Eq. (1-1).

There are several limitations to the simplified calculations presented in this report. The electrochemical reactions considered in this investigation are limited to the dissolution of the metals and the reduction of both O_2 and H_2O. While these are the primary corrosion reactions, the corrosion kinetics may be significantly accelerated by the presence of a highly oxidizing species such as H_2O_2 (the main radiolytic product) or Fe^{3+}ions (which can be produced by the oxidation of Fe^{2+} species in solution by the available O_2). At present, formation of these species within the repository has not been conclusively determined but it is expected that after thousands of years gamma radiolysis will decrease sufficiently to make the generation of H_2O_2 negligible. The thickness of the inner overpack is such that alpha radiolysis can be neglected at its outer surface. Yet another limitation in the present analysis is the lack of knowledge regarding the near-field environmental conditions. These conditions will be strongly dependent on the design and thermal loading strategy for the proposed repository. The time dependent variation of temperature, partial pressure of oxygen, chemistry of the water contacting the containers, and other environmental variables can have a significant impact on the container lifetimes. A third limitation is the lack of an appropriate estimate of the wetted area of the A516 steel overpack. Finally, a complete analyses of the resistance of the galvanic couple considering the impedances of the phases formed between WP barriers cannot be performed solely by modeling. Experimental work, currently being conducted under the ENFE KTI, is required for measuring the impedance associated with the presence of oxide layers and corrosion deposits affecting the flow of galvanic current. A more accurate assessment of the near-field

environment and information on the final WP detailed design are important to better define the conditions and configuration of the system under study.

Future efforts in the modeling of galvanic coupling of WP barriers will address the limitations listed here. Modeling of the repository environment will identify any additional redox species and other environmental parameters that should be included in calculation of the galvanic corrosion potentials of WP materials. Potential and current density distributions should be included through the use of more sophisticated modeling techniques to deal with the occurrence of a large number of pits of various sizes on different locations of the outer overpack surface. The boundary element method is perhaps the best choice for future modeling of galvanic interactions of WP barriers. This technique would incorporate the potential dependent kinetics of the anodic and cathodic reactions with the spacial variability as a result of the changing geometry of the WP expected as corrosion of the outer barrier proceeds. This would better define the amount of A516 steel necessary to protect the inner Alloy 825 barrier and provide an improved method to determine the amount of time over which the inner barrier can be galvanically protected.

6 REFERENCES

Adey, R.A., and S.M. Niku. 1992. Computer modeling of corrosion using the boundary element method. *Computer Modeling in Corrosion.* ASTM STP 1154. R.S. Munn, ed. Philadelphia, PA: American Society for Testing and Materials.

Adey, R.A., S.M. Niku, C.A. Brebbia, and J. Finnegan. 1985. Computer aided design of cathodic protection systems. *Boundary Elements VII.* C.A. Brebbia and G. Maier, eds. Berlin, Germany: Springer-Verlag.

Alavi, A., and R.A. Cottis. 1987. The determination of pH, potential and chloride concentration in corroding crevices on 304 stainless steel and 7475 aluminum alloy. *Corrosion Science* 27: 443–451.

Astley, D.J. 1983. A method for calculating the extent of galvanic corrosion and cathodic protection in metal tubes assuming unidirectional current flow. *Corrosion Science* 23: 801–832.

Astley, D.J. 1988. Use of the microcomputer for calculation of the distribution of galvanic corrosion and cathodic protection in seawater systems. *Galvanic Corrosion.* ASTM STP 978. H.P. Hack, ed. Philadelphia, PA: American Society for Testing and Materials.

Atkins, J.E., and J.H. Lee. 1996. *User's Guide to Waste Package Degradation (WAPDEG) Simulation Code. Version 1.0.* Preliminary Draft. Las Vegas, NV: INTERA, Inc.

Bard, A.J., R. Parsons, and J. Jordan, eds. 1985. *Standard Potentials in Aqueous Solutions.* New York: Marcel Dekker, Inc.

Bardal, E., R. Johnsen, and P.O. Gartland. 1984. Prediction of galvanic corrosion rates and distribution by means of calculation and experimental models. *Corrosion* 40: 628–633.

Bockris, J.O'M., and A.K.N. Reddy. 1977. *Modern Electrochemistry.* New York: Plenum Press.

Bockris, J.O'M., D. Drazic, and A.R. Despic. 1961. The electrode kinetics of the deposition and dissolution of iron. *Electrochimica Acta* 4: 325–361.

Calvo, E.J. 1979. *Study of the Electroreduction Reaction of Oxygen on Passive Metals in Different Aqueous Media* (in Spanish). Ph.D. dissertation, Universidad Nacional de La Plata (Argentina).

Calvo, E.J., and D.J. Schiffrin. 1988. The electrochemical reduction of oxygen on passive iron in alkaline solutions. *Journal of Electroanalytical Chemistry* 243: 171–185.

Cramer, S.D. 1982. *The Solubility of Methane, Carbon Dioxide and Oxygen in Brines from 0 to 300 °C.* Bureau of Mines Report of Investigations. RI 8706. Washington, DC: U.S. Department of the Interior.

Conway, B.E. 1952. *Electrochemical Data.* Amsterdam, Netherlands: Elsevier.

Damjanovic, A. 1969. Mechanistic analysis of oxygen electrode reactions. *Modern Aspects of Electrochemistry*. J.O'M. Bockris and B.E. Conway, eds. New York Plenum Press 5.

De Giorgi, V.G., E.D. Thomas II, and A.I. Kaznoff. 1992. Numerical simulation of impressed current cathodic protection systems using boundary element method. *Computer Modeling in Corrosion* ASTM STP 1154. R.S. Munn, ed. Philadelphia, PA: American Society for Testing and Materials.

De Waard, C., and D.E. Milliams. 1975. Carbonic acid corrosion of steel. *Corrosion* 31: 177–181.

Dunn, D.S., G.A. Cragnolino, and N. Sridhar. 1997. *An Electrochemical Approach to Predicting Long-Term Localized Corrosion of Corrosion Resistant Container Materials*. San Antonio, TX: Center for Nuclear Waste Regulatory Analyses.

Dunn, D.S., N. Sridhar, and G.A. Cragnolino. 1995. Effects of surface chromium depletion on localized corrosion of Alloy 825 as a high-level nuclear waste container material. *Corrosion* 51: 618–624.

Esteban, J.M., M.E. Orazem, K.J. Kennelley, and R.M. Degerstedt. 1995. Mathematical models for cathodic protection of an underground pipeline with coating holidays. *CORROSION/95*. Paper No. 347. Houston, TX: NACE International.

Galvele, J.R. 1978. Present state of understanding of the breakdown of passivity and repassivation. *Passivity of Metals*. R.P. Frankenthal and J. Kruger, eds. Princeton, NJ: The Electrochemical Society.

Gilroy, D., and J.E.O. Mayne. 1962. The deaeration of aqueous solutions. *Journal of Applied Chemistry* 12: 382–384.

Gruss, K., D.S. Dunn, G.A. Cragnolino, and N. Sridhar. 1997. Repassivation potentials for localized corrosion of Alloys 625 and C-22 in simulated repository environments. To be presented at *CORROSION/98*. Paper No. 149. Houston, TX: NACE International.

Heusler, K.E. 1976. Influence of temperature and pressure on the kinetics of electrode processes. *High Temperature, High Pressure Electrochemistry in Aqueous Systems*. D. deG. Jones and R.W. Staehle, eds. Houston, TX: National Association of Corrosion Engineers.

Hoare, J.P. 1967. *The Oxygen Electrode on Noble Metals*. Advances in Electrochemistry and Electrochemical Engineering. Volume 6: Electrochemistry. P. Delahay and C.W. Tobias, eds. New York: Interscience Publishers.

King, F., and M. Kolar. 1996. A numerical model for the corrosion of copper nuclear fuel waste containers. *Scientific Basis for Nuclear Waste Management XIX*. W.M. Murphy and D.A. Knecht, eds. Pittsburgh, PA: Materials Research Society: Symposium Proceedings 412: 555–562.

Lou, J.L., Y.C. Lu, and M.B. Ives. 1992. Use of microelectrodes to determine local conditions within active pits. *Materials Performance* 31: 44–47.

Macdonald, D.D., G.R. Shierman, and P. Butler. 1972. *The Thermodynamics of Metal-water Systems at Elevated Temperatures. Part 2: The Iron-Water System.* AECL-4137. Pinawa, Canada: Atomic Energy of Canada Limited.

Manteufel, R.D., R.G. Baca, S. Mohanty, M.S. Jarzemba, R.W. Janetzke, S.A. Stothoff, C.B. Connor, G.A. Cragnolino, A.H. Chowdhury, T.J. Martin, and T.M. Ahn. 1997. *Total-System Performance Assessment (TPA). Version 3.0 Code Module Descriptions and User's Guide.* San Antonio, TX: Center for Nuclear Waste Regulatory Analyses.

Marsh, G.P., and K.J. Taylor. 1988. An assessment of carbon steel containers for radioactive waste disposal. *Corrosion Science* 28: 289–320.

Marsh, G.P., K.J. Taylor, I.D. Bland, C. Wescott, P.W. Tasker, and S.M. Sharland. 1986. Evaluation of the localized corrosion of carbon steel overpacks for nuclear waste disposal in granite environments. *Scientific Basis for Nuclear Waste Management IX.* L.W. Werme, ed. Pittsburgh, PA: Materials Research Society: Symposium Proceedings 50: 421–428.

McCright, D. 1995. *Scientific Investigation Plan for Yucca Mountain Project (YMP) WBS Element 1.2.2.5.1. Metal Barrier Selection and Testing.* SIP-CM-01. Rev. 2. Livermore, CA: Lawrence Livermore National Laboratory.

Mohanty, S., G.A. Cragnolino, T. Ahn, D.S. Dunn, P.C. Lichtner, R.D. Manteufel, and N. Sridhar. 1997. *Engineered Barrier System Performance Assessment Code: EBSPAC Version 1.1 Technical Description and User's Manual.* CNWRA 97-006. San Antonio, TX: Center for Nuclear Waste Regulatory Analyses.

Morgan, J. 1993. *Cathodic Protection.* 2nd Edition. Houston, TX: NACE International.

Munn, R.S., and O.F. Devereux. 1991a. Numerical modeling and solution of galvanic corrosion systems. Part I: Governing differential equation and electrodic boundary conditions. *Corrosion* 47: 612–617.

Munn, R.S., and O.F. Devereux. 1991b. Numerical modeling and solution of galvanic corrosion systems. Part II: Finite-element formulation and descriptive examples. *Corrosion* 47: 618–634.

Ogundele, G.I., and W.E. White. 1986. Some observations on corrosion of carbon steel in aqueous environments containing carbon dioxide. *Corrosion* 42: 71–78.

Oldfield, J.W. 1988. Electrochemical theory of galvanic corrosion. *Galvanic Corrosion.* ASTM STP 978. H.P. Hack, ed. Philadelphia, PA: American Society for Testing and Materials.

Orazem, M.E., J.M. Esteban, K.J. Kennelley, and R.M. Degerstedt. 1997a. Mathematical models for cathodic protection of an underground pipeline with coating holidays. Part 1: Theoretical development. *Corrosion* 53: 264–272.

Orazem, M.E., J.M. Esteban, K.J. Kennelley, and R.M. Degerstedt. 1997b. Mathematical models for cathodic protection of an underground pipeline with coating holidays. Part 2: Case studies of parallel anode cathodic protection systems. *Corrosion* 53: 427–436.

Pourbaix, M. 1974. *Atlas of Electrochemical Equilibria in Aqueous Solutions*. Houston, TX: National Association of Corrosion Engineers.

Pryor, M.J., and D.J. Astley. 1994. Bimetallic corrosion. *Corrosion Metal/Environment Reactions. Volume 1*. L.L. Shreir, R.A. Jarman, and G.T. Burstein, eds. Oxford, United Kingdom: Butterworths Heinemann.

Roy, A.K., D.L. Fleming, and S.R. Gorton. 1996. Effect of chloride concentration and pH on pitting corrosion of waste package container materials. Paper 182. *190th Electrochemical Society Meeting*. Pennington, NJ: The Electrochemical Society.

Sagar, B., ed. 1997. *NRC High-Level Radioactive Waste Program Annual Progress Report: Fiscal Year 1996*. NUREG/CR–6513, No. 1. CNWRA 96-OIA. Washington, DC: Nuclear Regulatory Commission.

Scully, J.R., and H.P. Hack. 1984. Galvanic corrosion prediction using long- and short-term polarization curves. *CORROSION/84*. Paper No. 34. Houston, TX: NACE International.

Shoesmith, D.W., F. King, and B.M. Ikeda. 1996. The indefinite containment of nuclear fuel wastes. *Scientific Basis for Nuclear Waste Management XIX*. W.M. Murphy and D.A. Knecht, eds. Pittsburgh, PA: Materials Research Society: Symposium Proceedings 412: 563–570.

Sridhar, N., G.A. Cragnolino, and D.S. Dunn. 1993. *Experimental Investigations of Localized Corrosion of High-Level Waste Container Materials*. CNWRA 93-004. San Antonio, TX: Center for Nuclear Waste Regulatory Analyses.

Sridhar, N., G.A. Cragnolino, and D.S. Dunn. 1995. *Experimental Investigations of Failure Processes of High-Level Radioactive Waste Container Materials*. CNWRA 95-010. San Antonio, TX: Center for Nuclear Waste Regulatory Analyses.

Sridhar, N., G.A. Cragnolino, D.S. Dunn, and H.K. Manaktala. 1994. *Review of Degradation Modes of Alternate Container Designs and Materials*. CNWRA 94-010. San Antonio, TX: Center for Nuclear Waste Regulatory Analyses.

Sridhar, N., B.E. Wilde, C. Manfredi, S. Kesavan, and C. Miller. 1991. *Hydrogen Absorption and Embrittlement of Candidate Container Materials*. CNWRA 91-008. San Antonio, TX: Center for Nuclear Waste Regulatory Analyses.

Strommen, R.D. 1992. Computer modeling of offshore cathodic protection systems: method and experience. *Computer Modeling in Corrosion*. ASTM STP 1154. R.S. Munn, ed. Philadelphia, PA: American Society for Testing and Materials.

Sugimoto, K., and K. Asano. 1987. Analysis of localized corrosion on stainless steel by micro-complex pH-pCl electrode. *NACE-9 Advances in Localized Corrosion.* H.S. Isaacs, U. Bertocci, J. Kruger, and S. Smialowska, eds. Houston, TX: NACE International.

Suzuki, T., M. Yamabe, and Y. Kitamura. 1973. Composition of an anolyte within pit anode of austenitic stainless steels in chloride solution. *Corrosion* 29: 18–22

Szklarska-Smialowska, S. 1986. *Pitting Corrosion of Metals.* Houston, TX: National Association of Corrosion Engineers.

TRW Environmental Safety Systems, Inc. 1995. *Total System Performance Assessment—1995: An Evaluation of the Potential Yucca Mountain Repository.* B00000000-01717-2200-00136. Las Vegas, NV: TRW Environmental Safety Systems, Inc.

TRW Environmental Safety Systems, Inc. 1996. *Mined Geologic Disposal System Advanced Conceptual Design Report. Engineered Barrier Segment/Waste Package.* B00000000-01717-5705-00027. Las Vegas, NV: TRW Environmental Safety Systems, Inc.

Tsuru, T., A. Nishikata, and J. Wang. 1995. Electrochemical studies of corrosion under a water film. *Materials Science and Engineering* A198: 161–168.

Turnbull, A. 1983. The solution composition and electrode potentials in pits, crevices, and cracks. *Corrosion Science* 23: 833–870.

Uhlig, H.H., and R.W. Revie. 1985. *Corrosion and Corrosion Control.* New York: John Wiley and Sons.

U.S. Department of Energy. 1996. *Highlights of the U.S. Department of Energy's Updated Waste Containment and Isolation Strategy for the Yucca Mountain Site.* Concurrence Draft. Washington, DC: U.S. Department of Energy.

Varela, F.E., Y. Kurata, and N. Sanada. 1997. The influence of temperature on the galvanic corrosion of a cast iron-stainless steel couple (prediction by the boundary element method). *Corrosion Science* 39: 775–788.

Vetter, K.J. 1967. *Electrochemical Kinetics—Theoretical and Experimental Aspects.* New York: Academic Press.

Wagner, C. 1951. Theoretical analysis of the current density distribution in electrolytic cells. *Journal of The Electrochemical Society* 98: 116–128.

Wagner, C., and W. Traud. 1938. The interpretation of corrosion phenomena by superimposition of electrochemical partial reactions and the formation of potentials of mixed electrodes. *Z. Electrochem* 44: 391–398.

Wilhelm, S.M., 1988. Galvanic Corrosion Caused by Corrosion Products. *Galvanic Corrosion.* ASTM STP 978. H.P. Hack, ed. Philadelphia PA: 23–34.

Yan, J.F., S.N.R. Pakalapati, T.F. Nguyen, R.E. White, and R.B. Griffin. 1992. Mathematical modeling of cathodic protection using the boundary element method with a nonlinear polarization curve. *Journal of The Electrochemical Society* 139: 1,932–1,936.

Zamani, N.G. 1988. Boundary element simulation of the cathodic protection system in a prototype ship. *Applied Mathematics and Computation* 26: 119–134.

Zamani, N.G., J.F. Porter, and A.A. Mufti. 1986. A survey of computational efforts in the field of corrosion engineering. *International Journal for Numerical Methods in Engineering* 23: 1,295–1,311.

APPENDIX

ELECTROCHEMICAL PARAMETERS

The $i_{0,Fe/Fe^{2+}}$ for the dissolution of steel has a large effect on the E_{corr}^{steel} as shown in figure A-1. From Eq. 2-24 it is apparent that decreasing the $i_{0,Fe/Fe^{2+}}$ shifts the curve for the anodic dissolution of iron to higher potentials. Variations in $i_{0,Fe/Fe^{2+}}$ have no effect on E_{corr}^{825}. As noted in figure A-2a, however, a reduction in the $i_{0,Fe/Fe^{2+}}$ resulted in significant changes in both the $E_{corr}^{825,WP}$ and the $E_{corr}^{steel,WP}$. The value of η necessary to initiate localized corrosion is lowered from 0.4 to 0.35 when $i_{0,Fe/Fe^{2+}}$ is increased from 10^{-5} to 10^{-1} A/m^2. From figure A-2b, it may be observed that this will require the value of R_{couple} to rise from 300 to 500 ohms.

The effect of the i_{pass}^{825} on E_{corr}^{825} is presented in figure A-3. It is apparent that as the i_{pass}^{825} decreases, the intersection of the passive dissolution curve and the oxygen reduction curve is increased to higher potentials which results in higher values of E_{corr}^{825}. The i_{pass}^{825} has been experimentally measured to be in the range of 10^{-2} to 10^{-3} A/m^2 (Dunn et al., 1995). A poorly formed oxide such as that on a chromium depleted surface on Alloy 825 tends to result in a higher passive current density. On the other hand, aging of the passive film and the growth of an oxide film at elevated temperatures can be expected to reduce the passive current density. Figure A-4a shows the effect of i_{pass}^{825} on the $E_{corr}^{825,WP}$ and the $E_{corr}^{steel,WP}$. It may be observed that the increase in the $E_{corr}^{825,WP}$ as i_{pass}^{825} decreases tends to make the Alloy 825 barrier more susceptible to localized corrosion. This effect however, is limited to the region where η <0.5. As η increases, the active dissolution of steel decreases $E_{corr}^{825,WP}$ below E_{rp}. Although localized corrosion can be initiated at a higher value of η when the passive current density is reduced, the results plotted in figure A-4b indicate that the value of R_{couple} necessary to obtain η values where localized corrosion can be avoided are virtually the same for both values of passive current density plotted here and are approximately 400 ohms.

Figure A-5 the effect of variations in the i_{0,O_2} is provided. Increasing the i_{0,O_2} has a marked effect on the kinetics for the reduction of oxygen in the activation controlled region. As a result, the E_{corr}^{825} rises with i_{0,O_2}. Since increasing i_{0,O_2} does not alter the oxygen reduction kinetics in the diffusion limited region, no change in E_{corr}^{steel} is observed. Increasing the $E_{corr}^{825,WP}$ when i_{0,O_2} is elevated from 10^{-8} to 10^{-5} A/m^2 is shown in figure A-6a. For the most part, increases in $E_{corr}^{825,WP}$ are limited to η values corresponding to poor galvanic coupling. No change in $E_{corr}^{steel,WP}$ is observed with the variations in i_{0,O_2}. The value of R_{couple} necessary to create an inefficient galvanic couple where localized corrosion can be initiated is not affected by changes in the i_{0,O_2} (see figure A-6b).

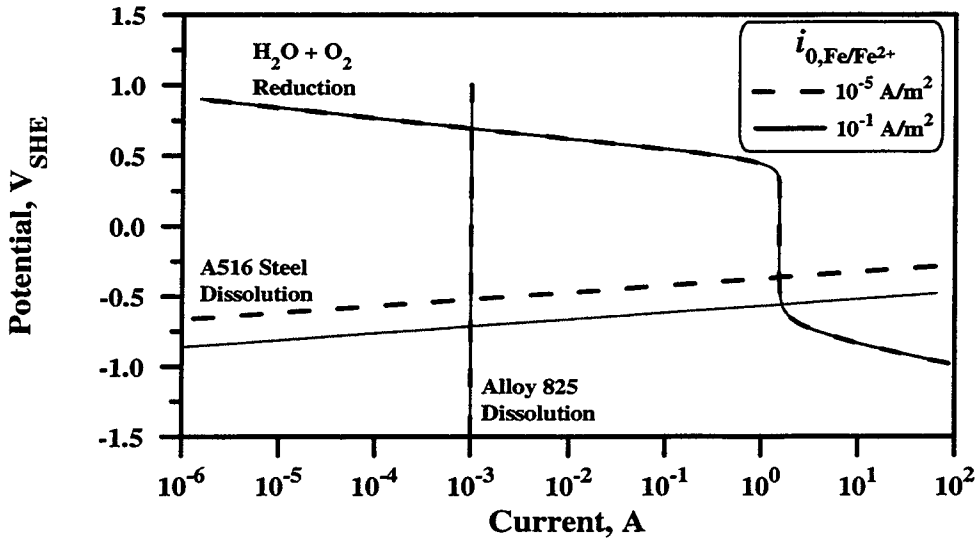

Figure A-1. Evans diagram showing the effect of the exchange current density for the active dissolution of A516 steel and the calculated total cathodic currents for the reduction of O_2 and H_2O as a function of potential in an air saturated solution of pH 5 at 368 K.

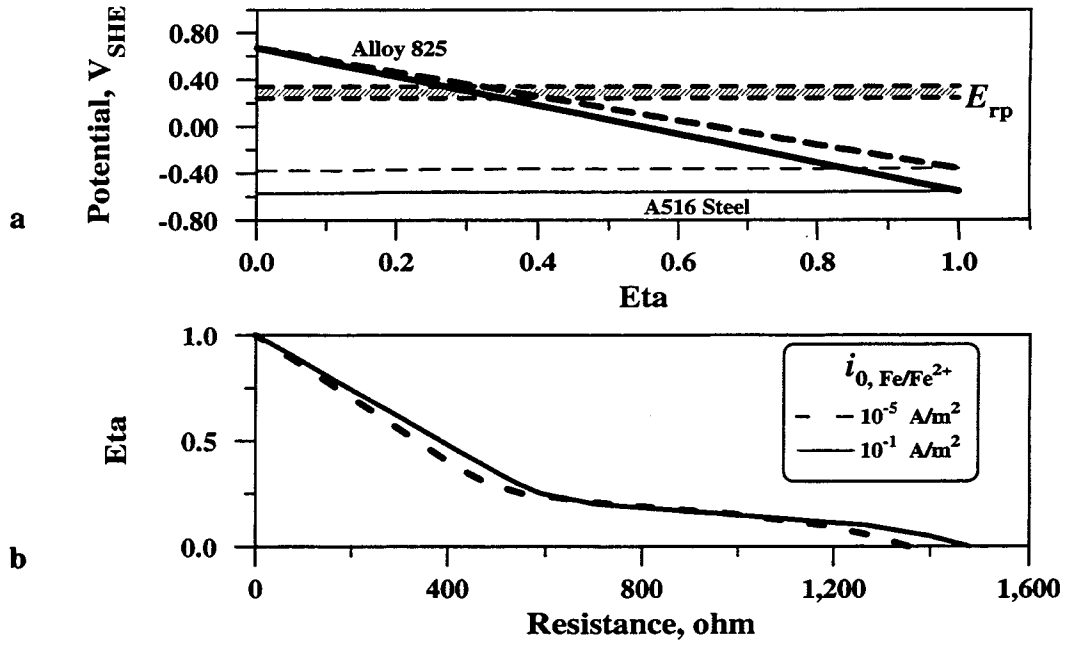

Figure A-2. (a)Plot of the calculated galvanic corrosion potentials of Alloy 825 and A516 steel as a function of the efficiency, η, of the galvanic coupling for two values of the exchange current density of the anodic dissolution of A516 steel (10^{-5} and 10^{-1} A/m^2). The value of the repassivation potential of Alloy 825 in a solution containing 1,000 ppm chloride at 368 K is included. (b) Variation of η as a function of the resistance of the galvanic couple.

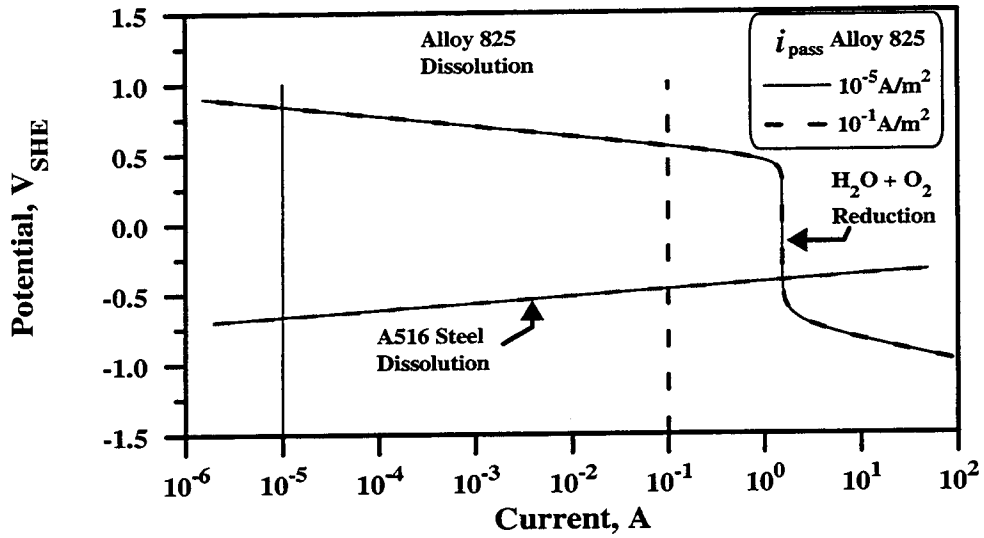

Figure A-3. Evans diagram showing the effect of the current density for the passive dissolution of Alloy 825 and the calculated total cathodic currents for the reduction of O_2 and H_2O as a function of potential in an air saturated solution of pH 5 at 368 K.

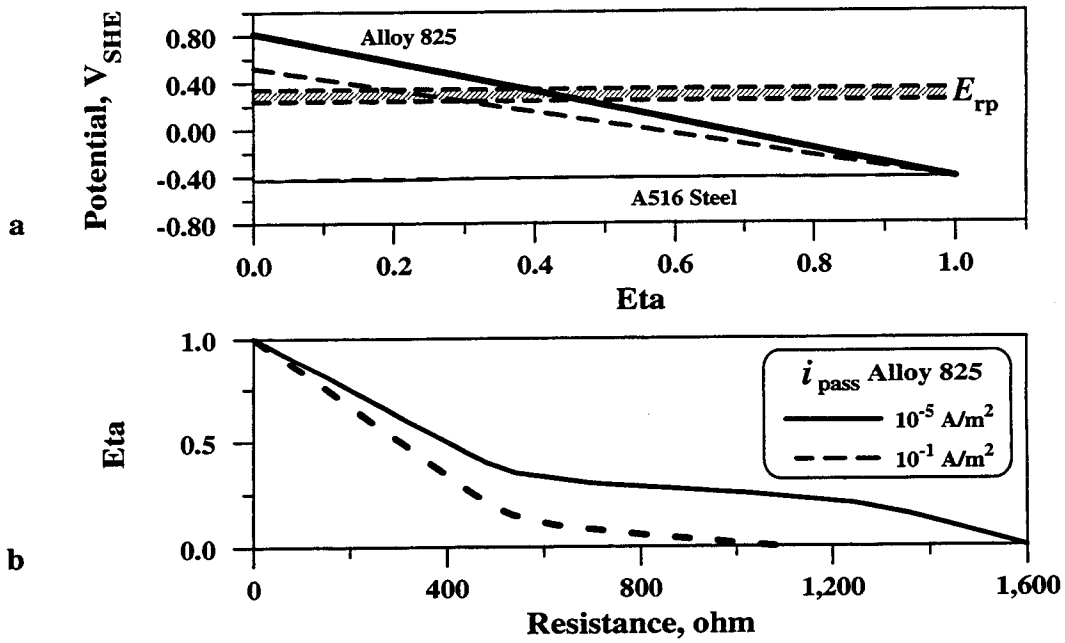

Figure A-4. (a) Plot of the calculated galvanic corrosion potentials of Alloy 825 and A516 steel as a function of the efficiency, η, of the galvanic coupling for two values of the current density for the passive dissolution of Alloy 825 (10^{-5} and 10^{-1} A/m^2). The value of the repassivation potential of Alloy 825 in a solution containing 1,000 ppm chloride at 368 K is included. (b) Variation of η as a function of the resistance of the galvanic couple.

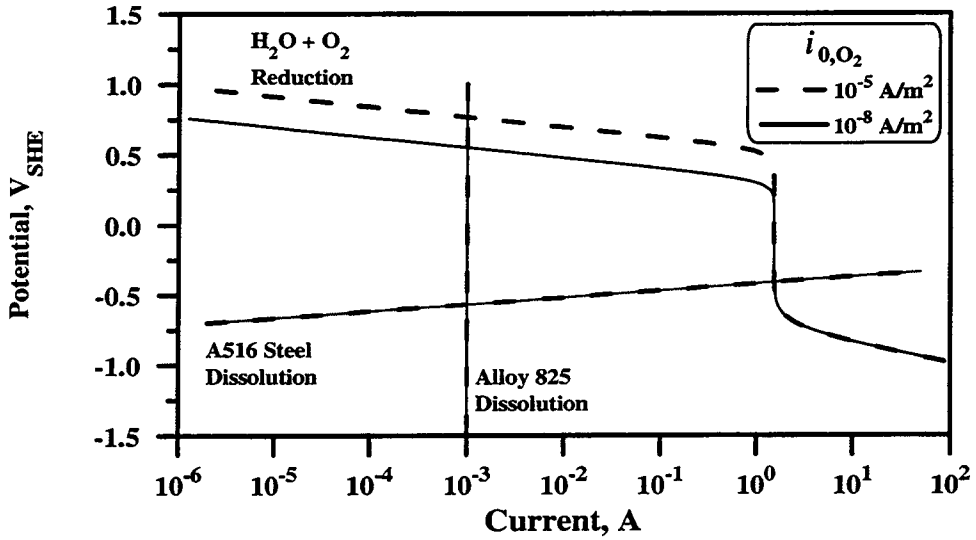

Figure A-5. Evans diagram showing the effect of the exchange current density for the reduction of O_2 on the calculated total cathodic currents for the reduction of O_2 and H_2O as a function of potential in an air saturated solution of pH 5 at 368 K.

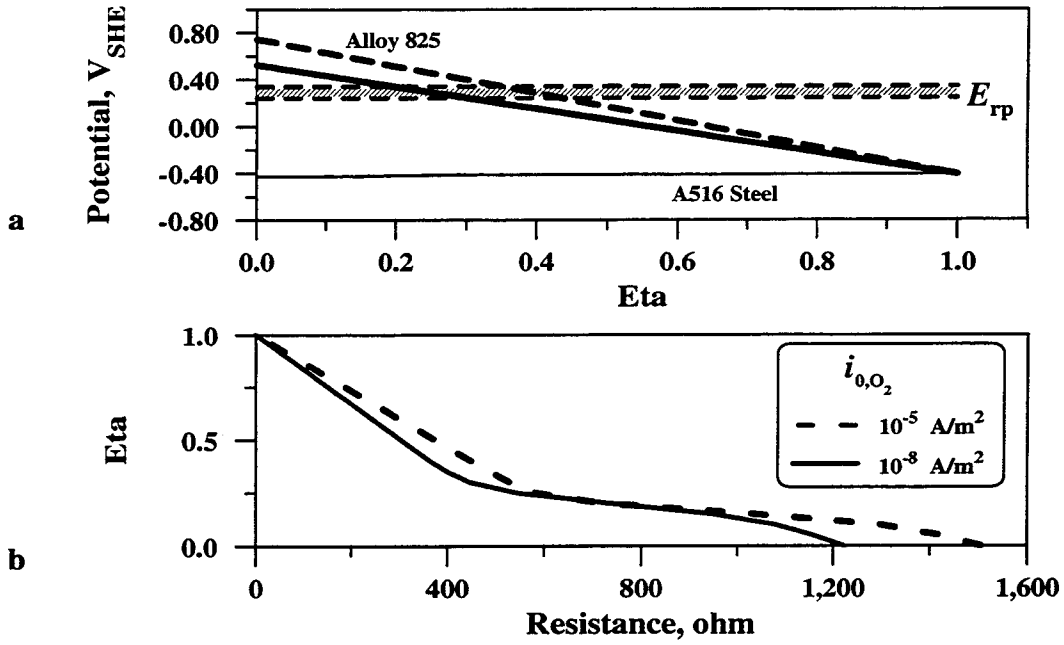

Figure A-6. (a) Plot of the calculated galvanic corrosion potentials of Alloy 825 and A516 steel as a function of the efficiency, η, of the galvanic coupling for two values of the exchange current density for the reduction of O_2 (10^{-5} and 10^{-8} A/m^2). The value of the repassivation potential of Alloy 825 in a solution containing 1,000 ppm chloride at 368 K is included. (b) Variation of η as a function of the resistance of the galvanic couple.

In figure A-7 the effect of β_{O_2} on the E_{corr}^{steel} and the E_{corr}^{825} is presented. Increasing the β_{O_2} raises the E_{corr}^{825} but has no effect on E_{corr}^{steel}. The changes in $E_{corr}^{825,WP}$, $E_{corr}^{steel,WP}$, and the value of R_{couple} necessary to initiate localized corrosion are minor as noted in figure A-8. This is again because variations in the β_{O_2} cause only slight changes in the kinetics in the activation controlled region of the oxygen reduction reaction. As a result, the kinetics of the iron dissolution reaction (independent of variations in β_{O_2}) become the dominant factor in determining corrosion potential of the galvanic couple and hence, reduce the $E_{corr}^{825,WP}$ to values below the E_{rp} for $\eta > 0.4$.

Figure A-9 illustrates that the E_{corr}^{steel} is strongly dependent on the value of α_{Fe}. Decreasing the α_{Fe} results of an increased polarization resistance. As shown in figure A-10a, both the $E_{corr}^{825,WP}$ and $E_{corr}^{steel,WP}$ escalate with lower values of α_{Fe}. As the Tafel slope for steel rises (α_{Fe} is reduced), the value of R_{couple} necessary to initiate localized corrosion is lowered from 400 to 300 ohms (figure A-10b). A Tafel slope of 40 mV/decade has previously been reported for the active dissolution of steel (De Waard and Milliams, 1975; Ogundele and White, 1986). An extension in the Tafel slope (reduction in α_{Fe}) can only occur was a result of a change in the dissolution kinetics of the steel. This may happen as a consequence of the steel surface becoming passivated in an alkaline environment. If passivation occurs, the dissolution kinetics of steel will approach the behavior observed for Alloy 825. As previously indicated, the formation of pits on the passivated carbon steel surface can easily be initiated in the presence of Cl^- containing electrolytes.

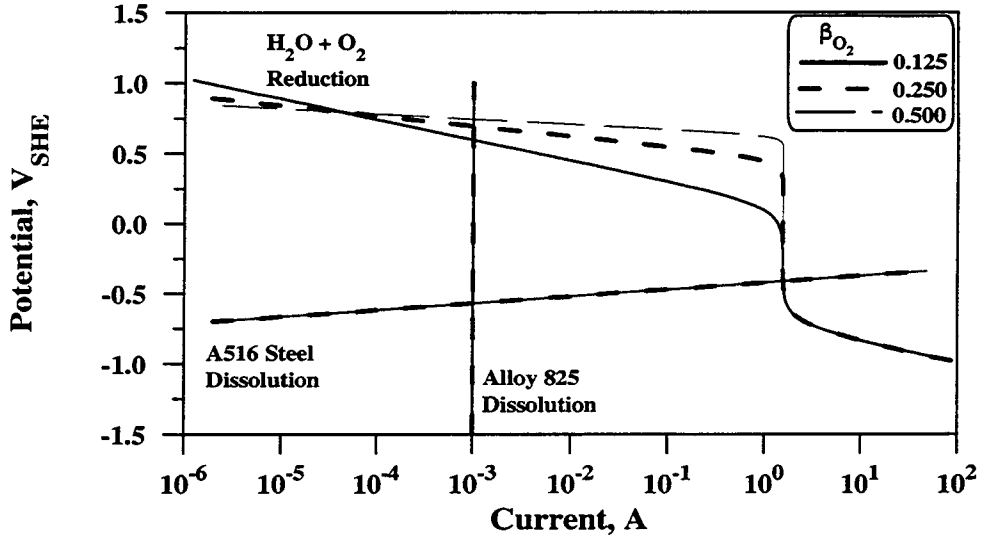

Figure A-7. Evans diagram showing the effect of the charge transfer coefficient for the reduction of O_2 on the calculated total cathodic currents for the reduction of O_2 and H_2O as a function of potential in an air saturated solution of pH 5 at 368 K.

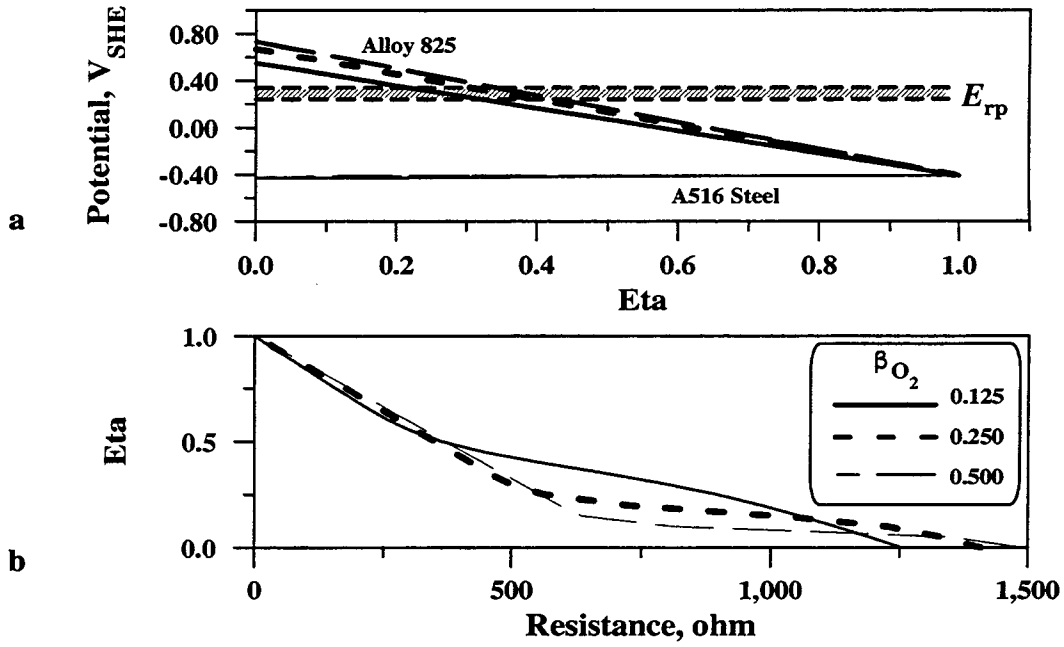

Figure A-8. (a) Plot of the calculated galvanic corrosion potentials of Alloy 825 and A516 steel as a function of the efficiency, η, of the galvanic coupling for three values of the charge transfer coefficient (β) for the reduction of O_2 (0.125, 0.250, and 0.750). The value of the repassivation potential of Alloy 825 in a solution containing 1,000 ppm chloride at 368 K is included. (b) Variation of η as a function of the resistance of the galvanic couple.

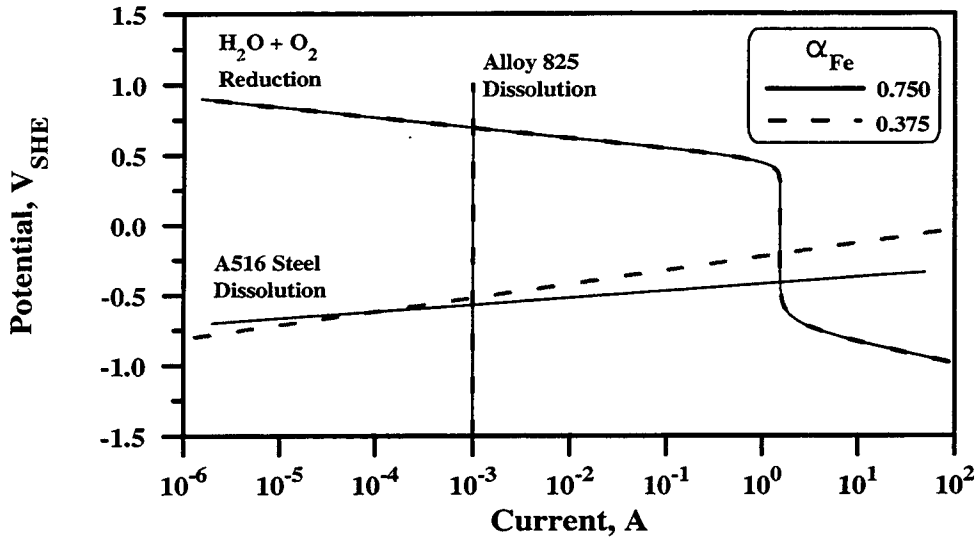

Figure A-9. Evans diagram showing the effect of the charge transfer coefficient (α) for the active dissolution of A516 steel on the calculated anodic current as a function of potential in an air saturated solution of pH 5 at 368 K.

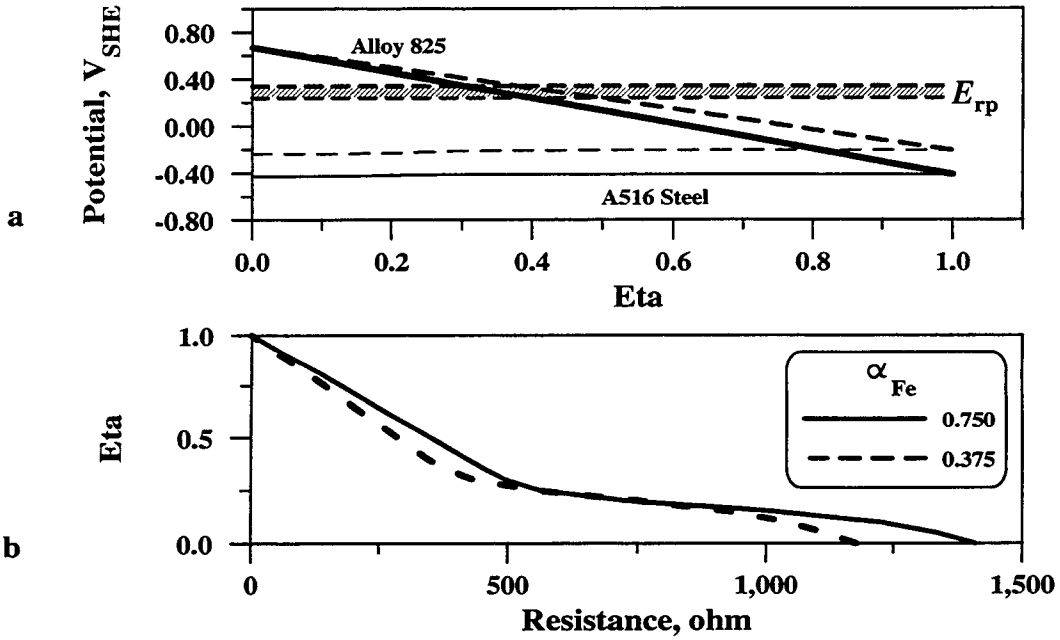

Figure A-10. (a) Plot of the calculated galvanic corrosion potentials of Alloy 825 and A516 steel as a function of the efficiency, η, of the galvanic coupling for two values of the charge transfer coefficient (α) for the active dissolution of A516 steel (0.750 and 0.375). The value of the repassivation potential of Alloy 825 in a solution containing 1,000 ppm chloride at 368 K is included. (b) Variation of η as a function of the resistance of the galvanic couple.